No PB # listed

Volume 1

Report No. FRA/ORD-80/52-1

PERFORMANCE OF A LINEAR SYNCHRONOUS MOTOR WITH LAMINATED TRACK POLES AND WITH VARIOUS MISALIGNMENTS

General Electric Company
P.O. Box 43
Schenectady, N.Y. 12305

William R. Mischler
Thomas A. Nondahl

SEPTEMBER 1980

Document is available to the public through the
National Technical Information Service
Springfield, Virginia 22161

Prepared for

U.S. DEPARTMENT OF TRANSPORTATION
FEDERAL RAILROAD ADMINISTRATION
Office of Research and Development
Washington, D.C. 20590

NOTICE

LIST OF RELATED REPORTS

All experimental and analytical work on linear electric motors, both synchronous and induction, performed by the General Electric Company under contract DOT-FR-64147 is contained in the following four reports:

Report No. FRA/ORD - 80/52

W.R. Mischler and T.A. Nondahl, Performance of a Linear Synchronous Motor with Laminated Track Poles and with Various Misalignments, The General Electric Company, Sept. 1980.

Volume 1 – This volume contains a description and summary of the linear synchronous motor work.

Volumes 2, 3, 4, 5, 6 – These volumes constitute Appendix I, and contain all test data and computer runs on the linear synchronous motor.

Report No. FRA/ORD - 80/53

G.B. Kliman, W.R. Mischler, and W.R. Oney, Performance of a Single-Sided Linear Induction Motor with Solid Back Iron and with Various Misalignments, The General Electric Company, Sept. 1980.

Volume I – This volume contains a description and summary of the linear induction motor work.

Volume II, Appendix B – Part 1 – This volume contains the first part of the reduced data on the linear induction motor work.

Volume II, Appendix B – Part 2 – This volume contains the second part of the reduced data on the linear induction motor work.

Report No. FRA/ORD -80/54

T.A. Nondahl and E. Richter, Comparisons Between Designs for Single-Sided Linear Electric Motors: Homopolar Synchronous and Induction, The General Electric Company, Sept.1980. (This report is complete in one volume.)

Report No. FRA/ORD - 80/73

G.B. Kliman, D.G. Elliott, V.B. Honsinger, T.A. Lipo, W.R. Mischler, T.A. Nondahl, and W.R. Oney, Performance of a Single-Sided Linear Induction Motor with Solid Back Iron and with Various Rail Configurations/Evaluation of the Claw-Pole Linear Synchronous Motor and Performance of the Homopolar Linear Synchronous Motor with Solid-Iron Poles, The General Electric Company, Sept.1980.

Volume 1 – This volume contains various experimental and analytical studies of three types of single-sided linear motors: induction, claw-pole, and homopolar synchronous.

Volume 2 – This volume contains all experimental runs connected with the studies of Volume 1.

TECHNICAL REPORT STANDARD TITLE PAGE

1. Report No. FRA/ORD-80/52-1	2. Government Accession No.	3. Recipient's Catalog No.
4. Title and Subtitle Performance of a Linear Synchronous Motor with Laminated Track Poles and with Various Misalignments		5. Report Date September 1980
		6. Performing Organization Code
7. Author(s) William R. Mischler and Thomas A. Nondahl		8. Performing Organization Report No. SRD-78-102
9. Performing Organization Name and Address General Electric Company Corporate Research and Development P.O. Box 43 Schenectady, New York 12301		10. Work Unit No.
		11. Contract or Grant No. DOT-FR-64147
12. Sponsoring Agency Name and Address U.S. Department of Transportation Federal Railroad Administration Office of Research and Development Washington, D.C. 20590		13. Type of Report and Period Covered Phase I - Final Report September 15, 1975 - June 30, 1978
		14. Sponsoring Agency Code
15. Supplementary Notes		

16. Abstract

A test facility was designed and built to measure the performance of a single-sided high speed homopolar Linear Synchronous Motor with laminated pole pieces over a wide range of frequency and excitation levels. The facility was instrumented to measure performance at the machine terminals, flux density in the air gap and machine, and forces in all six axes. The machine was tested under nominal conditions and with perturbations in five degrees of freedom: air gap, lateral, pitch, roll, and yaw. Equivalent circuit parameters and flux form coefficients were measured and compared to design values. Poor correlation forced a revision of the design programs. The modeling of the finite interpolar gap and interpolar leakage flux led to good agreement between test and revised design values. The test data show a high power factor, the absence of end effects, and a strong tendency of the machine to remain properly aligned relative to the track, with the exception of a destabilizing pitch torque.

17. Key Words (Selected by Author(s))	18. Distribution Statement
Linear synchronous motors Linear electric motors High-speed ground transportation	Document is available to the public through the National Technical Information Service, Springfield, VA 22161

19. Security Classif. (of this report)	20. Security Classif. (of this page)	21. No. of Pages	22. Price
UNCLASSIFIED	UNCLASSIFIED	115	

TABLE OF CONTENTS

TABLE OF CONTENTS (CONT'D)

LIST OF ILLUSTRATIONS

LIST OF ILLUSTRATIONS (CONT'D)

LIST OF ILLUSTRATIONS (CONT'D)

LIST OF ILLUSTRATIONS (CONT'D)

LIST OF ILLUSTRATIONS (CONT'D)

LIST OF TABLES

APPENDIX I - TEST DATA

Appendix I of Performance of a Linear Synchronous Motor with Laminated Track Poles and with Various Misalignments consists of five volumes of computer runs (Vol. 2-6) used in the analysis presented in Volume 1. The following is a catalog of these runs.

CATALOG OF TEST DATA

60 and 150 Hertz Performance Tests

Volume	Runs	Description
VOLUME 2	100 - 108	Preliminary 60 Hz Motoring
	109 - 116	60 Hz, 75 A Field, Motoring - Preliminary
	117 - 124	60 Hz, 40 A Field, Motoring - Preliminary
	125 - 133	60 Hz Angle Tests - 400 A
	134 - 140	60 Hz Angle Tests - 500 A
	141 - 146	60 Hz Motoring, 75 A Field
	147 - 152	60 Hz Motoring, 40 A Field
	153 - 160	60 Hz Open Ckt. Saturation
	161 - 167	150 Hz Open Ckt. Saturation
	168	Not Used
	169 - 176	60 Hz Short Ckt. Saturation
	177 - 184	150 Hz Short Ckt. Saturation
	185 - 190	60 Hz Motoring, 75 A Field
	191 - 197	60 Hz Generating, 75 A Field
	198 - 203	60 Hz Generating, 40 A Field
	204 - 211	60 Hz Angle Tests - 100 A
	212 - 219	60 Hz Angle Tests - 200 A
	220 - 227	60 Hz Angle Tests - 300 A
	228 - 235	60 Hz Angle Tests - 470 A
	236 - 240	60 Hz Motoring - 16.3 mm gap
	241 - 248	60 Hz Motoring - 11.2 mm gap
	249 - 256	60 Hz Open Ckt. Saturation - 11.2 mm
	257 - 264	150 Hz Open Ckt. Saturation - 11.2 mm
	265 - 272	60 Hz Short Ckt. Saturation - 11.2 mm
VOLUME 3	273 - 280	150 Hz Short Ckt. Saturation - 11.2 mm
	281 - 288	60 Hz Motoring - 21.3 mm gap
	289 - 296	60 Hz Open Ckt. Saturation - 21.3 mm
	297 - 304	150 Hz Open Ckt. Saturation - 21.3 mm
	305 - 312	60 Hz Short Ckt. Saturation - 21.3 mm
	313 - 320	150 Hz Short Ckt. Saturation - 21.3 mm
	321 - 327	150 Hz Motoring - Preliminary
	328 - 337	150 Hz Angle Tests - 500 A
	338 - 344	150 Hz Motoring - 75 A Field
	345 - 350	150 Hz Motoring - 40 A Field

351 - 352	Runs for DPO Data
353 - 359	150 Hz Generating - 40 A Field
360 - 365	150 Hz Generating - 75 A Field
366 - 370	150 Hz Motoring - 16.3 mm gap
371 - 378	150 Hz Motoring - 11.2 mm gap
379 - 384	150 Hz Motoring - 21.3 mm gap
385 - 398	150 Hz Generating - 75 A Field
399 - 403	150 Hz e = o
	150 Hz G - Table Tests
404 - 408	150 Hz e = o
409 - 413	150 Hz e = +12.5 mm
414 - 419	150 Hz e = +25 mm
420 - 424	150 Hz e = 12.5 mm
425 - 430	150 Hz e = 25 mm

VOLUME 4

431 - 435	150 Hz e = o, f = o
436 - 440	150 Hz b = +.0224 rad
441 - 445	150 Hz b = +.0448 rad
446 - 450	150 Hz b = -.0224 rad
451 - 455	150 Hz b = -.0448 rad
456 - 460	150 Hz b = o, a = o
461 - 465	150 Hz a = +.00148 rad
466 - 470	150 Hz a = -.00148 rad
471 - 475	150 Hz a = +.00296 rad
476 - 480	150 Hz a = +.00296 rad
481 - 485	150 Hz a = o, c = o
486 - 490	150 Hz c = +.00456 rad
491 - 495	150 Hz c = -.00456 rad
496 - 500	150 Hz c = o
501 - 505	60 Hz e = o
	60 Hz 6 - Table Tests
506 - 510	60 Hz e = +12.55 mm
511 - 516	60 Hz e = +25 mm
517 - 521	60 Hz e = -12.5 mm
522 - 527	60 Hz e = -25 mm
528 - 532	60 Hz e = o, b = o
533 - 537	60 Hz b = +.0224
538 - 542	60 Hz b = +.0448
543 - 547	60 Hz b = -.0224

548 - 532	60 Hz b = -.0448
533 - 557	60 Hz b = o, a = o
558 - 562	60 Hz z = +.00296 rad
563 - 567	60 Hz a = -.00296 rad
568 - 572	60 Hz a = o, c = o
573 - 577	60 Hz c = +.00456 rad
578 - 582	60 Hz c = -.00456 rad
583 - 587	60 Hz c = o

PREFACE

This report describes and summarizes the tests run on the General Electric/Department of Transportation laminated track single-sided homopolar Linear Synchronous Machine (LSM). These tests were part of a program to evaluate both linear induction and linear synchronous machines. In the part of the program described in this report, the measured performance of the laminated track LSM is summarized for frequencies of 60 hertz, 150 hertz, and 383 hertz, with several different field current values and a wide range of armature currents. The measured performance under off-nominal, or G-matrix conditions, wherein the stator was displaced by various offsets and angles, is also shown. Measurements of reluctance forces with dc armature excitation, values for the LSM equivalent circuit parameters, and flux desities are discussed, and the LSM design program modifications necessitated by poor condition between design and tested values are outlined.

Section 1 of this report describes the electromagnetic and mechanical design of the LSM. Section 2 describes open and short circuit tests, and Section 3 describes the performance of the machine under load. Curves showing the effect of displacing the motor (G-matrix) are shown in Section 4. Section 5 discusses the measurement of equivalent circuit parameters, air gap, and pole piece flux and dc static forces. Section 6 shows the corrections which were made to the LSM design program to account for the large difference between predicted and tested behavior. The resulting design program is discussed in detail in the Phase III report. Section 7 gives an introduction to the test data and data reduction program. All the test data for this phase of the test program are listed in Appendix I, Volumes 2 through 6.

Section 1

INTRODUCTION AND MACHINE DESIGN SUMMARY

The model Laminated Track Homopolar Linear Synchronous Motor was built in an effort to measure the available design procedures and refine them. A round track and segment stator were chosen to suit the available test facility, described in Section 1 of the Phase II Report on the Single-sided Linear Induction Motor (SLIM). The data acquisition system described therein was used in these tests, with appropriate adjustments and re-assignments of channels. The 112 kW model was tested at low, medium, and high speeds of 17.4, 43.5 and 111 meters per second, corresponding to 60, 150 and 382.5 hertz operating frequencies. Power for the machine was supplied by a rectifier and controlled current inverter. Synchronous operation was controlled by circuits which adjusted current levels and phase relationships of the inverter supply using opto-electronic sensors on the track and analog and digital processing of command and feedback signals.

ELECTROMAGNETIC DESIGN

Table 1-1 is a tabulation of the electromagnetic and related mechanical parameters of the test machine. The left column, dated 12/77, gives the characteristics and parameters of the machine as designed, while the right one, dated 4/78, gives these values as produced by the design program after it was corrected and adjusted for the actual performance of the test machine. Note that the original design was based on a 155 kW rating so as to provide operating margin if performance fell short of design. Further comparison and explanation of these two sets of information appear in Section 6 of this report, while details of the mechanical construction appear below.

TABLE 1-1. DESIGN DETAILS FOR 155 kW HOMOPOLAR INDUCTOR MOTOR MODEL

Computer Symbol		Value 12/77	Value 4/78
	General		
	Kilowatt Rating	155.00	96.00
	Linear Velocity, km/hr	402.00	402.00
	Voltage (line to neutral)	140.00	87.00
	Amperes	370.00	370.00
	Frequency, Hz	394.30	394.30
	Pole Ptch, cm	14.17	14.17
	Per Unit Pole Arc	0.50	0.50
	Gap Length, cm	1.52	1.52
	Winding Pitch	0.833	0.833
	Slotting and Armature Winding		
H14	Total Slot Depth, cm	1.98	1.98
$B_1 = B_4$	Slot Width (rectangular), cm	1.27	1.27
	Slot Pitch, T_s, cm	2.36	2.36
	Tooth Width W_t, cm	1.09	1.09
	Ratio Slot Width/Slot Pitch	0.54	0.54
SLOTS	Number of Slots	35.00	35.00
S/P/P	Slots/Pole/Phase	2.00	2.00
	Number Pole Pairs	2.50	2.50
TPC	Turns/Coil	2.00	2.00
CIR	Number Parallel Circuits	1.00	1.00
STR	Strands of Wire	4.00	4.00
T/PH	Turns/Phase	20.00	20.00
T/PHE	Effective T/PH = (T/PH)k_{pd}	18.66	18.66
WIRE	Rectangular, WWB, Width, cm	0.564	0.564
	HWB, Height, cm	0.183	0.183
	Wire Area, cm^2	0.096	0.096
	Current Density, A/cm^2	964.00	964.00
	Surface Current Density, A/cm	585.00	585.00
	Weights in Kilograms		
STCW	Stator Core	37.0	37.0
YW	Yoke	24.0	31.0
CUACU	Armature Copper	22.0	22.0
FCUW	Field Copper	87.0	87.0
STW	Total Motor (excludes track)	170.0	177.0
TRWPP	Track Weight Per Pole	10.0	10.0

TABLE 1-1. DESIGN DETAILS FOR 155 kW HOMOPOLAR INDUCTOR MOTOR MODEL (CONTINUED)

	Overall Lengths (cm)	12/77	4/78
HISP	Stack(s) plus Field Space	25.00	25.00
SPI	Field Space	13.00	13.00
HI	Stack Length	11.95	11.95
LOEDT	Length Over End Turns	41.10	41.10
H14	Slot Depth Total	1.98	1.98
HCOR	Core Depth Behind Slot	4.93	4.93
HY	Yoke Depth	2.17	2.82
TH	Total Machine Depth	9.08	9.73
TLM	Total Machine Length	85.00	85.00
HTR	Height of Track, maximum	7.62	7.62
WTR	Width of Track, maximum (Direction of Travel)	7.10	7.10
TPOLE	Pole Pitch	14.17	14.17
	Motor Estimated Parameters (V=600/phase, 394 Hz)		
RPH/RPU	Hot Resistance ac winding Ω /pu	.013/.035	.013/.057
XS/XSPU	Leakage Reactance Ω/pu	.16/.43	.14/.61
XAD/XADPU	Direct-Axis Mutual Ω/pu	.15/.39	.17/.70
XAQ/XAQPU	Quadrature-Axis Mutual Ω /pu	.12/.32	.14/.58
XF/XFP	Field Leakage Ω/pu	.15/.388	.47/2.0
XD1/XD1P	Direct-Axis Transient Reactance Ω/pu	.24/.63	.26/1.13
XC/XCP	Commutating Reactance Ω/pu	.26/.69	.27/1.16
	Flux, Flux Densities and Field Form Coefficients		
BGAP	Maximum Gap Density Tesla	0.81	0.81
BT	Maximum Stator Tooth Density	1.86	1.86
BMCOR	Maximum Stator Core Density	1.40	1.40
BMY	Maximum Yoke Density	1.55	1.55
BMTR	Maximum Track Density	1.55	1.55
FLDCT	Total Flux, dc in airgap (weber)	0.0136	0.0156
FLAC	ac Flux in Airgap	0.0048	0.0032
FLDCY	Flux dc in frame	0.0095	0.0124
KU	(Total Flux/ac Flux) in Pole	2.82	4.83
KM	Maximum Flux Density/ Average Flux Density	2.03	1.75
ATF	Ampere Turns Provided by Field	25,312.0	30,515.0
	Field Coil Data		
TURNS	Field Coil Turns	336.0	336.0
LAYERS	Coil Sides/Width (SPI)	24.0	24.0
CDF	Current Density in Field Coil (A/cm^2)	465.0	465.0

STATOR

Stator Winding

The model machine has been chosen to have a five-pole winding and two cores of 2.36 in. (6 cm) width. The five-pole length is dictated by the requirement of a constant number of saliencies over the stator to produce a constant reluctance in the dc circuit. Figure 1-1 shows the arrangement of the coils, the connections, and the rotor saliencies. The figure-eight winding pattern provides proper phasing of stator currents for use of straight-across trade poles, simplifying the track structure appreciably.

The constraints of construction and testing of the linear synchronous machine dictated that the model be built curved, with an air gap radius of approximately 27 in. (0.686 meter). This meant that, in curving the machine, some of the linear dimensions must change. The track pole pitch of 5.58 in. (14.17 cm) was maintained, and this necessitated an increase in the stator slot pitch from .93 (2.36 cm) to .951 in. (2.415 cm) at the air gap and .978 in. (2.48 cm) at the bottom of the slot.

Figure 1-2 shows the slot and tooth of the machine. The tooth width at the gap is the same as in the flat machine, so that the flux to saturate the teeth will be the same. The rectangular slot causes a slight widening of the tooth at its root.

Slot depth was held the same as in the flat machine, and the width was increased slightly, from 0.500 (1.27 cm) to 0.520 in. (1.32 cm). The dimensions of the slot allowed use of coils wound two turns per coil from four parallel wires of .070 in. x .225 in. (1.78 x 5.72 mm) copper with quadruple esterimide insulation. This wire was chosen as the most appropriate available size and insulation build. The insulation treatment of the coils in the slots is indicated in Figure 1-2. Although the peak voltage spikes delivered by the inverter were expected to be only about 700 volts, a 2300 volt insulation system was used to be on the safe side. This system was based on mica-mat tape and sheet insulation and on vacuum pressure impregnation.

Stator Core Construction

The construction of the stator core is detailed in Figures 1-3 and 1-4. The laminations are of .014 in. (.36 mm) silicon steel, and the vendor was given the option of manufacturing each one in two pieces. The split lines for the two-piece option are shown in Figure 1-3, one slot to each side of center. Accepted motor manufacturing standards for slot tolerances, burrs, and lineup have been applied to the lamination stacks. A total of nine bolts through each stack clamp the laminations together and hold the stacks to the steel yoke.

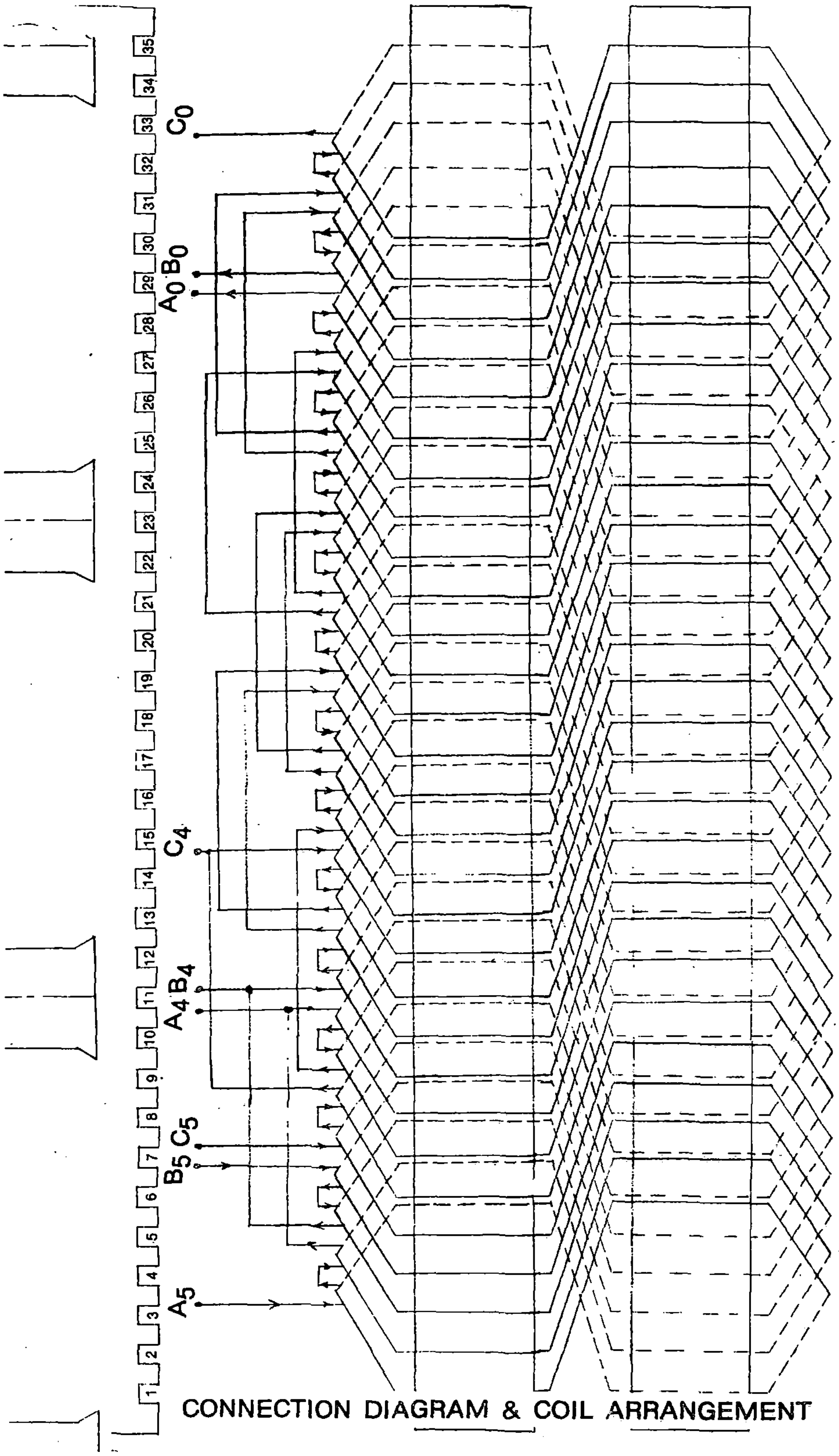

FIGURE 1-1. CONNECTION DIAGRAM AND COIL ARRANGEMENT.

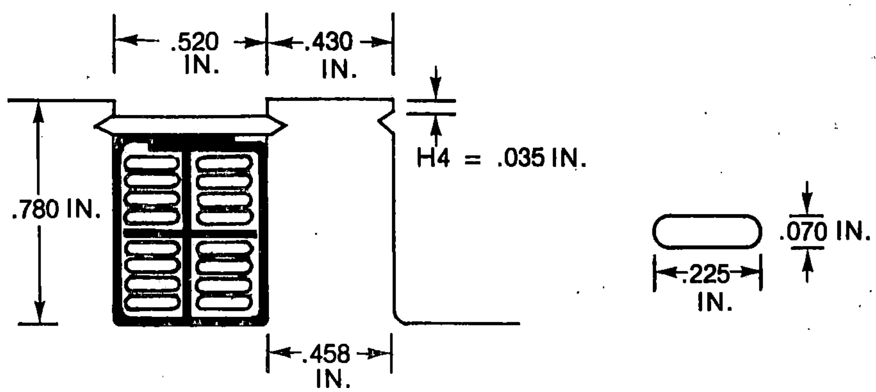

SLOT AND TOOTH (SCALE X 2)

STRANDS 4
T/C 2
CONNECTION 1Y

BARE CONDUCTOR (SCALE X 3)

H_{wb} = .070 IN.
W_{wb} = .225 IN.

HEIGHT:		.520 (1.32 cm)
COND	= 8 x .070	= .560 IN.
INS	= 16 x .003	= .048
S1 TUBE	= 2 x .015	= .030
SEP	=	= .015
STICK	=	= .065
H4	=	= .035
	.780 -	.753 = .027 DA (.068 cm)

WIDTH:		
COND	= 2 x .225	= .450 IN.
INS	= 4 x .003	= .012
S1 TUBE	= 2 x .015	= .030
		.502

W_A = .018 (.046 cm)

FIGURE 1-2. SLOT, TOOTH AND CONDUCTOR LAYOUT FOR 112 kW AIR-COOLED HOMOPOLAR MACHINE.

The yoke structure is a weldment which supports the stator stacks and field coils. The 1-9/16 in. (4 cm) thick plate has two plates welded near each end to carry the rods that run in the supporting linear bearings. A fifth piece is welded in the center as a post to push against the thrust sensors. The upper surface of the plate is machined to receive the stator stacks and their fastening hardware.

A clamp plate down each side of the structure secures the other side of the stacks to the yoke and aids in clamping the laminations together.

DC Field Winding

The design of the field winding was a rather simple construction using a low voltage (600 volts) insulation system. Two coils, each comprised of 168 turns of ten parallel strands, eight of .0480 in. (1.22 mm), and two of .0453 in. (1.15 mm) diameter esterimide insulated wire were wound on long rectangular forms, then taped and slipped onto the stator cores. Retaining clamps were

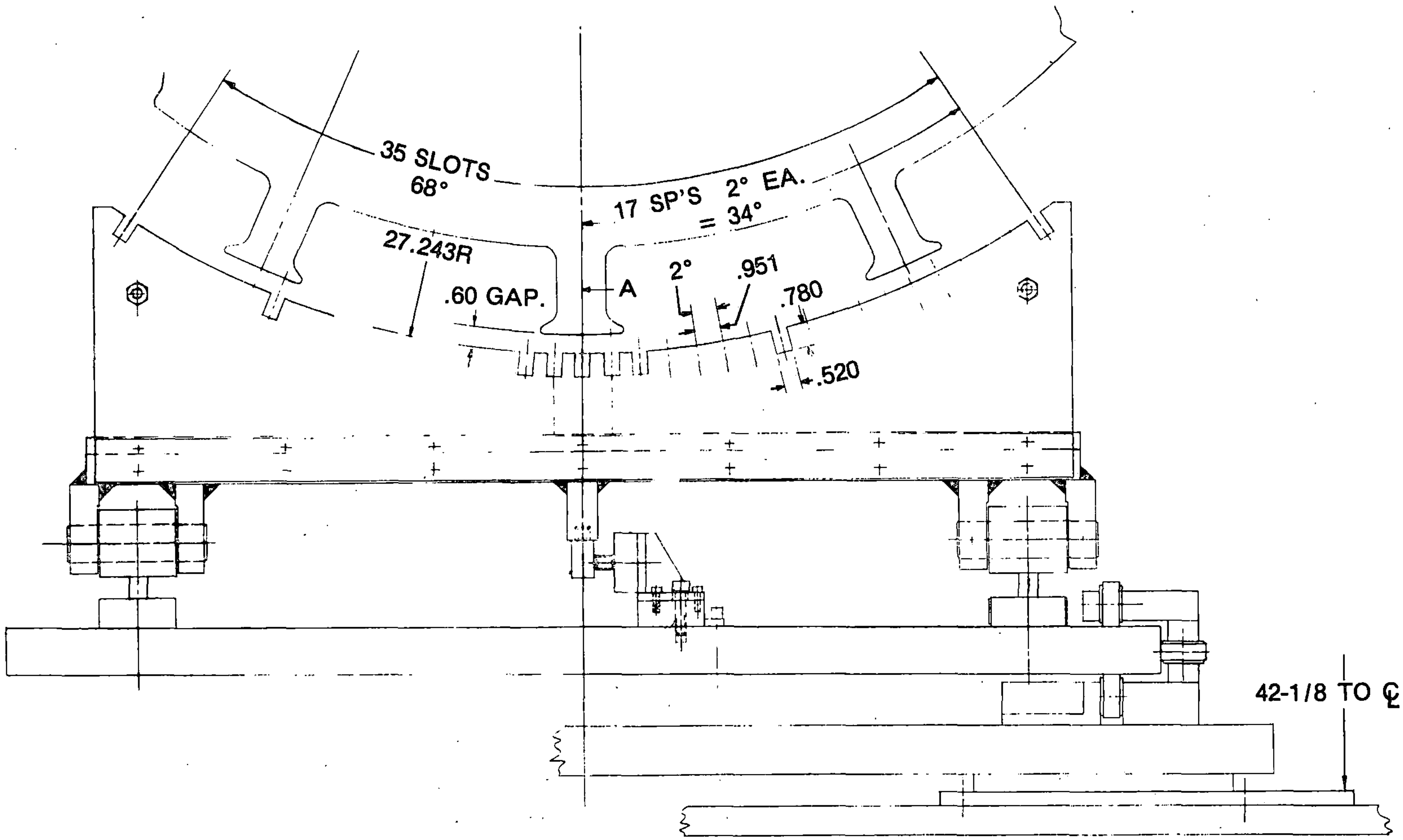

FIGURE 1-3. STATOR AND SUPPORT ASSEMBLY.

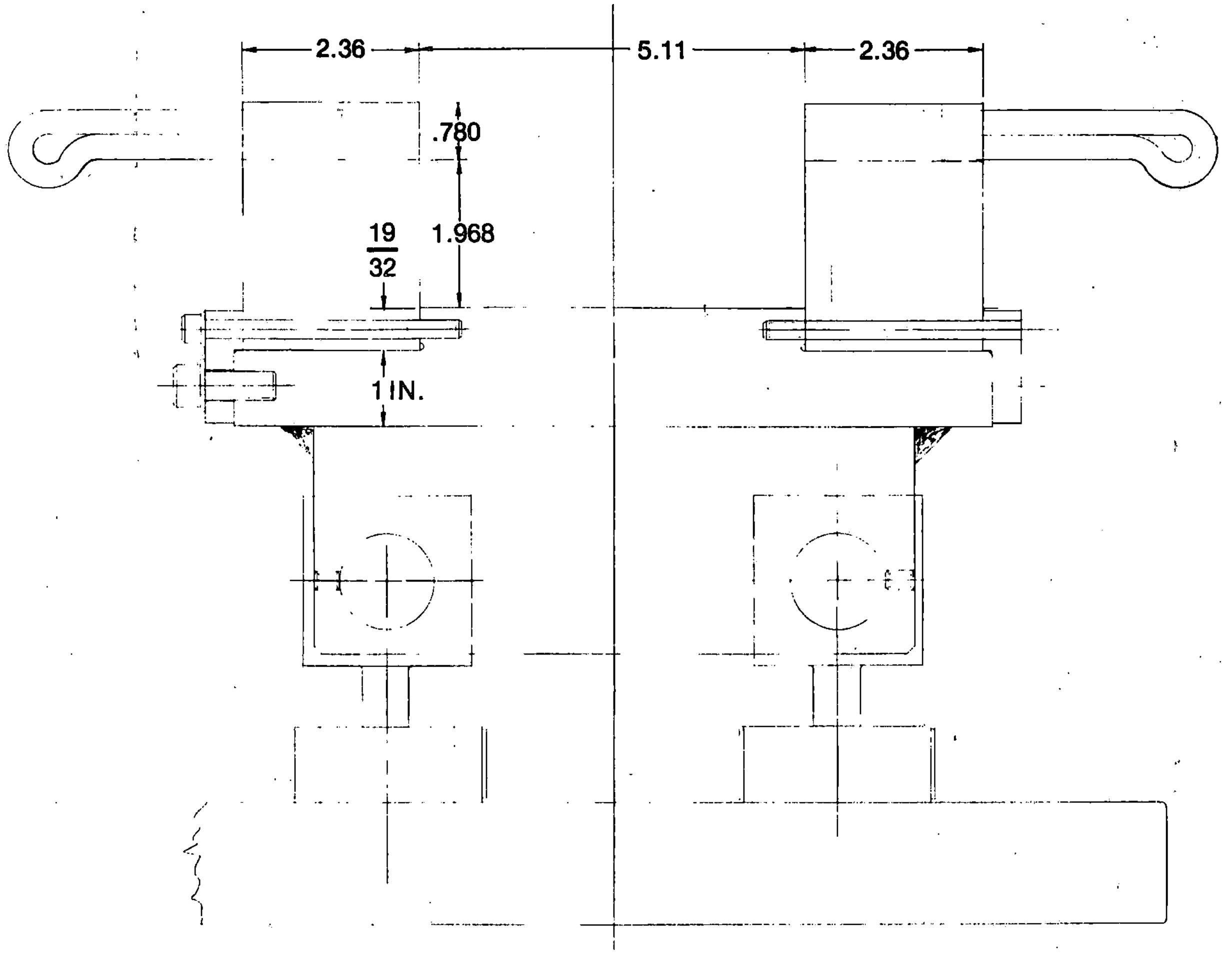

FIGURE 1-4. STATOR AND SUPPORT ASSEMBLY.

applied, the ac winding inserted and connected, and the entire stator assembly vacuum-pressure impregnated. For operation the two-field coils were connected in series.

SYNCHRONOUS MOTOR DESIGN AND FABRICATION: ROTOR

Factor of Safety

The 1.35 m (53.2 in.) diameter rotor has a top rated speed of 1530 rpm for 111 m/sec (250 miles per hour). At this speed the centrifugal "g" force on the outer surface is 1850, i.e., each pound on the surface has nearly a ton of centrifugal force on it. This produces stresses high enough to require care in design, but not so high that normally available materials cannot be used.

Design

The design of the rotor is shown in Figures 1-5 and 1-6. The two outer stacks of laminations with pole projections and the inner stack are made of 20 gage (0.0359 in.) cold-rolled sheet steel.

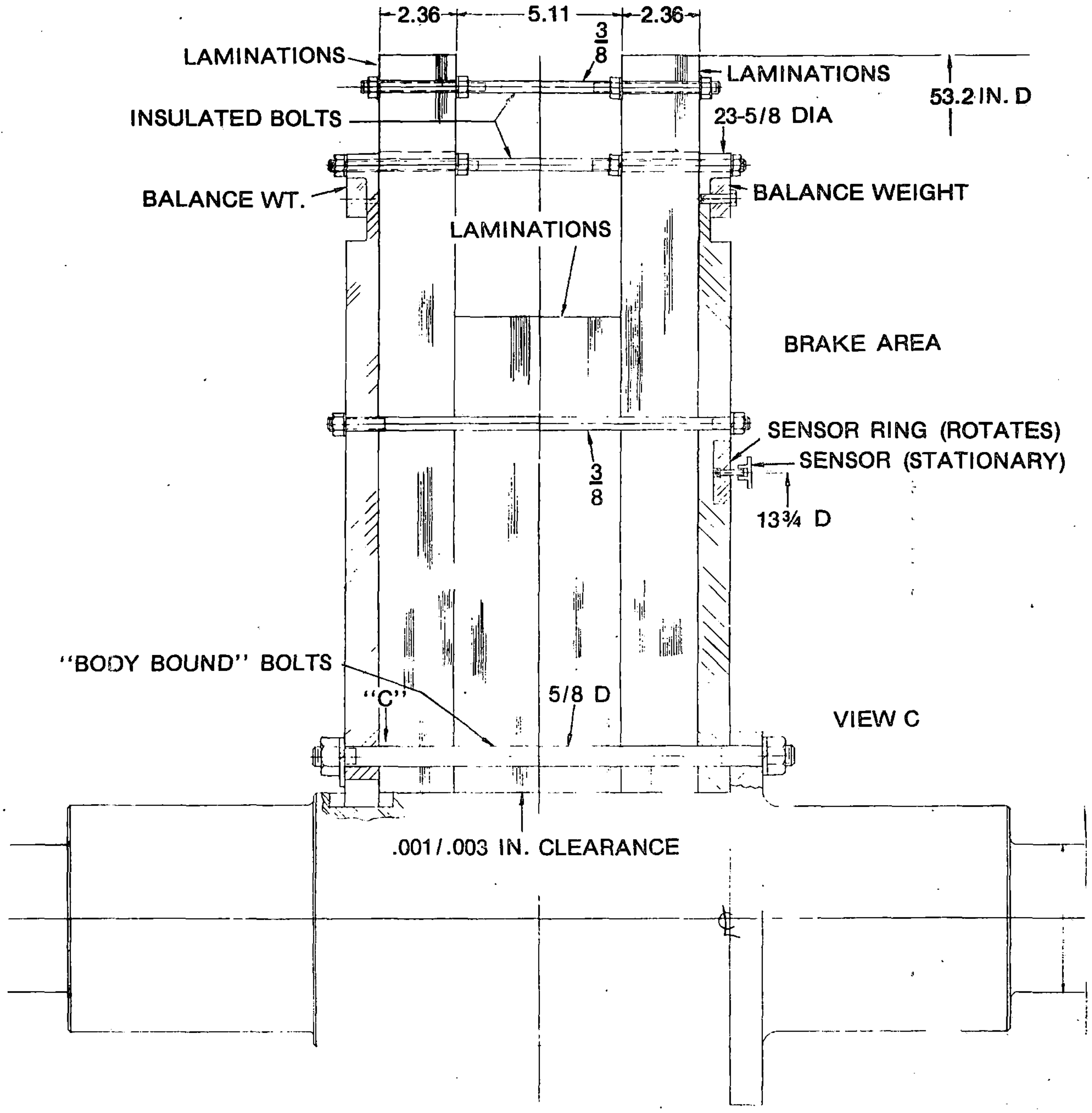

FIGURE 1-5. ROTOR DESIGN FOR THE SYNCHRONOUS MOTOR.

The flux in the outer sections must build up as the rotor passes over the field coil, at a rate dictated by the time constant. With the few number of stator poles of the sample, this reduction of flux can be large. To reduce the time constant, the pole projection and yoke section are "core plated" (interlaminar insulated) for a depth of 1 pole pitch, which is the outside diameter of the center stack. Below this diameter the flux pulsation was expected to be "averaged out" to a low enough value to not affect buildup time, and the laminations in all three stacks are uninsulated, to reduce the interlamination "air gap" where the flux is taken "across the grain."

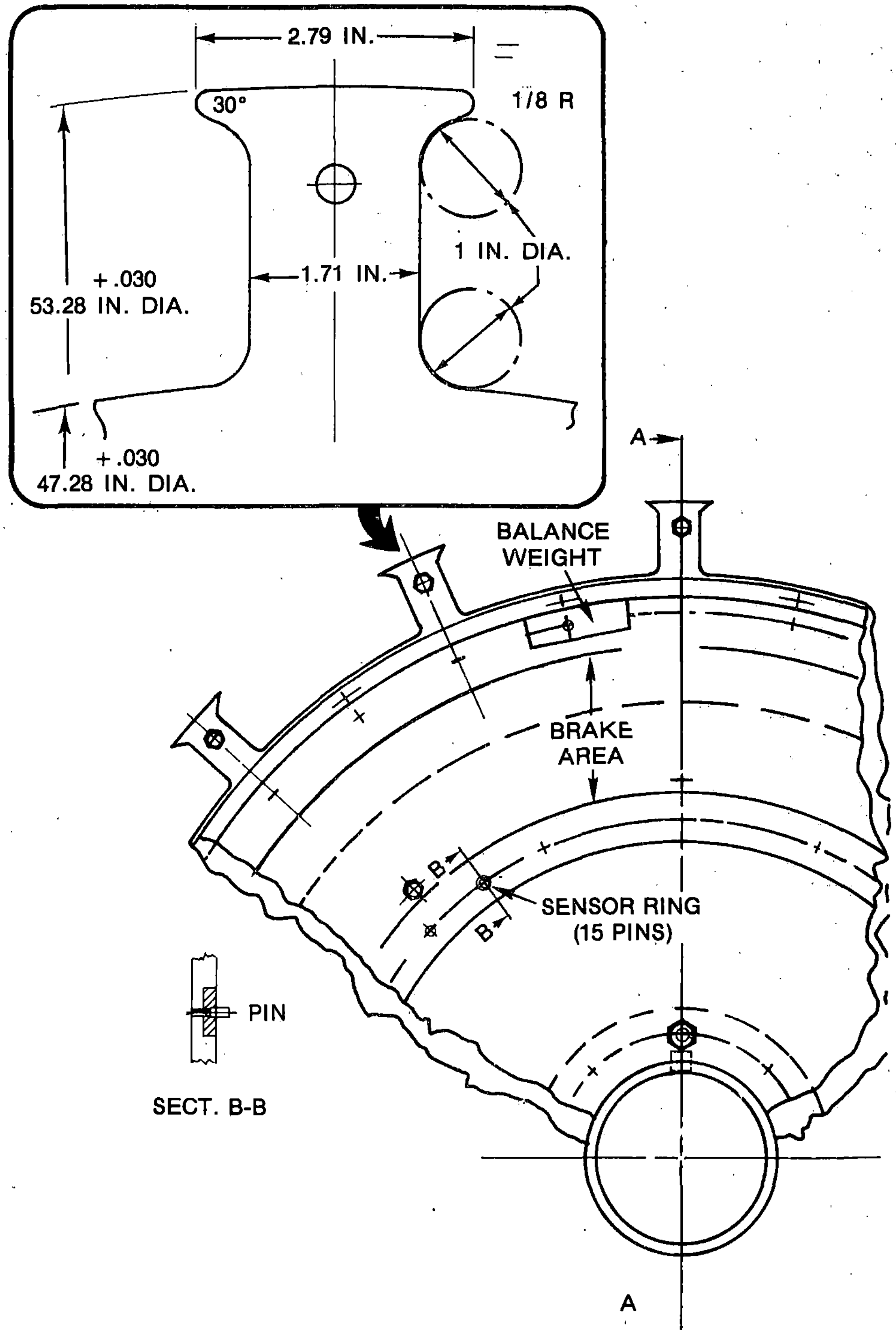

FIGURE 1-6. ROTOR DESIGN FOR THE SYNCHRONOUS MOTOR (CONTINUED).

In this design the rotor laminations are centered but not supported by the shaft, and at standstill have a 1 to 3 mils clearance. The stacks are held and driven by the eight through-bolts through the shoulder on the shaft on one end and the keyed ring on the other.

The outer tie bolts are insulated through the stacks so that the laminations will not be shorted.

Section 2

OPEN CIRCUIT AND SHORT CIRCUIT TESTS

This section describes and presents the results of tests of friction and windage, open circuit saturation and short circuit saturation tests on the laminated track machine.

FRICTION AND WINDAGE CORRECTIONS

The LSM was driven by the dc load motor at speeds near 240 rpm (60 hertz synchronous speed) and 600 rpm (150 hertz synchronous speed). The range of torque displayed by the torque transducer amplifier was plotted in Figure 2-1. A reasonably smooth curve was put through these torque ranges, and the square root, labeled $\sqrt{\tau}$, was plotted. A reasonable fit to the data was obtained as

$$\sqrt{\tau} = .0117 \times \text{rpm} + 0.9,$$

or

$$\tau = .0001369 \times \text{rpm}^2 + .0211 \times \text{rpm} + .81 \qquad (2\text{-}1)$$

and this relationship was used as the friction and windage contribution in all calculations of performance at 60 and 150 hertz. This contribution was added to the measured shaft torque for all motoring data and subtracted from the shaft torque for generating data, open circuit, and short circuit curves.

At full speed, the relationship of torque to speed was not exactly reflected by the expression developed for lower speeds. A new set of data was taken near 1530 rpm (382.5 hertz synchronous speed), and the results of this test are shown in Figure 2-2. The dashed line is the relationship

$$= .0001324 \times \text{rpm}^2, \qquad (2\text{-}2)$$

which was used as a simple correction in all performance data at 382.5 hertz.

OPEN CIRCUIT VOLTAGE AND LOSSES

The first test was to use the dc motor to drive the machine at 240 rpm (17.4 mps) with field applied and the ac terminals open. Figure 2-3 shows the three 60 hertz line-to-neutral voltages obtained with a 75 A field current. The voltages are quite sinusoidal, showing very little harmonic content, and appear in phase sequence C-B-A. The five-pole connection of the ac winding was used in this test, as in all subsequent tests presented here. The open cirucit voltage produced by the machine was 13.2 volts rms, measured by digital voltmeter, and the scope traces agree as nearly as can be measured.

The field current was varied in order to produce the open circuit saturation curve shown in Figure 2-4. Again, the speed was

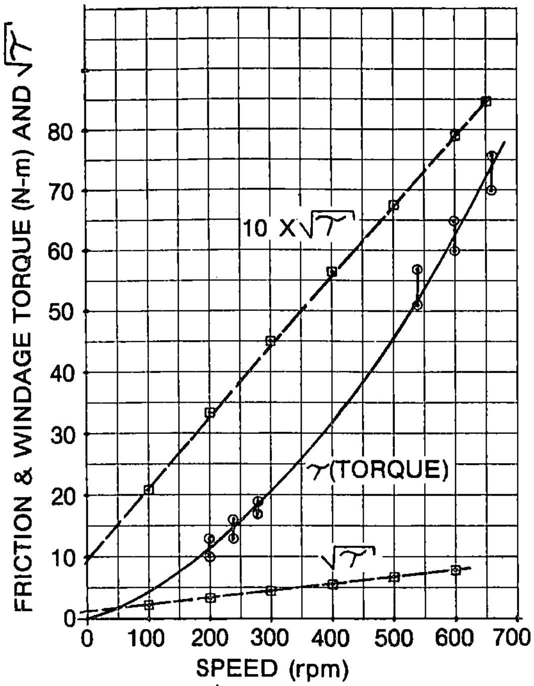

FIGURE 2-1. LSM LAMINATED TRACK FRICTION AND WINDAGE TORQUE VS. SPEED NEAR 240 AND 600 rpm OPERATING CONDITIONS.

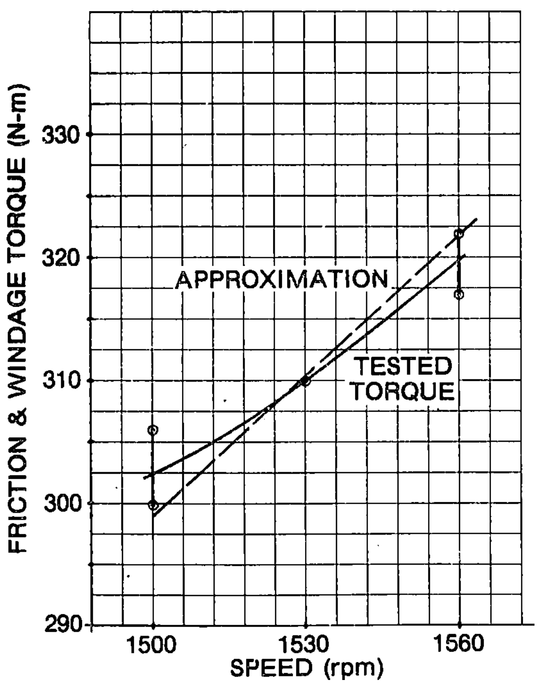

FIGURE 2-2. LSM LAMINATED TRACK FRICTION AND WINDAGE TORQUE VS. SPEED NEAR 1530 rpm OPERATING CONDITIONS.

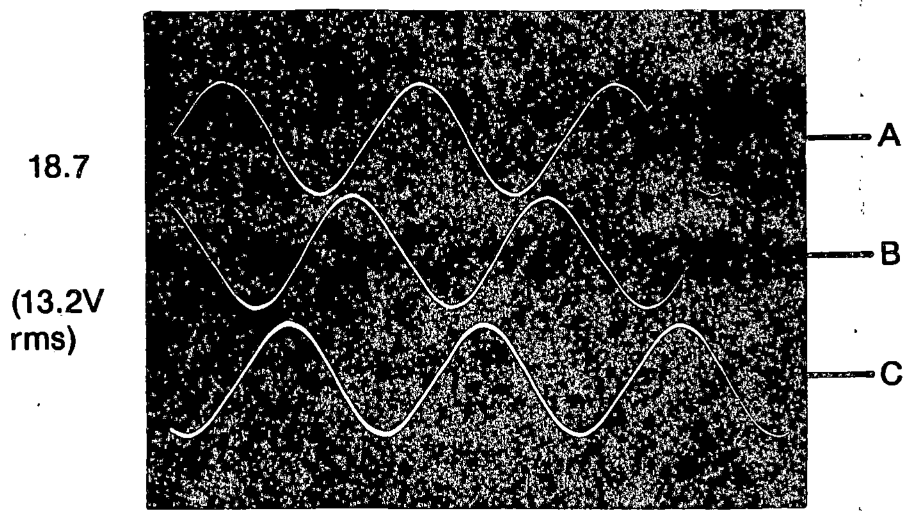

FIGURE 2-3. LSM LAMINATED TRACK LINE-TO-NEUTRAL VOLTAGES AT 75 AMPERE FIELD - 240 rpm (12.4 mps), 60 Hertz.

240 rpm to produce 60 hertz output. The shape of the saturation curve produced for this machine differs from that of a conventional synchronous machine, as can be seen in the decreased voltage output at high field currents. The output voltage increases linearly with field current from zero to about 30 A, then begins to show saturation. At about 87 A, the voltage actually starts to decrease for increasing field current. Saturation of either the stator teeth, the track saliencies, or both, apparently causes the effective alternating component of flux in the air gap to decrease. The ratio of the gap between saliencies to the gap over saliencies decreases, resulting in this reduction of flux variation. In this case, the maximum measured output voltage with the nominal air gap of 16.3 mm was 13.33 volts, at about 87 A field. The curves for the increased air gap of 21.3 mm and for the decreased gap of 11.2 mm show the inverse nature of variation of voltage with gap dimension. While the magnitude of open circuit voltage changes with air gap, the shape of the excitation curve remains very similar.

Figure 2-5 shows the mechanical (shaft) input (less friction and windage) to the machine as a function of field current and gap dimension. The point-to-point variation in this data is the result of limitations in the speed control loop and the torque transducer's resolution. These curves represent the magnetic losses in the stator and track associated with the buildup and decay of flux in the track poles and the alternating component of flux seen in the stator core as track poles pass over it. For the nominal gap at 75 A field, this amounts to about 440 watts, or about 2.5% of machine rating at this speed. These losses vary generally upward with decreasing air gap, downward with increasing gap.

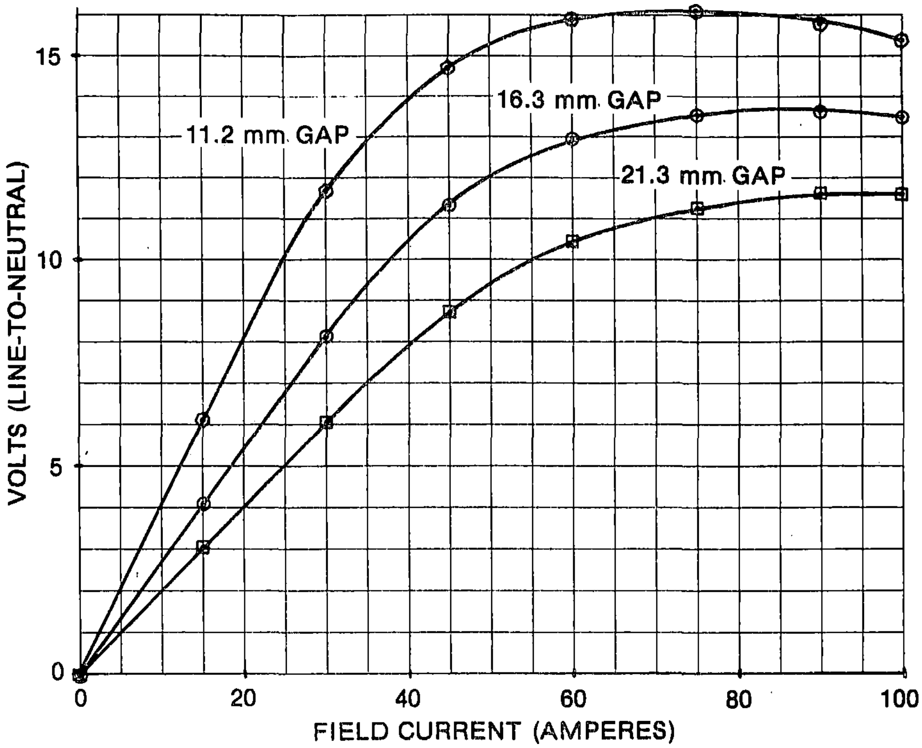

FIGURE 2-4. LSM LAMINATED TRACK OPEN CIRCUIT VOLTAGE VS. FIELD CURRENT AND AIR GAP - 60 Hertz, 240 rpm; g = 11.2, 16, 3, 21.3 mm.

Figures 2-6 and 2-7 show the open circuit voltage and magnetic losses as obtained at 150 hertz. The maximum voltage obtained with the nominal air gap was 34.0 volts, just 2.5 times the voltage at 60 hertz. Within the limitations of measurement of speed, field current and terminal voltage, the machine displayed a constant volts-per-hertz characteristic. The magnetic losses at nominal gap and 75 A field were about 2100 watts, 4.8 times those at 60 hertz, indicating a variation with $(speed)^{1.7}$.

Tests of open circuit characteristics at 382.5 hertz are presented in Figures 2-8 and 2-9. The maximum open circuit voltage at the nominal air gap was 86.4, within 1-1/2% of the constant volts-per-hertz relationship. This error is well within the limits of speed, field current and terminal voltage measurements. Magnetic losses at 75 A field were about 7000 watts, giving a relationship of $(speed)^{1.5}$ when compared to the 60 hertz measurements. The scatter in data observed in Figure 2-9 is the result of difficulty in stabilizing the dc motor speed at the weak field required to run this fast. This difficulty appears as an oscillation in shaft torque at this high speed, but its effects were limited to 2 or 3% of rated thrust, further reduced by attempting to take data in the center of the band of variation of shaft torque.

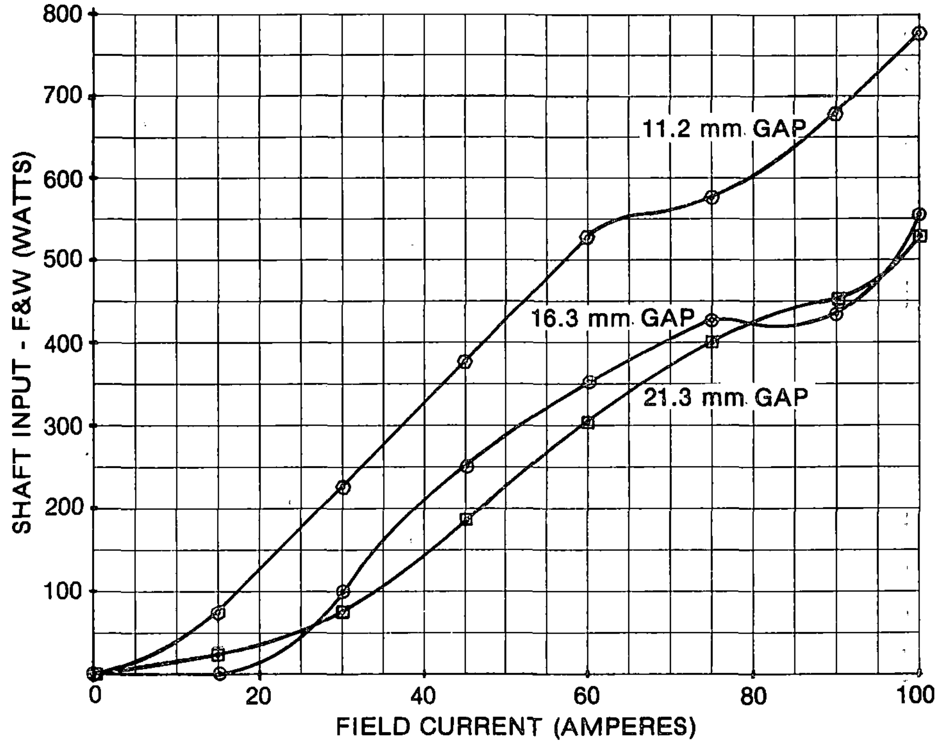

FIGURE 2-5. LSM LAMINATED TRACK MAGNETIC LOSS VS. FIELD CURRENT AND AIR GAP - 60 Hertz, 240 rpm; d = 11.2, 16.3, 21.3 mm.

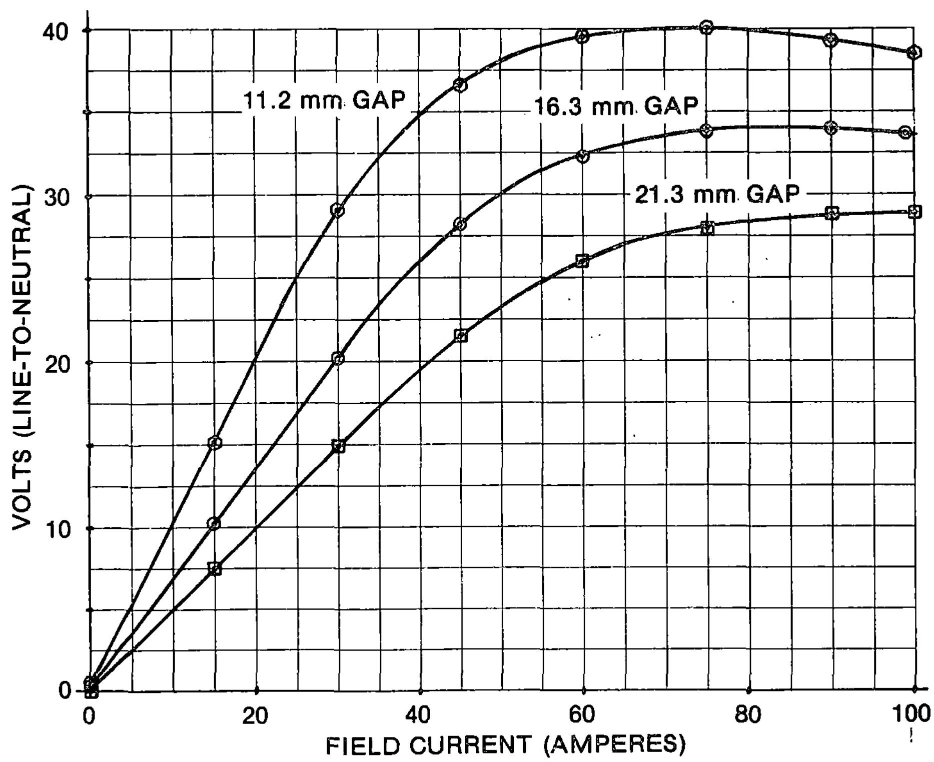

FIGURE 2-6. LSM LAMINATED TRACK OPEN CIRCUIT VOLTAGE VS. FIELD CURRENT AND AIR GAP - 150 Hertz, 600 rpm; d = 11.2, 16.3, 21.3 mm.

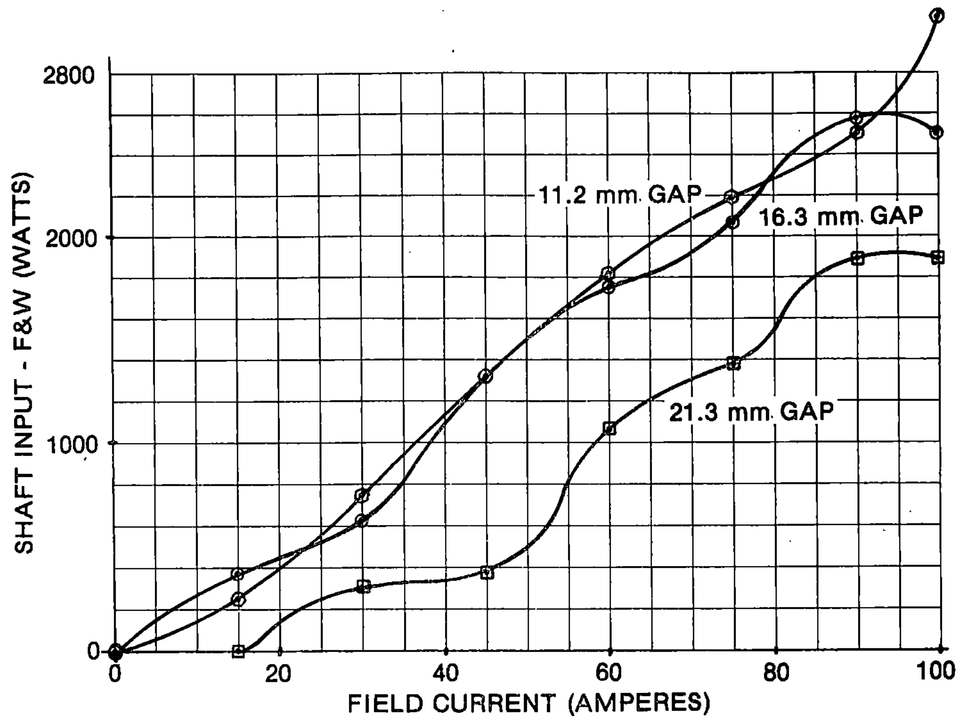

FIGURE 2-7. LSM LAMINATED TRACK MAGNETIC LOSSES VS. FIELD CURRENT AND AIR GAP - 150 Hertz, 600 rpm; d = 11.2, 16.3, 21.3 mm.

SHORT CIRCUIT CURRENT AND LOSSES

The terminals of the machine were shorted with a copper strap, and the dc machine used to spin the motor at 240 rpm. Field was applied, and the short circuit current and shaft input recorded. These are plotted in Figures 2-10 and 2-11 for the three air gaps tested. Note that the losses plotted have had friction and windage and stator I^2R subtracted, and so represent the stray loss. The cold (25^oC) resistance of the stator was measured at .0109 Ω per phase. By subtracting the approximate stator losses, assuming the windings to be cool, this stray loss plot was obtained. The short circuit current for a 75 A field and the nominal air gap is 305 A, and some 700 watts of stray loss are experienced. The waveform of the current is sinusoidal, as shown in Figure 2-12. The short circuit current varies in a manner similar to the open circuit voltage with changing air gap, while stray loss seems to be related to short circuit current regardless of air gap.

Figures 2-13 and 2-14 show the results of short circuit tests at 150 hertz. The current at 74 A field and nominal air gap was 329 A, 8% higher than the 60 hertz value. This variation is due to the presence of both resistance and inductance in the stator windings. As the frequency is increased, the ratio of inductive reactance to resistance increases, and the short circuit current increases slightly, assuming negligible change in resistance. The stray losses for the same nominal condition were 2000 watts.

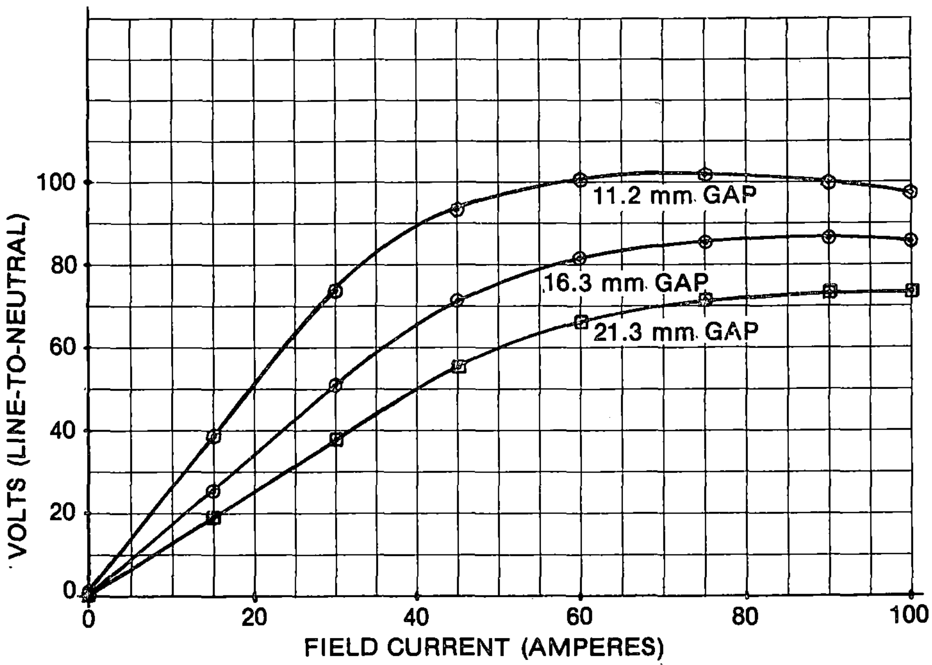

FIGURE 2-8. LSM LAMINATED TRACK OPEN CIRCUIT VOLTAGE VS. FIELD CURRENT AND AIR GAP - 382.5 Hertz, 1530 rpm; d = 11.2, 16.3, 2.13 mm.

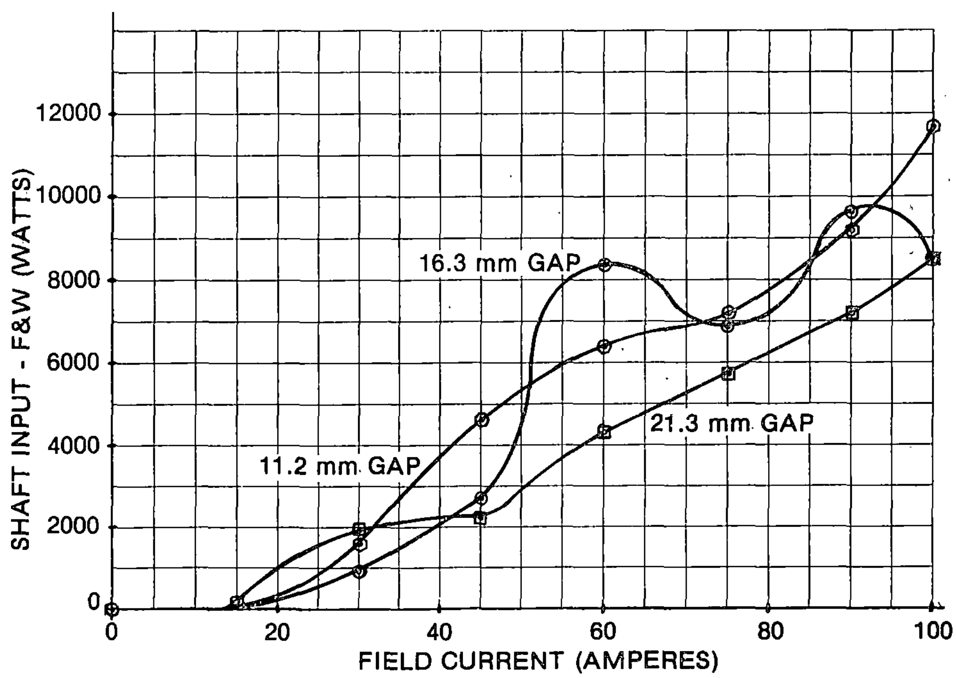

FIGURE 2-9. LSM LAMINATED TRACK MAGNETIC LOSSES VS. FIELD CURRENT AND AIR GAP - 382.5 Hertz, 1530 rpm; d = 11.2, 16.3, 21.3 mm.

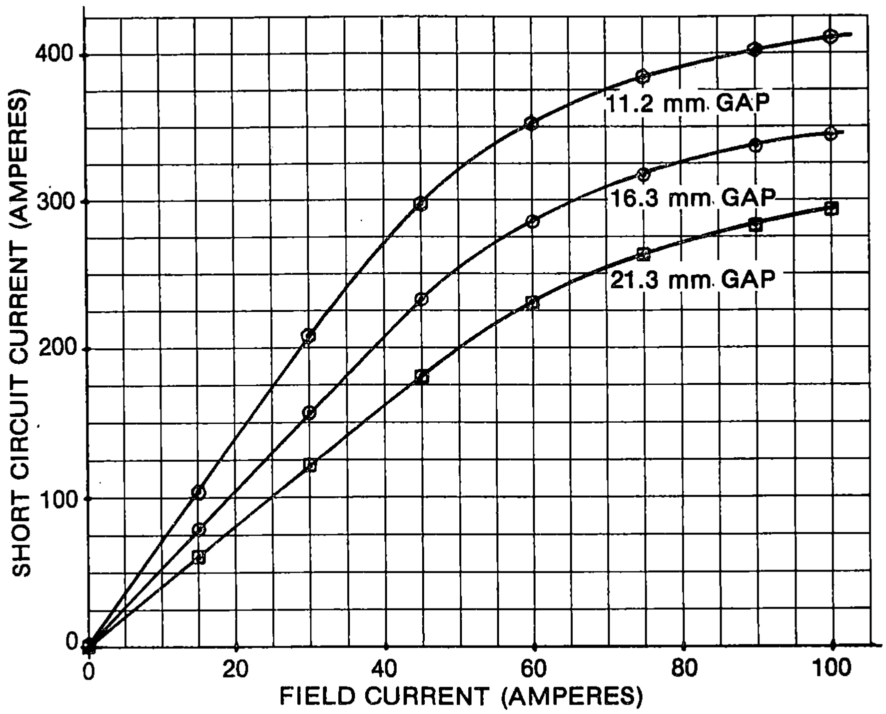

FIGURE 2-10. LSM LAMINATED TRACK SHORT CIRCUIT CURRENT VS. FIELD CURRENT AND AIR GAP - 60 Hertz, 240 rpm; d = 11.2, 16.3, 21.3 mm.

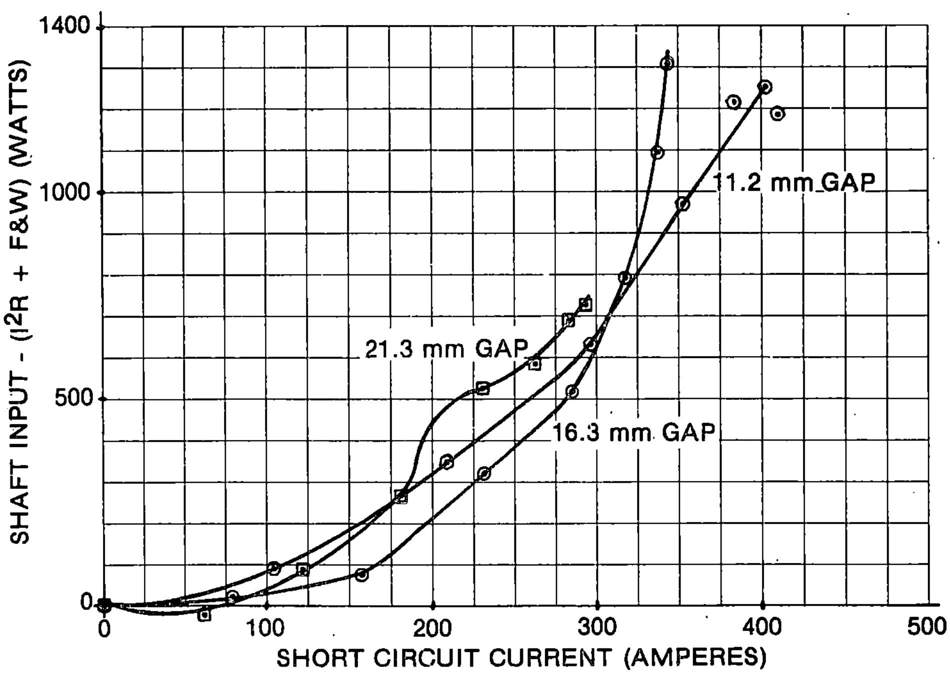

FIGURE 2-11. LSM LAMINATED TRACK STRAY LOSS VS. SHORT CIRCUIT CURRENT AND AIR GAP - 60 Hertz, 240 rpm; d = 11.2, 16.3, 21.3 mm.

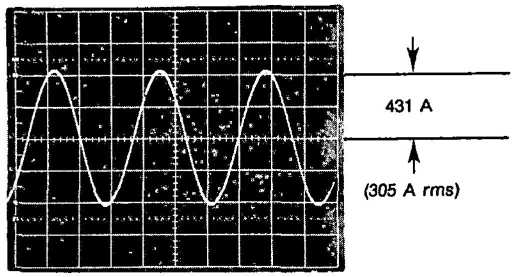

75 A Field

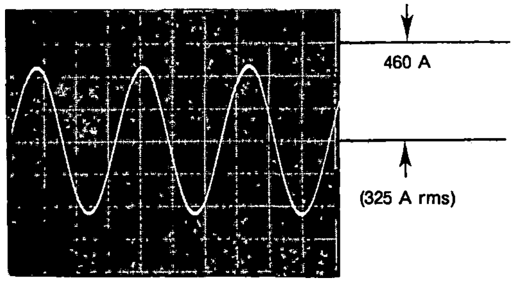

90 A Field

FIGURE 2-12. LSM - LAMINATED TRACK SHORT CIRCUIT CURRENT AT 240 rpm (17.4 m/sec).

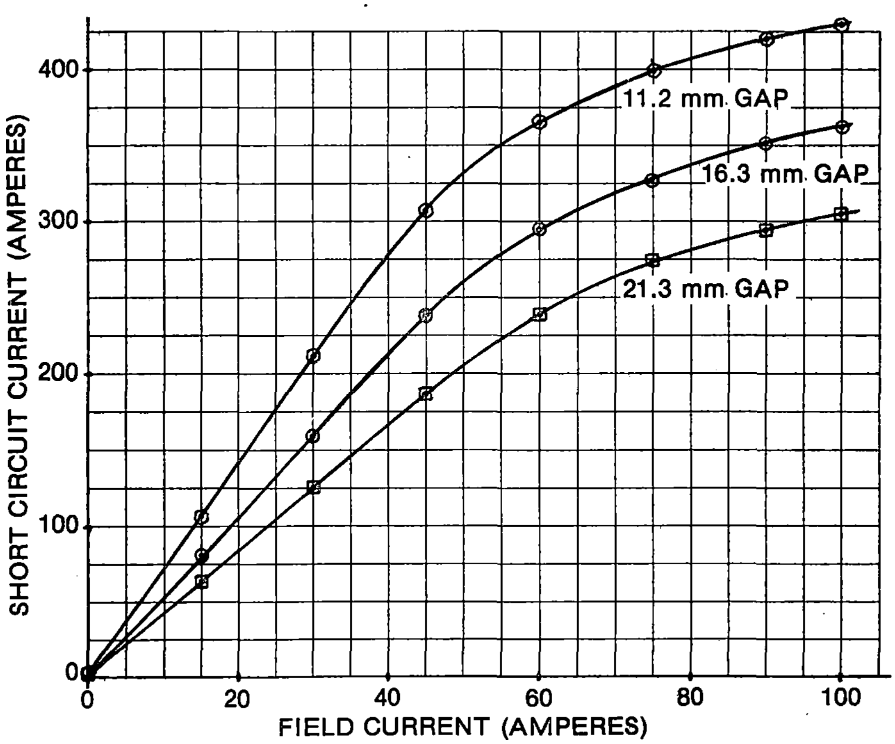

FIGURE 2-13. LSM LAMINATED TRACK SHORT CIRCUIT CURRENT VS. FIELD CURRENT AND AIR GAP - 150 Hertz, 600 rpm; d = 11.2, 16.3, 21 mm.

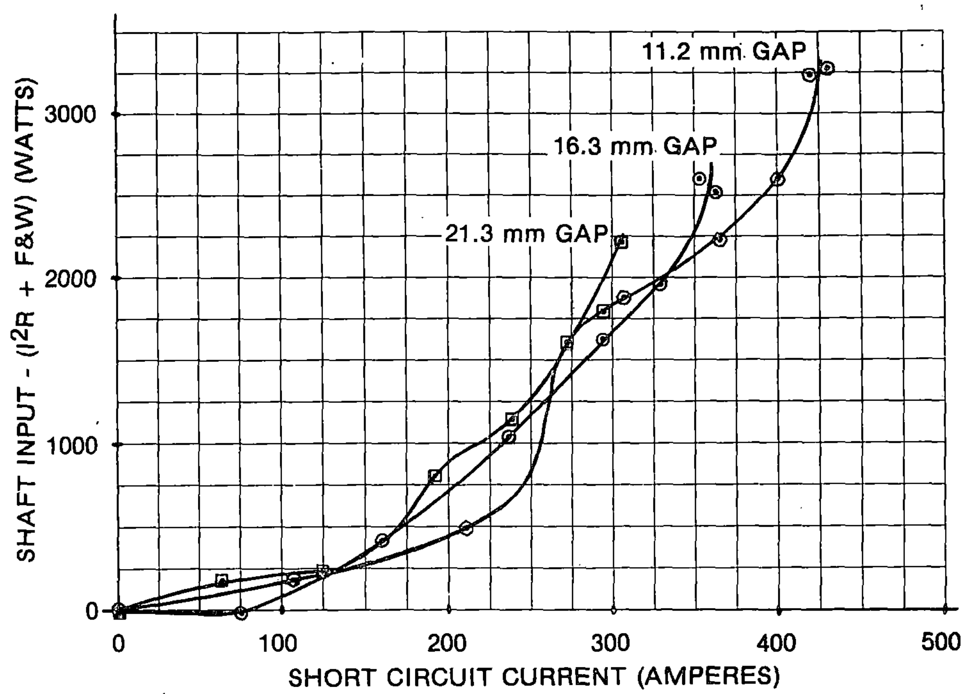

FIGURE 2-14. LSM LAMINATED TRACK STRAY LOSS VS. SHORT CIRCUIT CURRENT AND AIR GAP - 150 Hertz, 600 rpm; d = 11.2, 16.3, 21.3 mm.

When the speed was increased to 1530 rpm (382.5 hertz), the short circuit current increased only very slightly from the 150 hertz case. The 75 A, nominal gap value was 330 A, essentially the same as at 150 hertz. The stray losses at this current and speed are about 9000 watts, or about 8% of the machine rating. Figures 2-15 and 2-16 show these results. It should be remembered that all of these stray loss figures are based on a cool stator with its minimum I^2R loss, and may be higher than the actual stray loss. Runs were taken rapidly, using an initially cool machine, so that these assumptions should be fairly accurate.

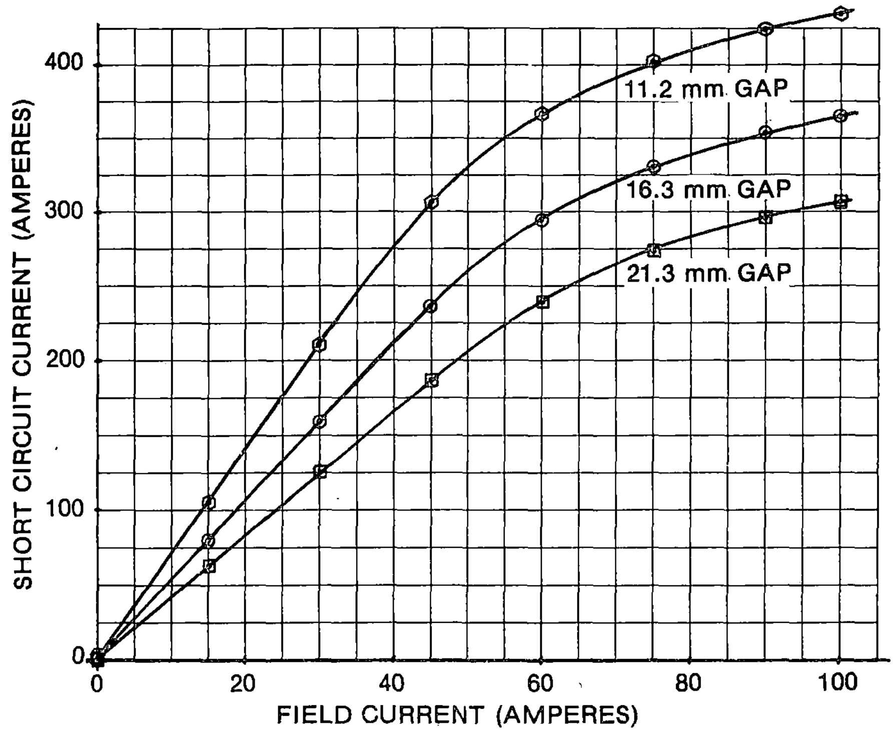

FIGURE 2-15. LSM LAMINATED TRACK SHORT CIRCUIT CURRENT VS. FIELD CURRENT AND AIR GAP - 382.5 Hertz, 1530 rpm; d = 11.2, 16.3, 21.3 mm.

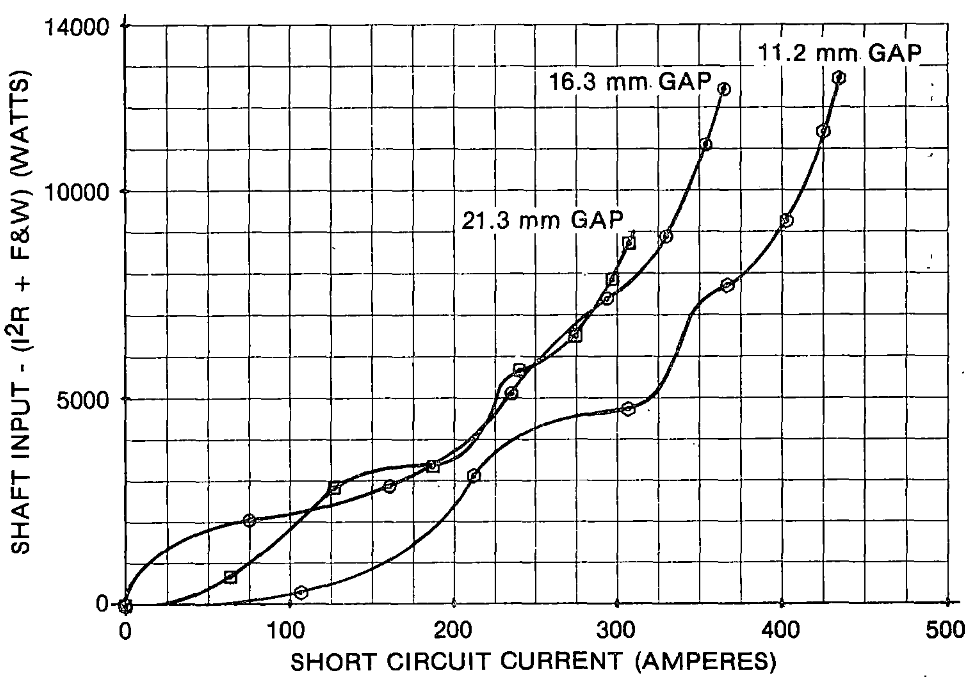

FIGURE 2-16. LSM LAMINATED TRACK STRAY LOSS VS. SHORT CIRCUIT CURRENT AND AIR GAP 382.5 Hertz, 1530 rpm; d = 11.2, 16.3, 21.3 mm.

Section 3

MACHINE PERFORMANCE UNDER LOAD

In this section the motoring and generating performance are described in detail, including thrust, normal force, efficiency and power factor information. The operation of the inverter control system is also described in so far as it affects the motor performance. All testing was performed with the dc load machine in a speed control loop and the LSM under current control.

MOTORING PERFORMANCE

After initial tests of the inverter, control, and LSM, an investigation of motor output versus inverter firing angle was undertaken. The control was adjusted so that the center of the 120° inverter firing pulse was from 0 to 64° ahead of the peak of the motor internal, or open circuit, voltage. This resulted in a set of firing pulses whose fundamental component varied from a 0 to 64° phase angle leading the internal voltage, which was the full range available from the control in the motoring mode. Figure 3-1 shows the thrust produced by the motor at 60 hertz with a 75 A field and rms stator currents from 100 to 500 A. These curves show a strong peak in thrust around 20 degrees of advance for currents of 400 to 500 A, and also indicate a current of about 470 A should produce the rated thrust of 1009 newtons at approximately this angle.

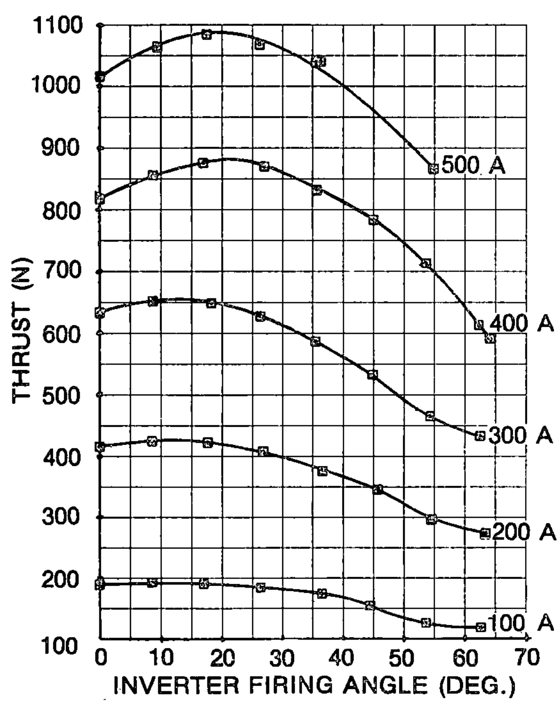

FIGURE 3-1. LSM LAMINATED TRACK THRUST VS. FIRING ANGLE - 100-500 rms Armature Amperes, 75 Amperes Field Current, 60 Hertz.

The inverter control circuitry was checked for drift, readjusted, and the curves of thrust versus firing angle with frequency as a parameter were obtained and are shown in Figure 3-2. The machine produced thrust exceeding the rated 1009 newtons for rms currents of 470 A at all three frequencies, corresponding to operation at 17.4, 43.5, and 111 meters per second. All subsequent tests reported here were performed with the inverter controls set for the maximum thrust per ampere as shown in Figure 3-2.

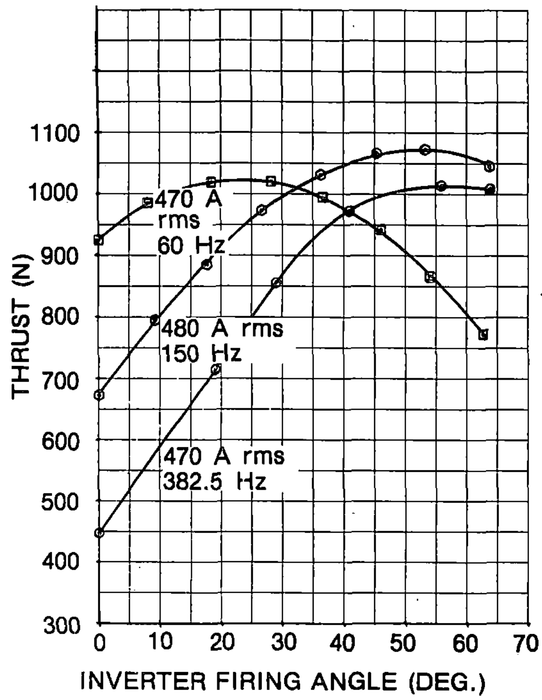

FIGURE 3-2. LSM LAMINATED TRACK THRUST VS. FIRING ANGLE - 75 Amperes Field Current; 60, 150, 382.5 Hertz.

The thrust produced by the machine as a function of stator current at 75 A field excitation and for the three testing frequencies is shown in Figure 3-3. As would be expected, thrust is a linear function of current within the measurement errors of the tests, and rated thrust is produced at 465 to 470 rms A for all three test frequencies. If the machine had significant end effects, the thrust for a given current would be expected to decrease at higher frequencies, but no such effect is observed in this laminated track machine. The thrust curve for full-speed operation deviates from the others at light loads, probably as a result of the difficulty of measuring thrust which is significantly less than the windage force encountered. Friction and windage at 1530 rpm amounted to about 310 newton meters of torque, or 447 newtons of thrust, nearly half of the machine rating.

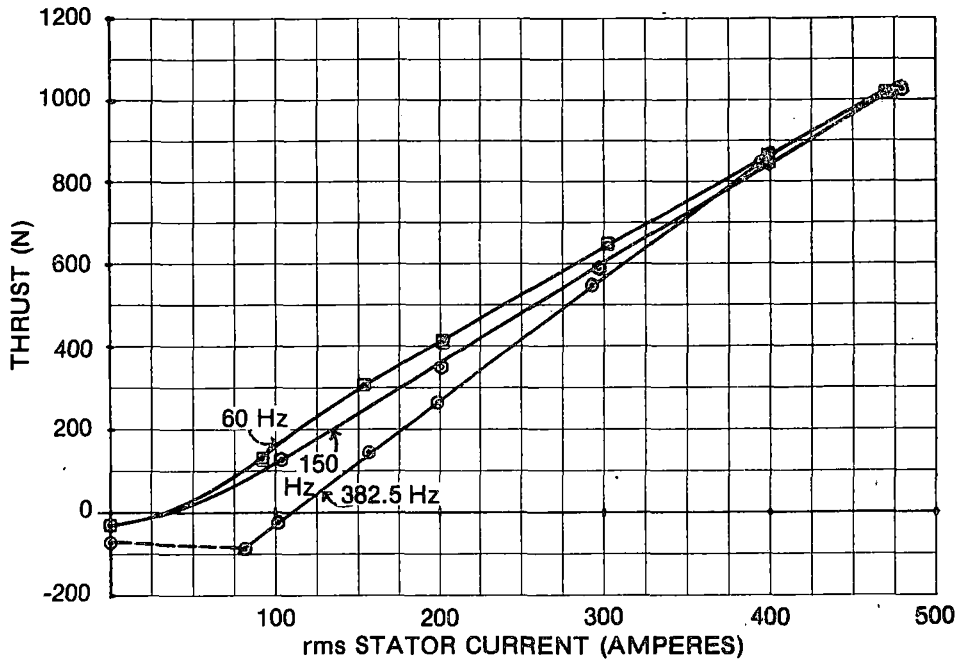

FIGURE 3-3. LSM LAMINATED TRACK THRUST VS. STATOR CURRENT - 75 Amperes Field Current; 60, 150, 382.5 Hertz.

The force of attraction between the stator and the track for a 75 A field was approximately 7000 newtons, or seven times rated thrust. The curves of Figure 3-4 show the effect of armature current on the normal force. The attraction increased at low currents, then decreased at higher currents as the angle and magnitude of armature reaction flux decreased the total air gap flux. It should be noted, however, that the effect of armature reaction is small compared to the total force.

Figures 3-5 and 3-6 show the same type of results for thrust and normal force at 40 A field excitation. The thrust produced at 470 A of stator current was 800 newtons, and the normal force was about 3500 newtons. The value of 40 A was chosen for field current as the upper end of the linear region of operation for the machine. In the <u>9th Quarterly Report</u>[1] it was noted that saturation appeared in the open circuit voltage of the machine for field currents exceeding 40 A.

Efficiency and power factor data as calculated using the data acquisition system information, are presented in Figures 3-7 and 3-8. Note that these are plotted against thrust, not current. The efficiency results are higher than expected, a result which also appeared in the induction motor tests. The problem appears to be in the watts calculation in the hardware of the data acquisition system. Several attacks were made on this, including calculation of input power by point-by-point analysis of voltage and current waveforms usng a digital processing oscilloscope (DPO), segregation of losses, and estimation of the input power from the inverter dc link power.

[1]SLEM Program, <u>9th Quarterly Report</u>, DOT-FR64147.

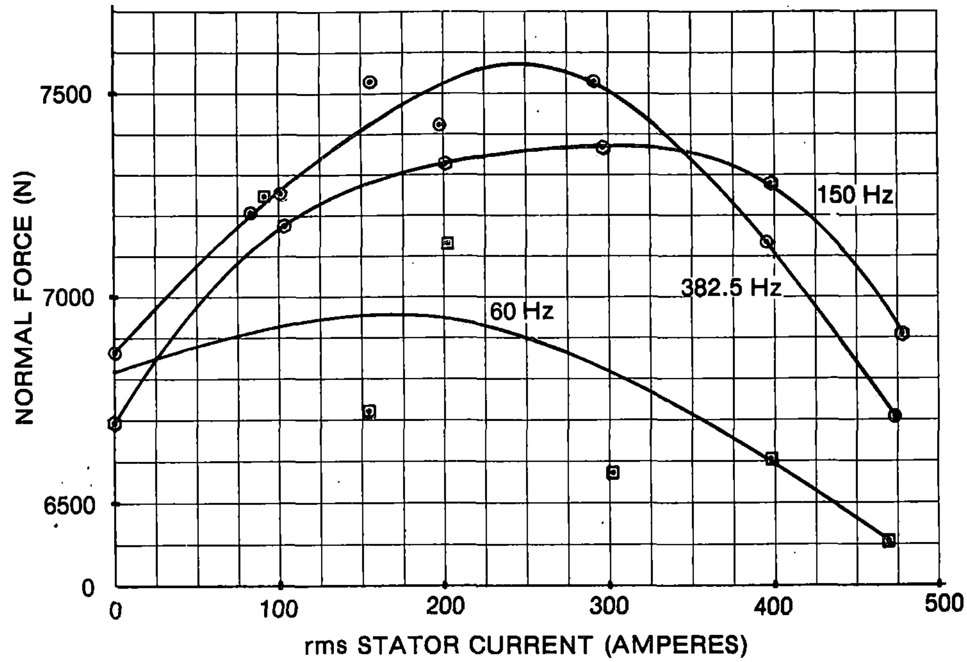

FIGURE 3-4. LSM LAMINATED TRACK NORMAL FORCE VS. STATOR CURRENT - 75 Amperes Field Current; 60, 150, 382.5 Hertz.

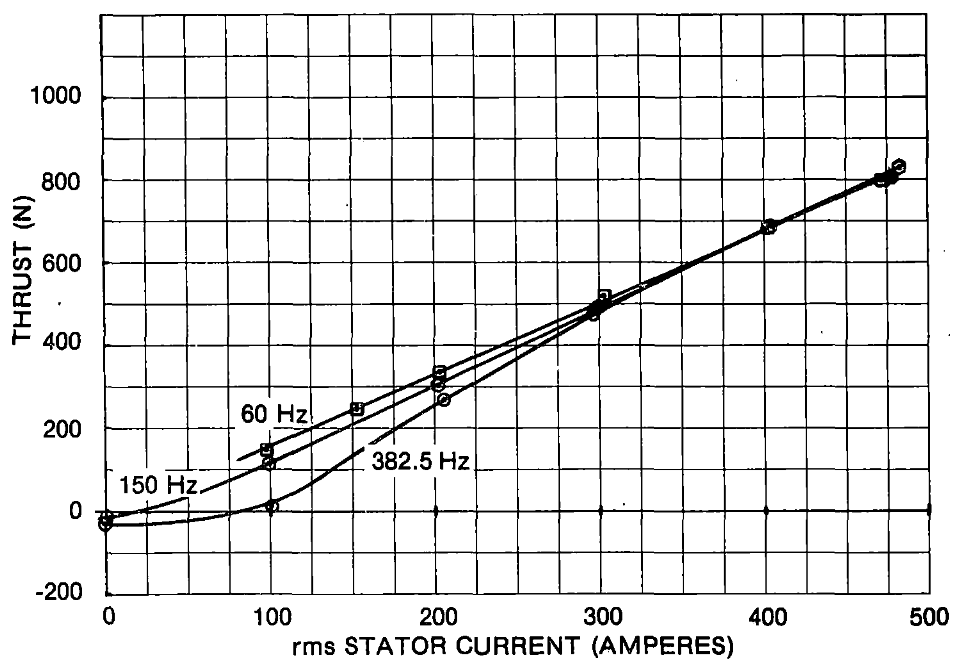

FIGURE 3-5. LSM LAMINATED TRACK THRUST VS. STATOR CURRENT - 40 Amperes Field Current; 60, 150, 382.5 Hertz.

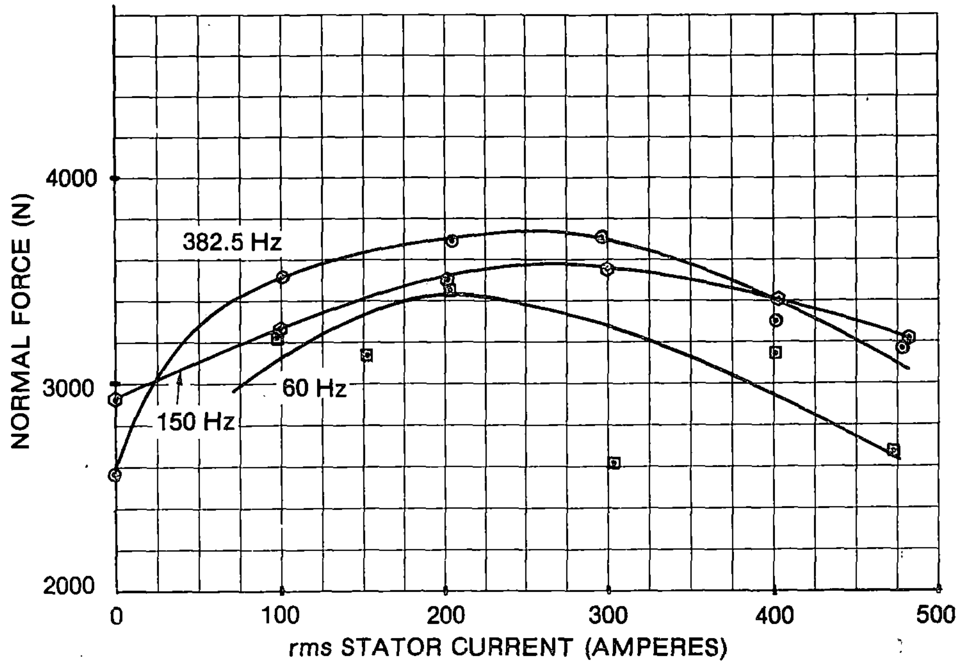

FIGURE 3-6. LSM LAMINATED TRACK NORMAL FORCE VS. STATOR CURRENT - 40 Amperes Field Current; 60, 150, 382.5 Hertz.

The machine was run at rated load and rated speed, and the waveforms of terminal voltage and phase current simultaneously recorded with the digital processing oscilloscope. Figure 3-9 shows the recorded voltage waveform, and Figure 3-10 shows the current waveform. The nature of the waveforms, a slight jitter from cycle to cycle, and the scanning rate resulted in some small jumps in the recorded traces. These did not appear to make significant differences in the resulting power calculations. The harmonic analysis of each waveform as calculated by the DPO is presented in Figures 3-11, 3-12 and 3-13, and the point-by-point calculation of power appears in Figure 3-14. The figure of 129.12 kW is based on the assumption of balanced three-phase conditions. Tests conducted on a phase-by-phase basis were used to produce an average power input figure to attempt to compensate for load oscillation and sampling rate limitations. The average power input over the three phases and several runs at the same load conditions was 136.9 kW, for an output of 111.0 kW, so that the calculated efficiency is 81%. This input is some 20% higher than the 114 kW indicated by the data acquisition system. The nature of the DPO sampling scheme is to broaden peaks and overemphasize the width of spikes, so that the 136.9 kW may be greater than the actual input. The results of other runs at 60 and 150 hertz showed the DPO to calculate inputs 7 and 12% higher, respectively, than the data acquisition system. These two methods of measurement, neither of them completely accurate, served to put a range on the electrical input and efficiency.

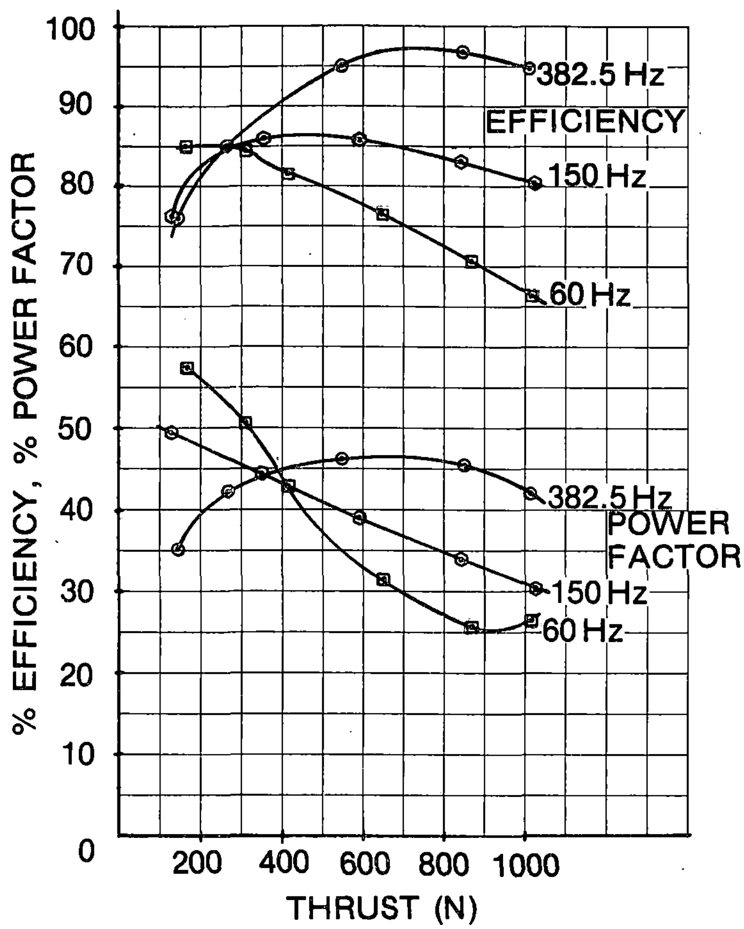

FIGURE 3-7. LSM LAMINATED TRACK EFFICIENCY AND POWER FACTOR VS. THRUST - 75 Ampere Field Current; 60, 150, 382.5 Hertz.

In an attempt to order the confusion concerning power measurement, a segregation of the losses for operation of the motor over the range of thrusts, frequencies, and field currents tested was undertaken. The magnetic loss for the field, the stator I^2R loss, adjusted for temperature of the windings, and the mechanical output were summed. This was subtracted from the electrical input provided by the data acquistion system and found to produce a negative stray loss figure. The input was increased by some percentage, and the difference taken again. The most satisfactory stray loss figures, compared to those obtained with the machine short circuited, were then used to select the most suitable percentage to add to the data acquisition system input. The results of this calculation for low-speed operation, 60 hertz, with a 40 A and a 75 A field current are shown in Table 3-1. The electrical input was increased by 4% to obtain the most reasonable distribution of losses for the range of test points taken. This same procedure was performed on 150 hertz and 382.5 hertz data, with results as tabulated in the remainder of Table 3-1.

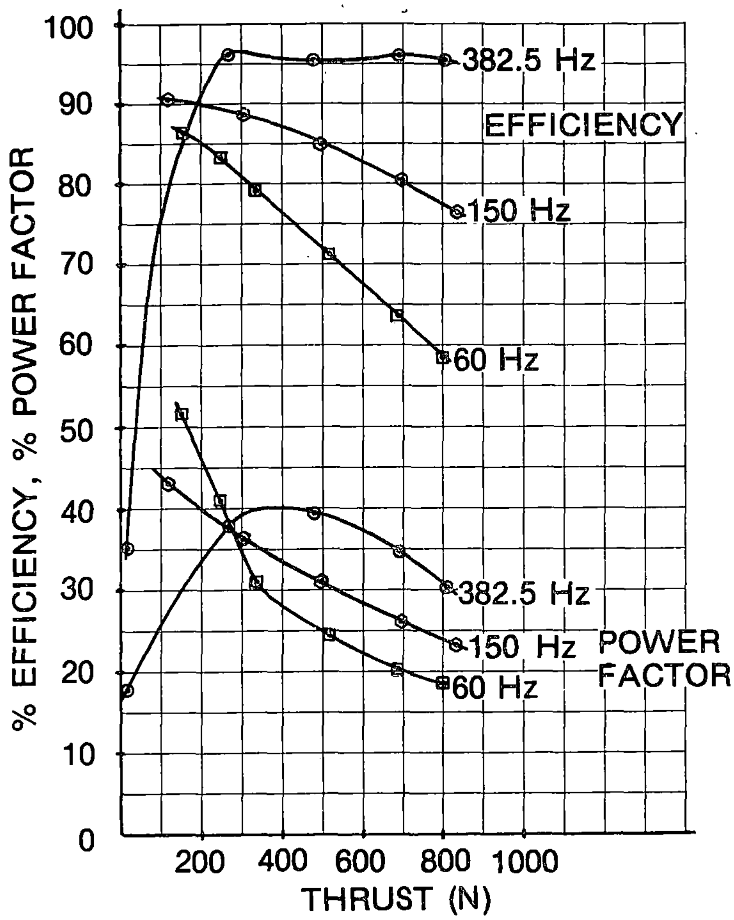

FIGURE 3-8. LSM LAMINATED TRACK EFFICIENCY AND POWER FACTOR VS. THRUST - 40 Ampere Field Current; 60, 150, 382.5 Hertz.

Table 3-2 summarizes the efficiency, power factor and displacement factor data obtained by the various methods discussed above, as well as the efficiency calculated for the combined inverter and motor. This figure was obtained from the average power in the dc link, as measured by the data acquistion system. Comparison of the combined efficiency figure to the motor efficiency shows the inverter efficiency to be approximately 79% for the 40 A field runs and 81% for the 75 A field runs. The column headed "Displacement Factor" gives the cosine of the angle between the fundamental components of voltage and current as calculated by the DPO.

COMMUTATION DELAY

In Figures 3-1 and 3-2, machine motoring performance was plotted as a function of inverter firing angle. If there were no commutation delay in the operation of the inverter, this angle would be the electrical angle by which the phase current leads the machine's internal voltage. Investigation of the performance of the inverter,

Table 3-1

LSM LAMINATED TRACK PERFORMANCE ADJUSTMENT

60 Hertz, 240 rpm

	Run No.	Armature Amperes	Armature Volts	Input kW	Output kW	Magnetic Loss	Stator I^2R	Stray Loss	Efficiency Estimates %	Power Factor %
40 Ampere Field (Input Adjusted by +4%)	147	97.8	20.12	3.17	2.63	0.2	0.3	0.04	83.0	53.7
	148	152.2	27.65	5.38	4.34	0.2	0.8	0.04	80.7	42.6
	149	201.7	39.60	7.68	5.88	0.2	1.4	0.20	76.6	32.1
	150	302.6	56.40	13.18	9.07	0.2	3.3	0.61	68.8	38.0
	151	401.2	77.15	19.44	11.91	0.2	6.0	1.33	61.3	20.9
	152	472.4	89.84	24.59	13.95	0.2	9.5	0.94	56.7 (52.5 with 2 kW Field Loss)	19.3
75 Ampere Field (Input Adjusted by +4%)	141	91.3	21.3	3.47	2.86	0.45	0.3	-0.14	82.4	59.5
	142	153.5	27.3	6.61	5.40	0.45	0.8	-0.04	81.7	52.6
	143	201.4	33.86	9.16	7.21	0.45	1.4	+0.10	78.7	44.8
	144	302.0	51.40	15.28	11.31	0.45	3.3	+0.22	74.0	32.8
	145	399.1	69.30	22.15	15.08	0.45	6.0	+0.62	68.1	26.7
	146	469.6	71.67	27.71	17.72	0.45	9.5	+0.04	63.9 (49.6 with 8 kW Field Loss)	27.4

150 Hertz, 600 rpm

	Run No.	Armature Amperes	Armature Volts	Input kW	Output kW	Magnetic Loss	Stator I^2R	Stray Loss	Efficiency Estimates %	Power Factor %
40 Ampere Field (Input Adjusted by +6%)	345	99.7	44.6	6.08	5.26	1.0	0.3	-0.48	86.5	45.5
	346	202.0	67.62	15.77	13.25	1.0	1.4	0.05	84.4	38.5
	347	299.1	90.84	26.90	21.61	1.0	3.2	1.09	80.3	33.0
	348	402.9	118.9	39.82	30.28	1.0	6.0	2.54	76.0	27.7
	349	482.5	141.1	50.17	36.38	1.0	9.5	3.29	72.5	24.6
	350	0	0	0	(-0.52)	1.0	0	0	(69.7 with 2 kW Field Loss)	
75 Ampere Field (Input Adjusted by +6%)	338	0	0	0	-0.36	0	0	+0.36	0	0
	339	0	34.75	0	-1.40	2.0	0	-0.60		
	340	103.0	48.76	7.88	5.71	2.0	0.4	-0.23	73.2	52.2
	341	200.6	66.62	18.86	15.32	2.0	1.4	+0.14	81.2	47.0
	342	297.3	86.10	31.70	25.70	2.0	3.2	+0.80	81.1	41.3
	343	398.8	108.40	46.74	36.70	2.0	5.9	2.14	78.5	36.0
	344	479.1	127.50	58.99	44.74	2.0	9.5	2.75	75.8 (66.8 with 8 kW Field Loss)	32.2

382.5 Hertz, 1530 rpm

	Run No.	Armature Amperes	Armature Volts	Input kW	Output kW	Magnetic Loss	Stator I^2R	Stray Loss	Efficiency Estimates %	Power Factor %
40 Ampere Field (Input Adjusted by +12%)	632	0	0	0	0	0	0	0	-	-
	633	0		0	-3.0	3.0	0	0	-	-
	634	100.4	100.9	6.1	1.9	3.0	0.4	0.8	31.1	20.0
	635	205.5	133.0	34.9	30.0	3.0	1.5	0.4	86.0	42.5
	636	296.4	159.8	62.5	53.2	3.0	3.5	2.8	85.1	44.0
	637	401.2	190.5	89.5	76.8	3.0	6.7	3.0	85.8	39.0
	638	478.1	215.9	105.2	89.6	3.0	10.0	2.6	85.2 (83.5 with 2 kW Field Loss)	34.0
75 Ampere Field (Input Adjusted by +12%)	623	0		0	0	0	0	0	0	0
	624	0		0	-8.0	8.0	0	0	0	0
	625	82.0	108.8	1.6	-9.1	8.0	0.2	2.5	-	6.0
	626	100.8	114.8	3.9	-2.4	8.0	0.3	2.0	-	11.2
	627	155.4	127.7	23.4	15.9	8.0	0.8	-1.3	67.9	39.3
	628	198.6	137.8	38.8	29.5	8.0	1.3	0	76.0	47.3
	629	292.5	158.9	72.0	61.1	8.0	2.8	0.1	84.9	51.6
	630	394.8	180.4	109.0	94.3	8.0	6.1	0.6	86.5	51.0
	631	473.9	198.8	133.2	112.7	8.0	9.9	2.6	84.6 (79.8 with 8 kW Field Loss)	47.1

Table 3-2

LSM LAMINATED TRACK PERFORMANCE ADJUSTMENTS

		Data Acquisition System		Digital Processing Scope			Adjusted Segregated Losses			
	Frequency	Efficiency (%)	Power Factor (%)	Efficiency (%)	Power Factor (%)	Displacement Factor (%)	Efficiency (%)	Power Factor (%)	Efficiency of Inverter & Motor (%)	Efficiency Including Field Losses (%)
40 Ampere Field - Approx. 800 N Thrust, 480 Armature Amperes	60 Hz	58.8	18.5	-	-	-	56.7	19.3	43.8	52.5
	150 Hz	76.6	23.4	-	-	-	72.5	24.6	57.9	69.7
	382.5 Hz	95.5	30.2	-	-	-	85.2	34.0	66.4	83.5
70 Amperes Field - Approx. 1000 N Thrust, 480 Armature Amperes	60 Hz	66.6	26.5	65.0	28.5	68.8	63.9	27.4	51.3	49.6
	150 Hz	81.1	30.5	72.5	33.0	65.0	75.8	32.2	62.3	66.8
	382.5 Hz	95.0	42.0	81.5	43.2	58.0	84.6	47.1	69.7	79.8

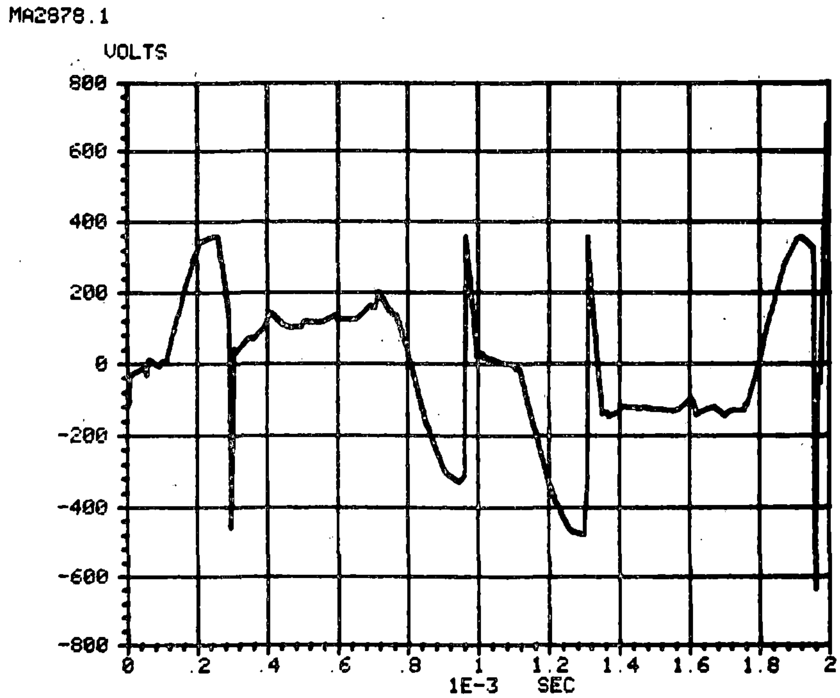

FIGURE 3-9. LSM LAMINATED TRACK LINE-TO-NEUTRAL VOLTS - Rated Load, 382.5 Hertz.

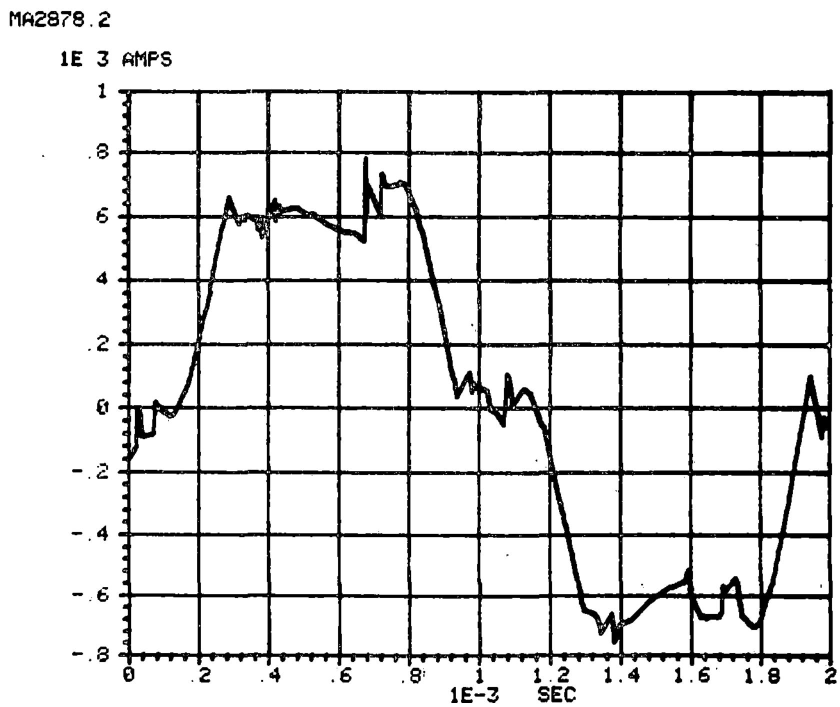

FIGURE 3-10. LSM LAMINATED TRACK PHASE CURRENT - Rated Load, 382.5 Hertz.

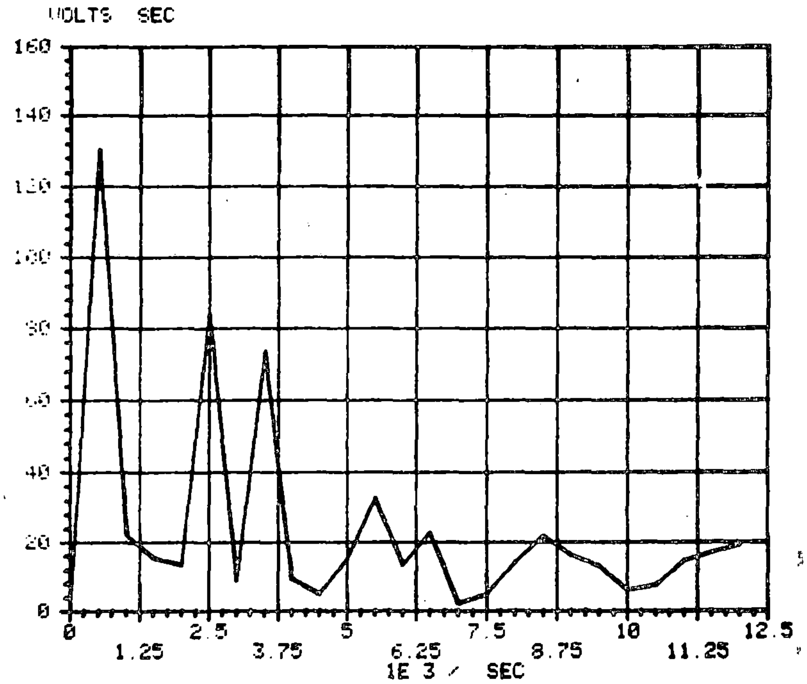

FIGURE 3-11. LSM LAMINATED TRACK LINE-TO-NEUTRAL VOLTS - Rated Load, 382.5 Hertz.

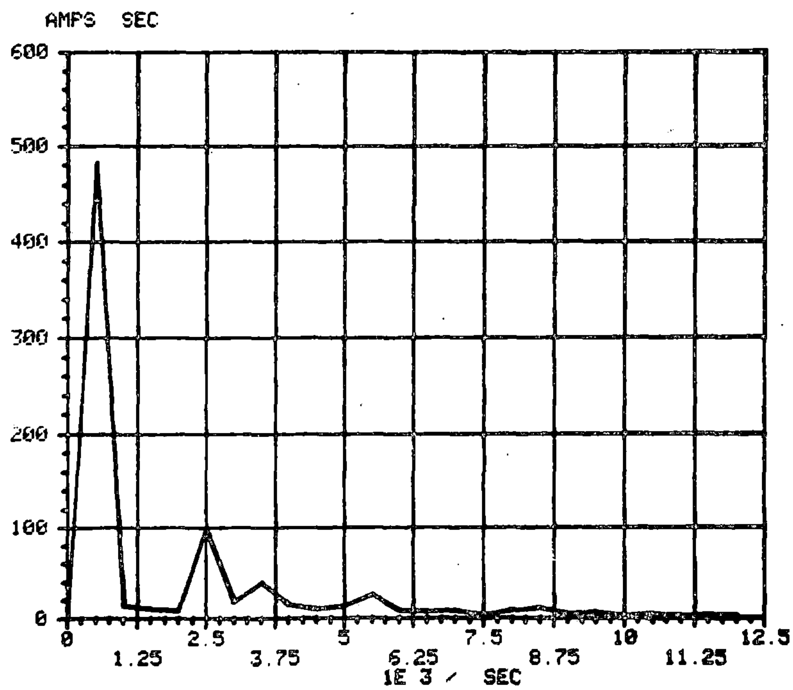

FIGURE 3-12. LSM LAMINATED TRACK PHASE CURRENT - Rated Load, 382.5 Hertz.

```
FILE NAME        MA2878.1
WAVEFORM         A
SCALE FACTOR=    100
UNITS            VOLTS
HARMONIC       AMPLITUDE(RMS)     PHASE(DEGREES)
 1                130.325         -50.8652
 3                15.3233          21.9967
 5                84.1344          124.854
 7                73.574           112.947
 9                4.57557          7.04387
 11               32.4388         -118.746
 13               22.7228          174.508
RMS VALUE         202.451
ANOTHER WAVEFORM  ENTER 1?

FILE NAME        MA2878.2
WAVEFORM         B
SCALE FACTOR=    2020.2
UNITS            AMPS
HARMONIC       AMPLITUDE(RMS)     PHASE(DEGREES)
 1                482.734         -101.012
 3                9.96369          179.086
 5                99.3791          42.8566
 7                38.5738          42.3529
 9                10.1018          166.835
 11               25.3393          171.454
 13               6.59775          176.909
RMS VALUE         497.038
```

FIGURE 3-13. LSM LAMINATED TRACK VOLTAGE AND CURRENT HARMONICS - Rated Load, 382.5 Hertz.

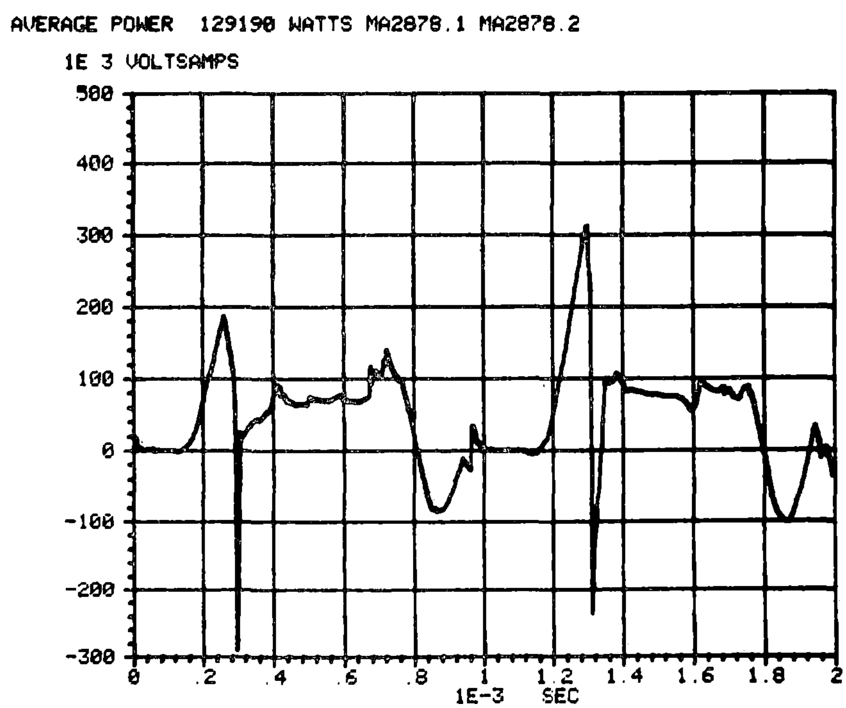

FIGURE 3-14. LSM LAMINATED TRACK WATTS INPUT - Rated Load, 382.5 Hertz.

however, shows that a significant commutation delay exists. Oscilloscope photographs of the firing pulses and the corresponding current waveforms were taken, and the delay angle measured, as shown in Figure 3-15. This angle varies with speed and with the amplitude of the current. To obtain meaningful data on the angular relationships in the various test runs, a correction curve must be made.

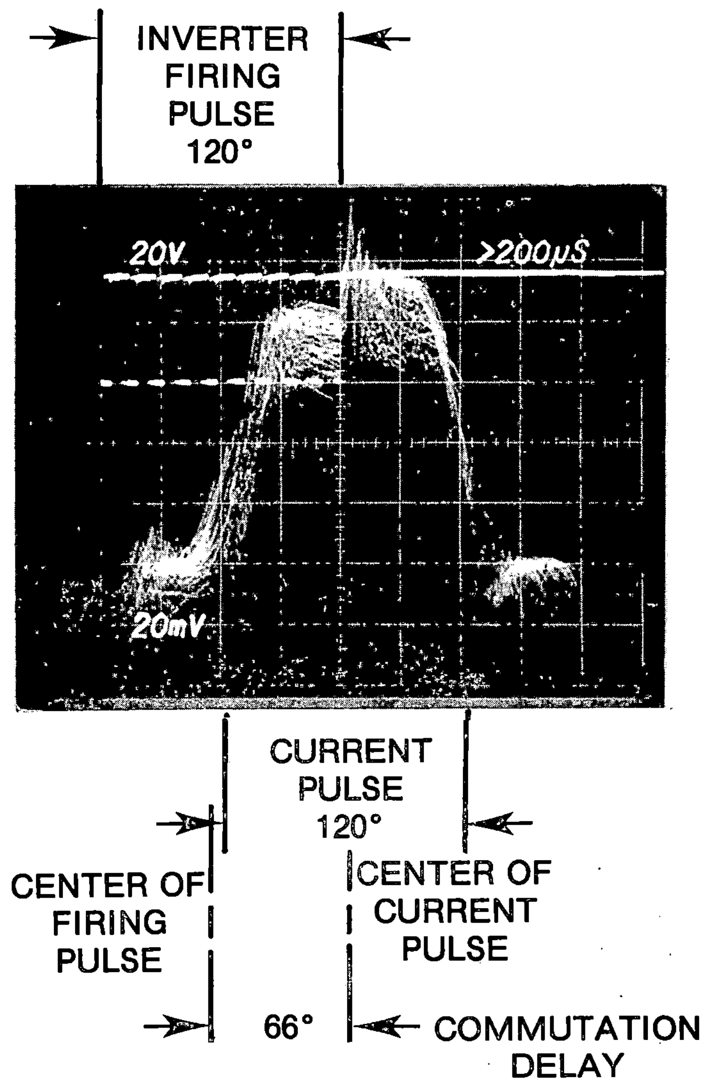

FIGURE 3-15. LSM LAMINATED TRACK COMMUTATION DELAY - 382.5 Hertz, 125 Ampere rms Stator Current.

Figure 3-16 shows examples of the way the inverter delay angle enters the machine performance in both motoring and generating. In motoring, the delay causes the angle of advance of current to be decreased. The angle printed on the output from the data

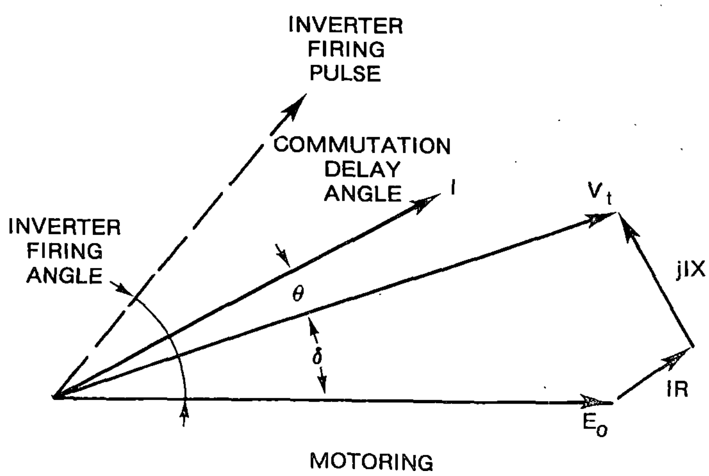

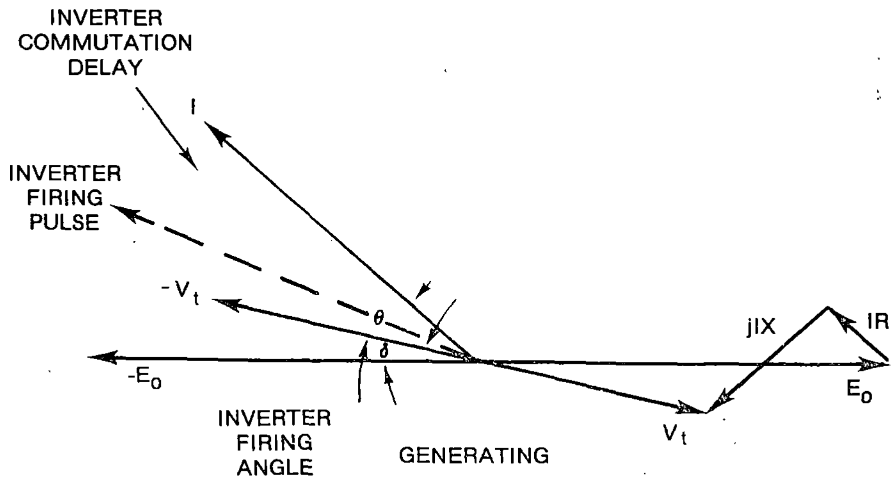

FIGURE 3-16. LSM LAMINATED TRACK VOLTAGE CURRENT RELATIONSHIPS WITH INVERTER DELAY.

acquisition system is larger than the actual angle of advance of current ahead of internal voltage. Compensation within the control involving both the frequency and the magnitude of current would be required to correct this, with more advance at high speed and low current. In generating, the delay increases the angle between the current and the reflection of the internal voltage. The nature of the control is such as to define the firing and delay angles, as shown in these two diagrams, and one can easily see the kind of correction required to compensate for these effects.

The top three lines in Figure 3-17 are the firing angles for various currents at the three test frequencies. These relationships were set up to give optimum thrust per ampere at 470 A rms stator current. These are the values printed out and called "DELTA ANGLE" on the data runs. The three curves on the lower half of figure are the commutation delay angles for each speed, and were taken from test points, as shown in Figure 3-15.

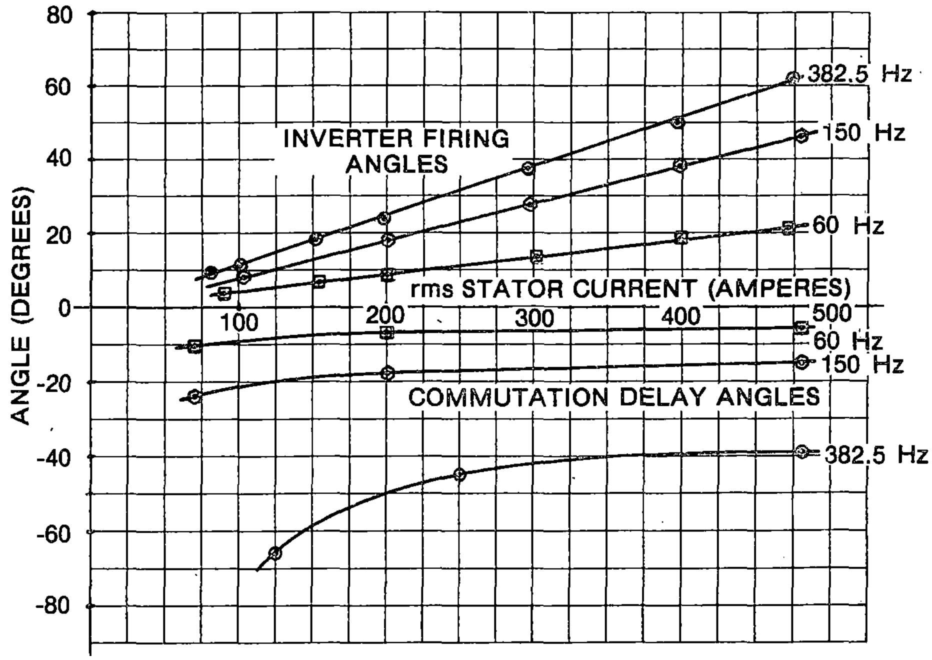

FIGURE 3-17. LSM LAMINATED TRACK INVERTER FIRING ANGLE AND COMMUTATION DELAY ANGLE VS. STATOR CURRENT - 60, 150, 382.5 Hertz.

Figure 3-18 illustrates the calculated angle ($\delta + \theta$) between current and internal voltage for the three frequencies under motoring conditions. The negative angles observed below 200 to 300 A armature current indicate operation that is not optimum for the amplitude of current, and may help to explain the variation in thrust curves at low current, as seen in Figures 3-3 and 3-5. The operation of the machine was optimized around rated thrust and appeared to suffer at reduced loads. Figure 3-19 shows the calculated angle for generating conditions. The angle at 60 hertz is reasonable, while at 150 hertz, it is becoming too large. At 382.5 hertz, the angle between current and internal voltage is sufficiently large to make operation as a generator questionable. The angle relationships for the generating region, derived from those producing the optimum motoring performance, are far from the optimum generating conditions. No attempt was made to adjust the control to optimum conditions for generating.

GENERATING TESTS

As explained previously, tests of the LSM in the generating region were limited, as the control was optimized for motoring. The generating tests at 60 hertz, presented in Figure 3-20, show a nearly linear increase of mechanical input with increasing current, but an electrical output that initially increased, then decreased toward zero. The control strategy, with a forced current amplitude and a forced angular relation between current and internal voltage, produced this rather unusual characteristic.

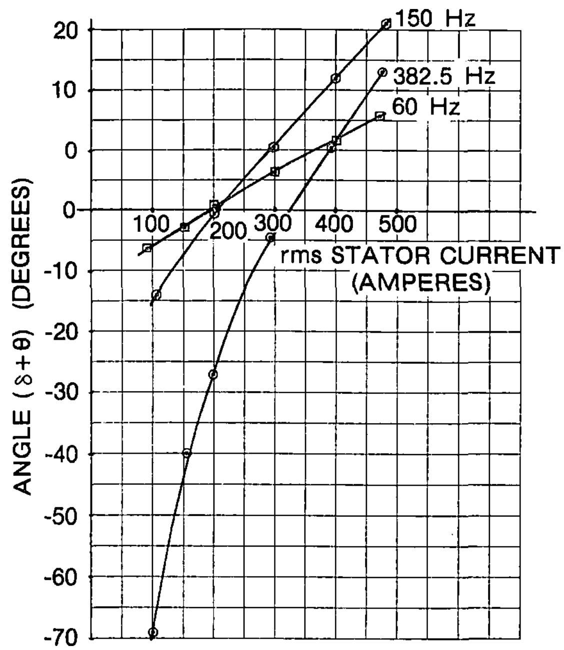

FIGURE 3-18. LSM LAMINATED TRACK MACHINE ANGLE (δ+θ) VS. rms STATOR CURRENT - 60, 150, 382.5 Hertz Motoring.

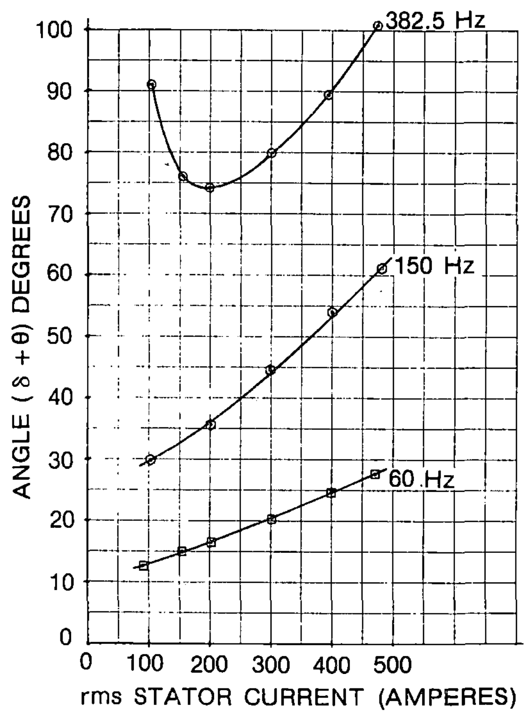

FIGURE 3-19. LSM LAMINATED TRACK MACHINE ANGLE (δ+θ) VS. rms STATOR CURRENT - 60, 150, 382.5 Hertz Generating.

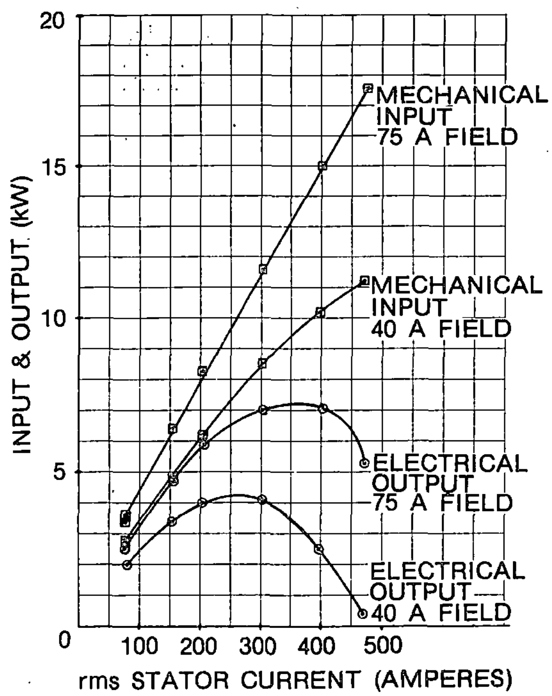

FIGURE 3-20. LSM LAMINATED TRACK GENERATING INPUT AND OUTPUT VS. STATOR CURRENT - 60 Hertz, 40 and 75 Ampere Fields.

At 150 hertz, the situation with angle control was more critical, and electrical output was actually driven negative. The machine entered a braking region, as shown in Figure 3-21, and increased current resulted in increased electrical input combined with decreased mechanical input. Motoring conditions were not achieved, but generating, then braking performance, were both degraded by increasing current.

At rated speed and frequency, 382.5 hertz, the inverter could not be made to commutate properly in the generating mode, and no data was obtained. Again it must be noted that the control was not adjusted for generating.

The curves of Figures 3-22 show the variation of normal force with current. Apparently, there is some random variation from point to point in the data, but the effect of armature reaction is obvious and much stronger here than in the motoring case. Forcing the machine in the manner of this control scheme significantly impairs its performance in the generating region, evidenced by the appreciable reduction in normal force, hence in air gap flux.

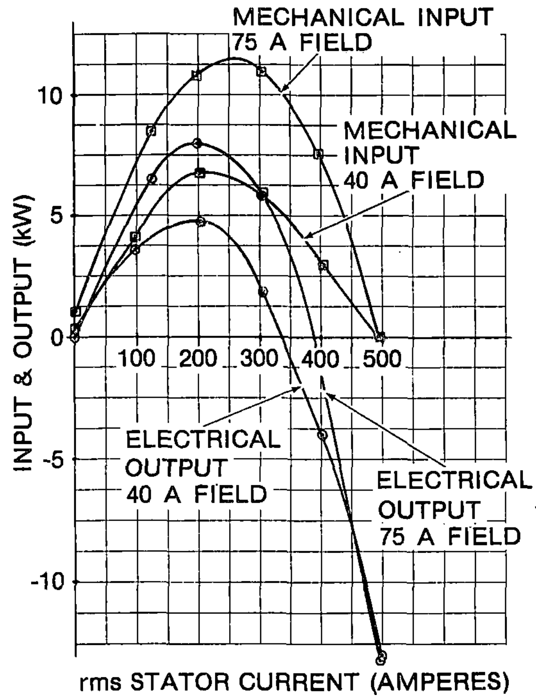

FIGURE 3-21. LSM LAMINATED TRACK GENERATING INPUT AND OUTPUT VS. STATOR CURRENT - 150 Hertz, 40 and 75 Ampere Fields.

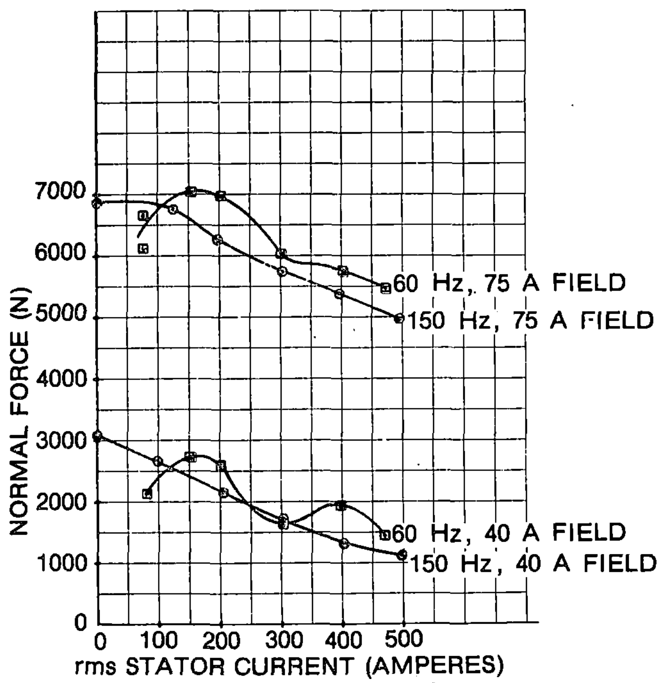

FIGURE 3-22. LSM LAMINATED TRACK NORMAL FORCE VS. STATOR CURRENT GENERATING - 60 and 150 Hertz; 40 and 75 Ampere Fields.

Section 4

G-TABLE TESTS

Tests of the Laminated Track Linear Synchronous Motor were made at 60, 150, and 382.5 hertz with 75 A field current and armature currents that produced approximately 10%, 40%, and 100% of rated thrust. The insensitivity of the motor's performance to speed and frequency, as mentioned in the motoring test section, appears again since data from the three frequencies are in very close agreement. High speed (382.5 hertz) data are not clear at low-thrust levels, due to the controls and to the large friction and windage of the "track" wheel. The conventions for displacements of the stator were the same as for the induction motor (see Figure 4-1).

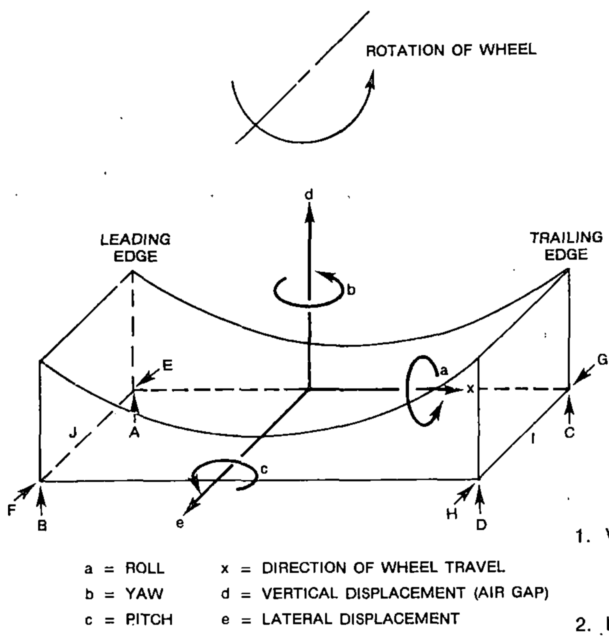

"G - Table" Paramters Tested

1. Vertical: (nominal d = 18.2 mm)
   d' = 13.1 mm (d-5.1 mm)
   d'' = 23.3 mm (d+5.1 mm)
2. Lateral: e' = 12.5 mm
   e'' = 25 mm
3. Roll: a' (.00148 rad)
   2.1 mm tilt between rails
   1/4 mm tilt across width of stator

   a'' (.00296 rad)
   4.2 mm tilt between rails
   1/2 mm tilt across width of stator
4. Yaw: b' (.0224 rad)
   ±12.5 mm across length of machine (total 25 mm)

   b'' (.0448 rad)
   ± mm across length of machine (total 50 mm)
5. Pitch: c' (+.00456 rad)
   +5 mm across length of machine
   largest gap at leading end

   c'' (-.00456 rad)
   -5 mm across length of machine
   largest gap at trailing end

FIGURE 4-1. DEFINITIONS OF DIRECTIONS FOR "G-MATRIX" TESTS.

VARIATION OF AIR GAP

Figures 4-2, 4-3 and 4-4 present the thrust obtained for air gaps of d = 11.2, 16.3 and 21.3 mm at 60, 150, and 382.5 hertz, respectively. As expected, the thrust per ampere is increased for the reduced gap, decreased for the increased gap. The increase and decrease in thrust amount to about 17% for a 30% change in air gap. In all cases, the thrust varies linearly with current.

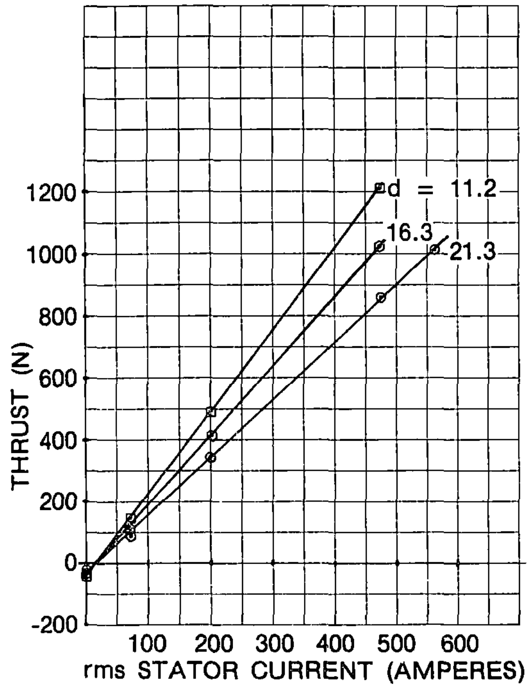

FIGURE 4-2. LSM THRUST VS. STATOR CURRENT - d = 11.2, 16.3, 21.3 mm; 75 Ampere Field Current, 60 Hertz.

Figure 4-5 summarizes the normal force data for the runs at three different gaps and the three speeds. Again there is no significant variation with speed, and the force varies inversely with the air gap. From the average force of 7500 newtons at the nominal gap, the force increases to about 9250 newtons at the reduced, 11.2 mm gap, and diminishes to about 5750 newtons at the increased, 21.3 mm gap.

Figures 4-6, 4-7, and 4-8 show the pitch torque recorded at the three gaps. The data have a good deal of scatter, but there is a general trend to a greater pitch torque for reduced air gap under load. The calculation of pitch torque from the force sensors includes a positive component due to thrust. This is due to the manner in which the stator is constrained.

Efficiency and power factor for the three air gaps at the three test frequencies are shown in Figures 4-9, 4-10, and 4-11. As expected, both efficiency and power factors improve with the

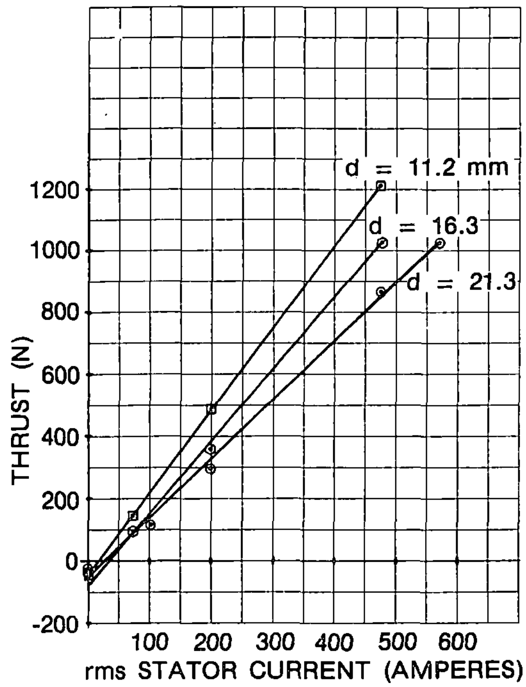

FIGURE 4-3. LSM THRUST VS. STATOR CURRENT - d = 11.2, 16.3, 21.3 mm; 75 Ampere Field Current, 150 Hertz.

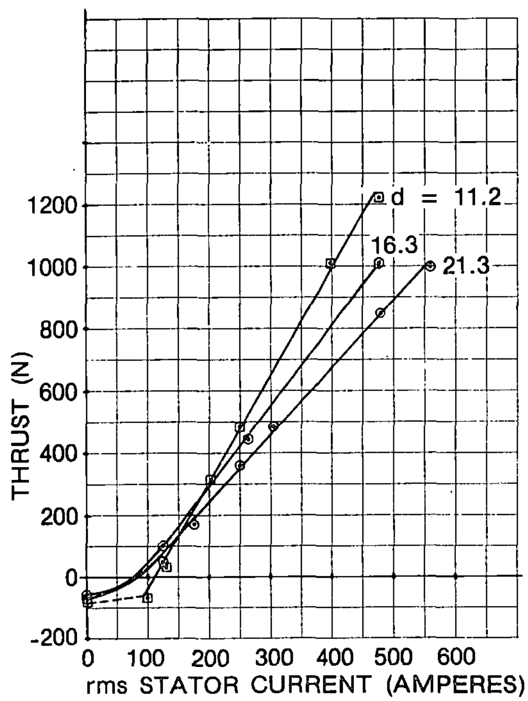

FIGURE 4-4. LSM THRUST VS. STATOR CURRENT - d = 11.2, 16.3, 21.3 mm; 75 Ampere Field Current, 382.5 Hertz.

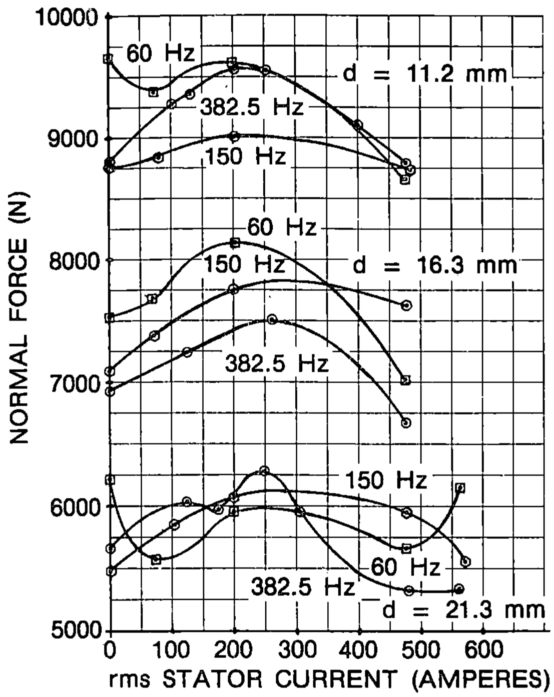

FIGURE 4-5. LSM NORMAL FORCE VS. STATOR CURRENT - d = 11.2, 16.3, 21.3 mm; 75 Ampere Field Current; 60, 150, 382.5 Hertz.

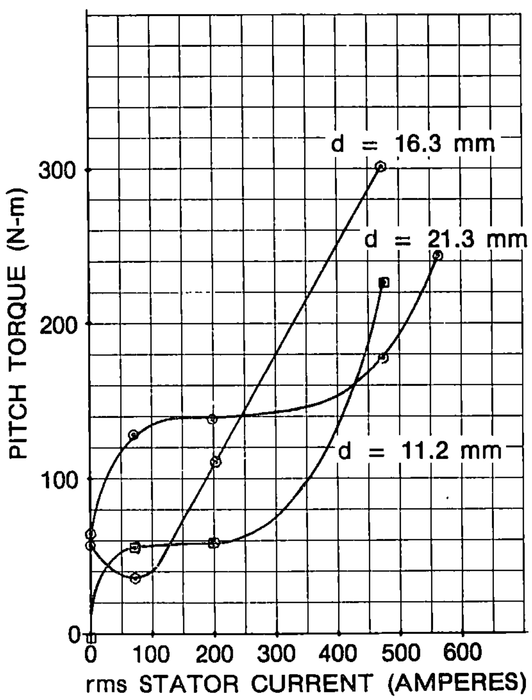

FIGURE 4-6. LSM PITCH TORQUE VS. STATOR CURRENT - d = 11.2, 16.3, 21.3 mm; 75 Ampere Field Current; 60 Hertz.

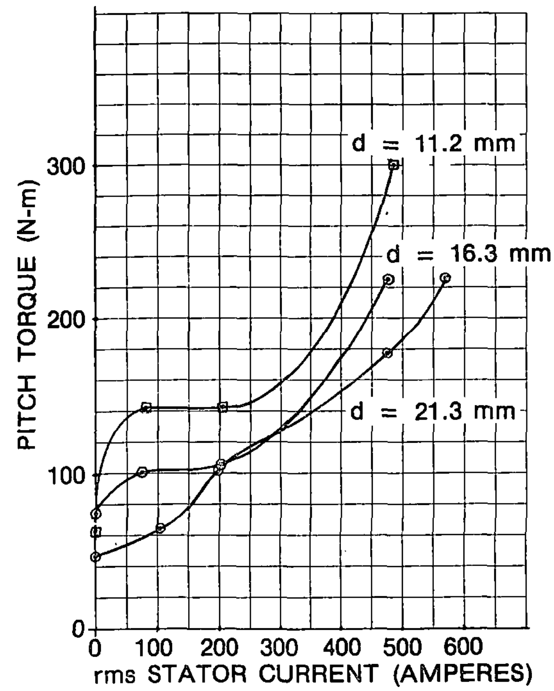

FIGURE 4-7. LSM PITCH TORQUE VS. STATOR CURRENT - d = 11.2, 16.3, 21.3 mm; 75 Ampere Field Current; 150 Hertz.

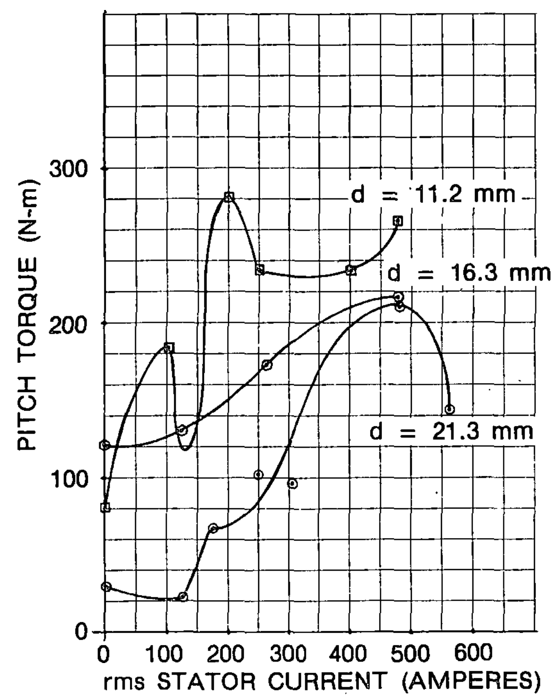

FIGURE 4-8. LSM PITCH TORQUE VS. STATOR CURRENT - d = 11.2, 16.3, 21.3 mm; 75 Ampere Field Current; 382.5 Hertz.

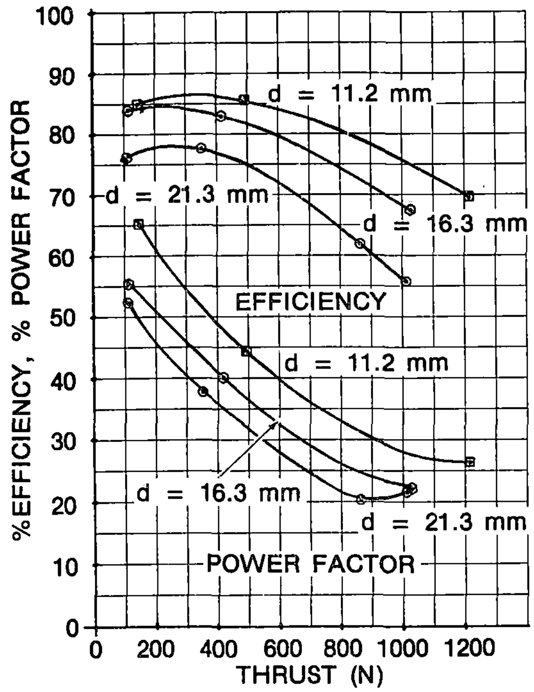

FIGURE 4-9. LSM EFFICIENCY AND POWER FACTOR VS. THRUST - d = 11.2, 16.3, 21.3 mm; 75 Ampere Field Current; 60 Hertz.

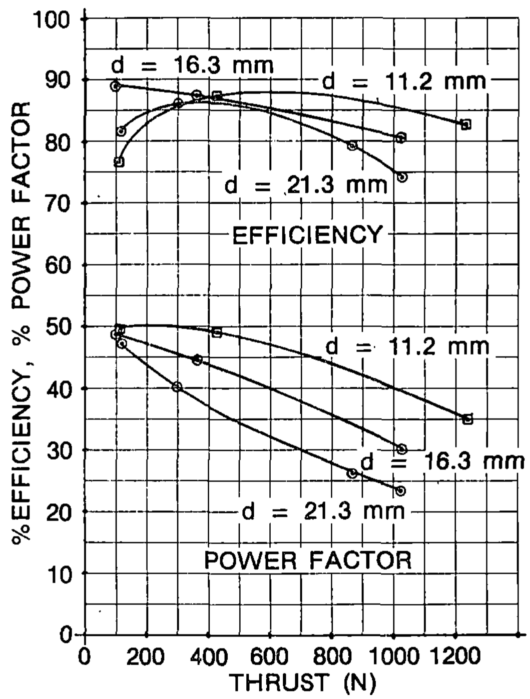

FIGURE 4-10. LSM EFFICIENCY AND POWER FACTOR VS. THRUST - d = 11.2, 16.3, 21.3 mm; 75 Ampere Field Current; 150 Hertz.

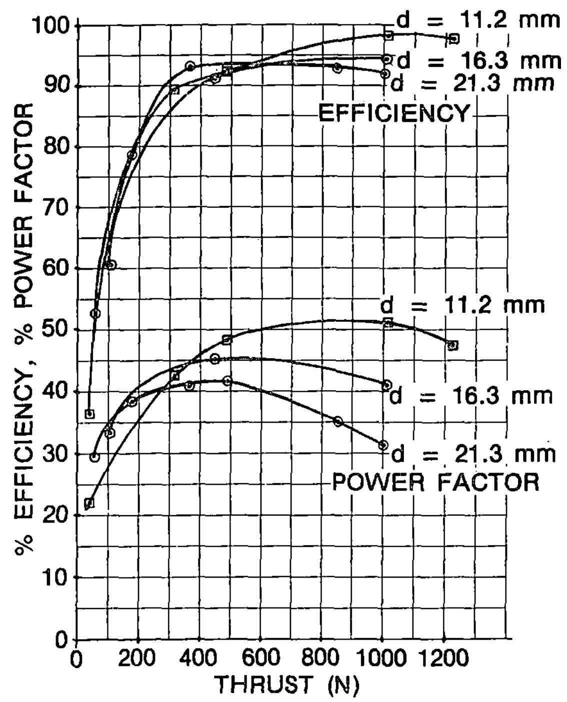

FIGURE 4-11. LSM EFFICIENCY AND POWER FACTOR VS. THRUST - d = 11.2, 16.3, 21.3 mm; 75 Ampere Field Current; 382.5 Hertz.

smaller gap, degrade with the larger gap. The 382.5 hertz data suffer somewhat from confusion at low-thrust levels, but are consistent at and near rated load. As was mentioned in the motoring performance section, the efficiency curves are all higher than they should be, the power factor ones lower.

LATERAL OFFSETS

The stator was offset under the track to displacements of e=0, ±12.5, ±25 mm, and the resulting lateral forces in operation are plotted in Figure 4-12. The sense of the lateral force is to restore the stator to the centered position, and the magnitude of the "spring constant" is about 700 newtons per centimeter. The yaw torque data indicated no noticeable trend with lateral displacement, and only a slight reduction in normal force was detected with displacement. As can be seen in Figure 4-13, a reduction of thrust of about 10% was suffered when the maximum offset was tested. The data in Figure 4-12 and in Figures 4-13, 4-14 and 4-15 indicate that the stator was not perfectly centered under the track at the location called e=0. The variations in core heights of the two halves of the stator, as well as the slight difference in width of the stator and track, result in a limitation on the ability to align the stator exactly centered under the track. In fact, the amount of lateral force experienced in the e=0 data corresponds to a displacement of about e=+1.5 mm. This initial offset is in a direction to cause the slight differences seen in Figures 4-14 and 4-15 between the thrust curves of +12.5 and -12.5 mm, of

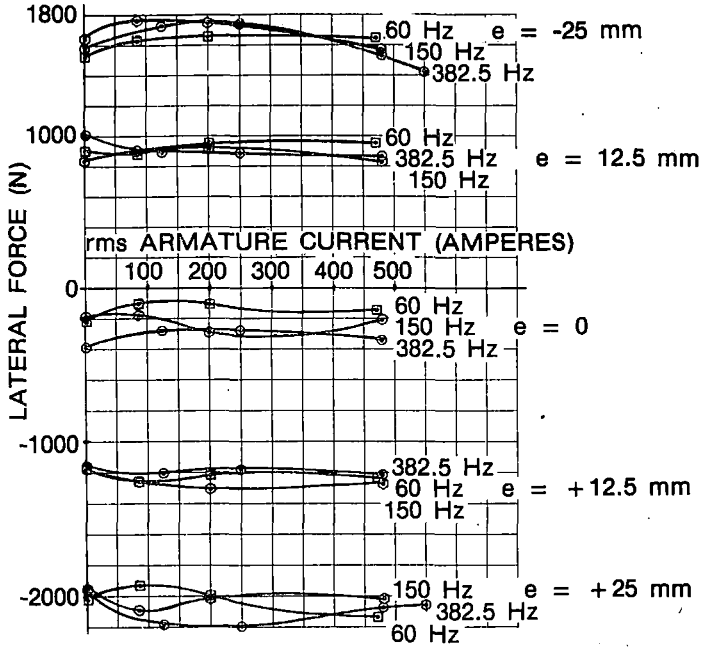

FIGURE 4-12. LSM LATERAL FORCE VS. STATOR CURRENT FOR LATERAL DISPLACEMENTS - e=0, ±12.5, ±25 mm; 75 Ampere Field Current; 60, 150, 382.5 Hertz.

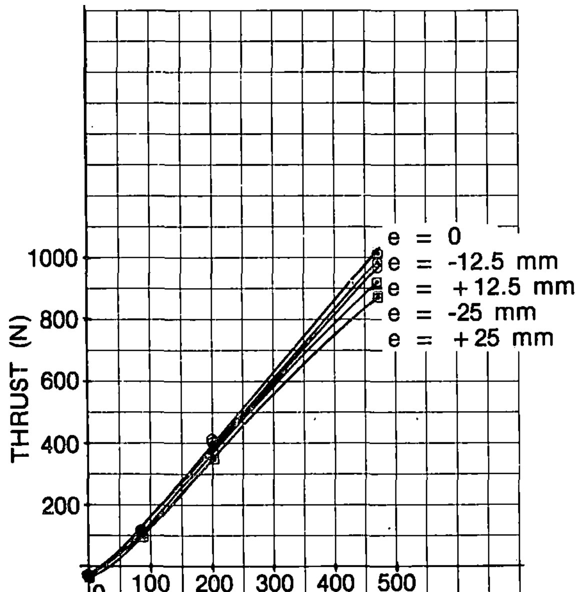

FIGURE 4-13. LSM THRUST VS. STATOR CURRENT FOR LATERAL DISPLACEMENTS - e=0, ±12.5 mm, ±25 mm; 75 Ampere Field Current; 60 Hertz.

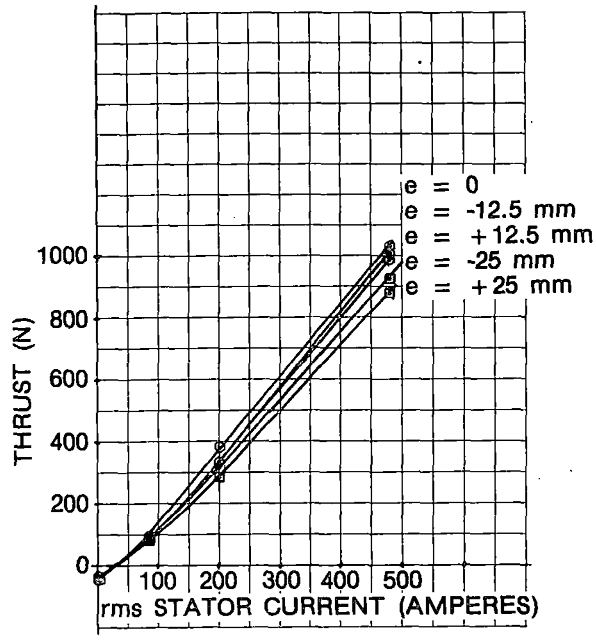

FIGURE 4-14. LSM THRUST VS. STATOR CURRENT FOR LATERAL DISPLACEMENTS - e=0, ±12.5 mm; 75 Ampere Field Current; 150 Hertz.

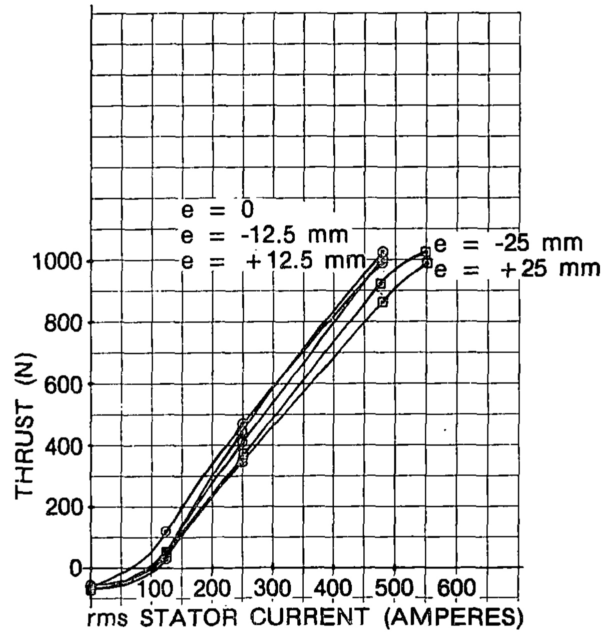

FIGURE 4-15. LSM THRUST VS. STATOR CURRENT FOR LATERAL DISPLACEMENTS - e=0, ± 12.5 mm, ±25 mm; 75 Ampere Field Current; 382.5 Hertz.

+25 and -25 mm. In fact, the positive initial displacement causes all positive displacements to be about 3 mm more than the negative corresponding ones, with the values probably being e=-23.5, -11, +1.5, +14, +26.5 mm.

Yaw Angle Displacements

The stator was turned under the trade to yaw angles of b=0, ±.0224, and ±.0448 radians, and motoring tests made. No noticeable effect was present in lateral force data, and only a slight reduction in normal force was observed. The yaw torque produced is shown in Figure 4-16, and it should be noted that the force was strongly restoring. Figure 4-17 shows the relatively small effect of these yaw displacements on thrust, amounting to only about 8% at the maximum angles.

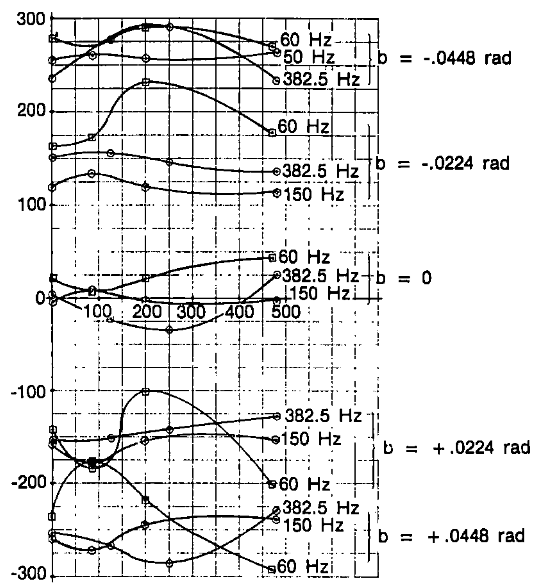

FIGURE 4-16. LSM TORQUE VS. STATOR CURRENT FOR YAW DISPLACEMENTS - b=0, ±.0224, ±.0448 Radian; 75 Ampere Field Current; 60, 150, 382.5 Hertz.

Roll Angle Displacements

The stator was rolled to angles of a=0, and ±.00296 radian, but no noticeable effects were seen in any performance or force measurements.

Pitch Angle Displacements

The stator was shimmed to angles of pitch of c=0 and ±.00456 radians, and the pitch torque data obtained is plotted in Figure 4-18. In this case, a positive pitch creates more of a positive pitch torque, and the force tends to aggravate rather than correct the displacement. The slope of the curves to increasing torque

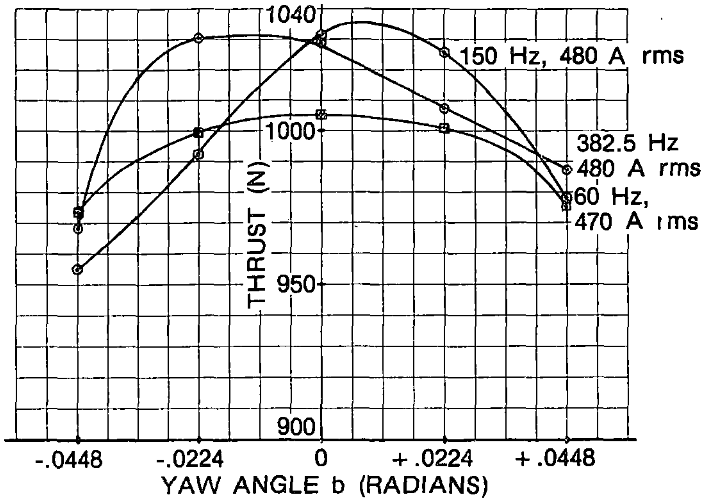

FIGURE 4-17. LSM THRUST VS. YAW DISPLACEMENT - b=0, $\pm$.0224, $\pm$.0448 Radian; 75 Ampere Field Current; 60, 150, 382.5 Hertz.

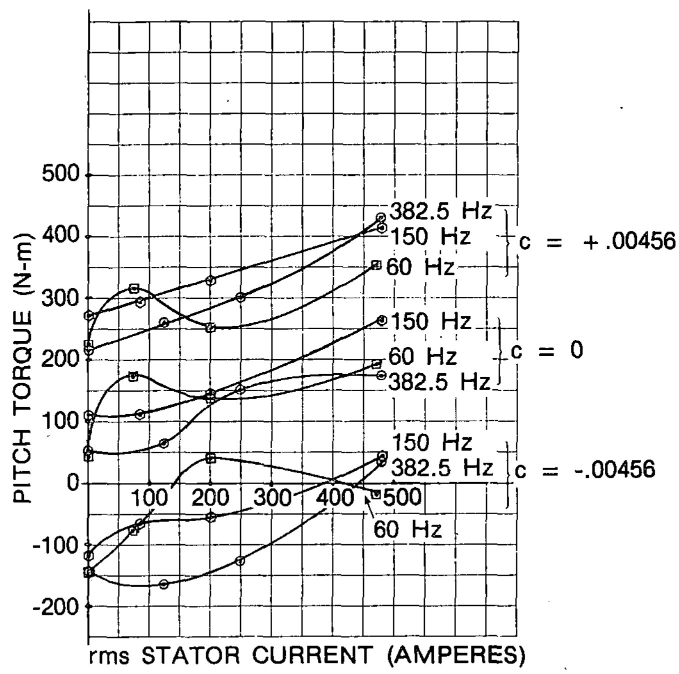

FIGURE 4-18. LSM PITCH TORQUE VS. STATOR CURRENT FOR PITCH ANGLE DISPLACEMENTS - c=0, $\pm$.00456 Radian; 75 Ampere Field Current; 60, 150, 382.5 Hertz.

with increasing load is partially due to the method of stator support and force measurement, which introduces a component of pitch torque due to thrust. No consistent effect of pitch angle was observed in thrust, normal force, nor in any other measurement.

Section 5

RESISTANCE, REACTANCE, FORCE AND FLUX MEASUREMENTS

This section describes the static force, resistance, reactance, and flux measurements performed on the laminated track machine.

DC RESISTANCE MEASUREMENTS

The resistances of the three armature phases were measured with a resistance bridge at a temperature of approximately 25°C and found to be balanced and equal to 0.0109Ω. The resistance of the field winding was calculated from the measurement of voltage and current while connected to its power supply in the test stand. At approximately 25°C, this winding was found to have a resistance of 1.08Ω.

FORCES WITH DC ARMATURE CURRENT

To determine the space harmonics present in the air gap of the LSM, the force on the periphery of the wheel was measured as a function of wheel displacement while the armature windings were excited with direct current ($I_c = -2I_a = -2I_b$). The force measuring system consisted of a scale suspended from a crane which was raised or lowered as necessary to compensate for movement of the wheel. Friction was reduced as much as possible by decoupling the wheel from the load machine. The effect of the remaining frictional force was minimized by taking two sets of force readings, one with clockwise wheel rotation, the other with counter-clockwise wheel rotation, and then averaging the results at each wheel displacement value. The displacement values were measured by a flexible scale attached to the periphery of the wheel. A diagram of the test setup is shown in Figure 5-1.

The resulting force versus displacement diagram for zero field current is shown in Figure 5-2. North and south armature poles are drawn on the diagram in the shape of pole pieces to indicate the orientation of the forces relative to the armature. In an ideal synchronous machine this reluctance force measurement would result in a sinusoidal force distribution similar to that of Figure 5-2 except that the magnitude of the two force peaks would be equal. In Figure 5-2 the higher force peak is about 20% above the lower for 200 A and about 45% above the lower for 400 A armature current (I_c). Since the static friction causes a force of almost 3.5 newtons, the force readings at the higher current are probably more accurate.

The reason for the difference in the force peaks may be seen in Figure 5-3. The upper, stepped waveform shows the armature mmf during the experiment as obtained by counting conductors. Part (b) of the figure shows the position of the saliencies relative to the first harmonic approximation of the armature mmf during two force measurements. The force measurement for Position Number 1

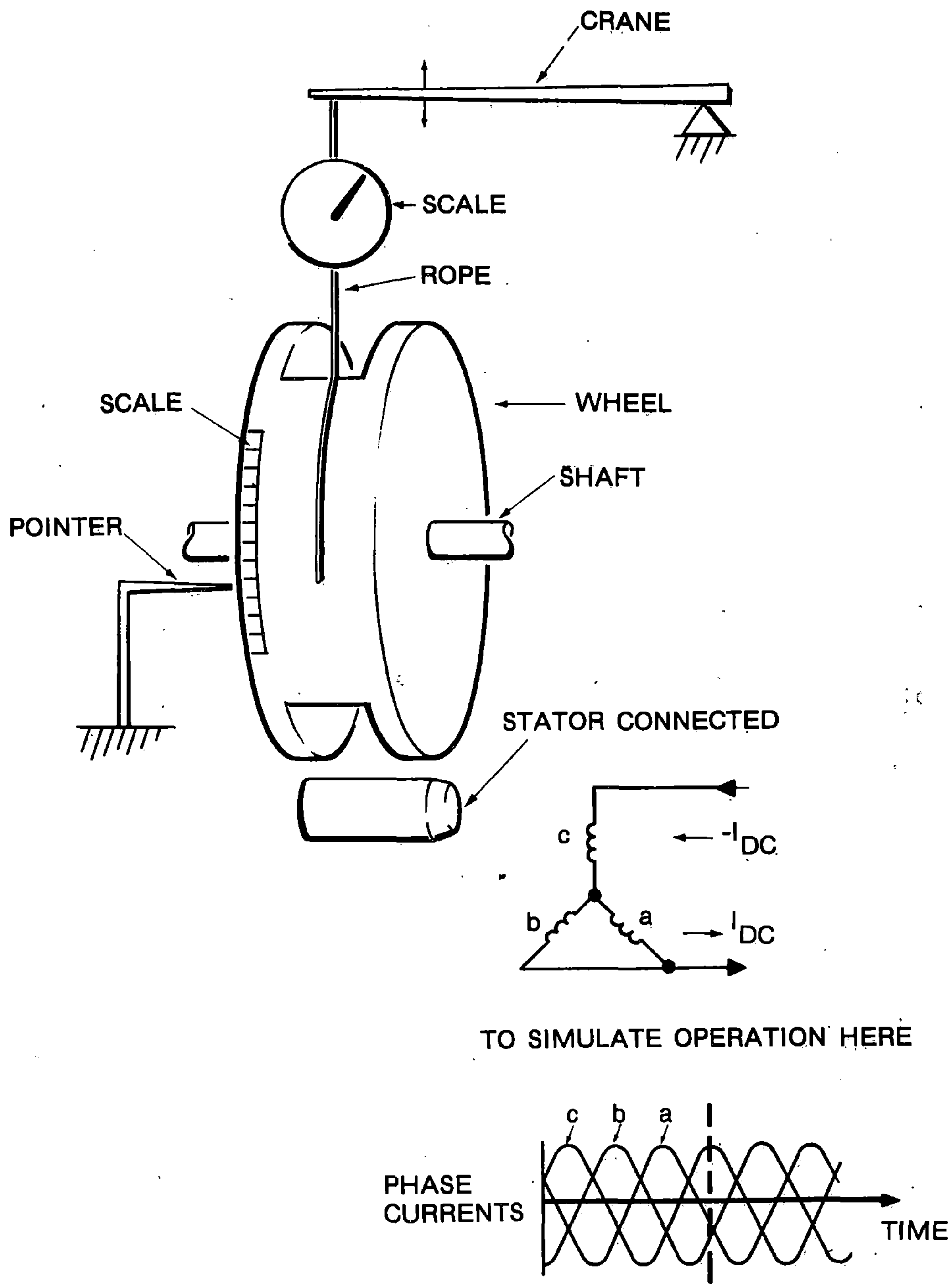

FIGURE 5-1. EXPERIMENTAL SETUP FOR DC FORCE MEASUREMENTS.

yielded the higher peak value, while the measurement for Position Number 2 yielded the lower peak value. One easily sees that three rail saliencies are under armature mmf in Position Number 1 but that only two saliencies are under the armature mmf for Position Number 2. Thus the force in Position Number 1 should be 3/2 times

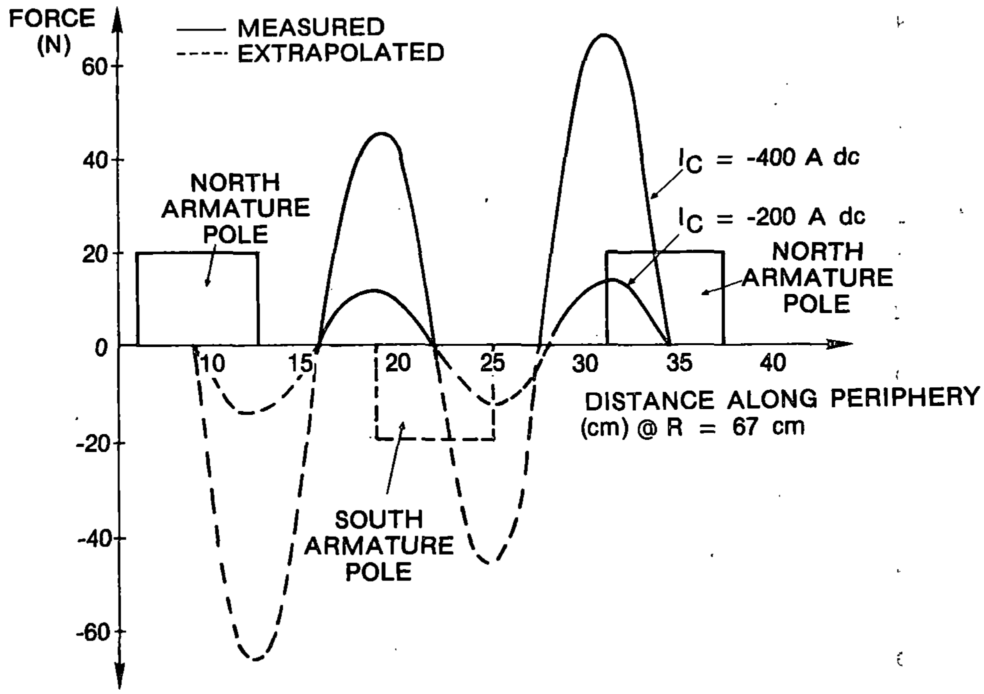

FIGURE 5-2. RELUCTANCE FORCE VS. DISTANCE FOR HOMOPOLAR LSM:

$$I_a = I_b = -I_c/2$$
$$I_f = 0$$

the force in Position Number 2, a result verified by the 400 A force data.

The result of repeating the same force measurements with a non-zero field current is shown in Figure 5-4a. The measurement at 40 A gives a fairly good sinewave curve, but as the field current is increased to 75 A the force waveform becomes quite distorted as saturation, perhaps of the pole tips or teeth, begins to distort the air gap flux waveform. This reluctance force seen in Figure 5-2 is replotted in Figure 5-4a to show a comparison of the relative magnitudes. It is seen that only a small portion of the total force waveform distortion is caused by the reluctance force. Thus most of the distortion must be the result of the highly non-sinusoidal air gap.

D-AXIS AND Q-AXIS REACTANCES

Figure 5-4b shows the value of synchronous reactance, X_d, as a function of field current. This value is calculated from the ratio of open circuit voltage to short circuit current at 382.5 hertz. The high frequency was chosen to minimize the effect of stator resistance on the ratio. The unsaturated value of 0.32 ohm decreases to about 0.26 ohm at 75 A field. (The calculated value for the machine was 0.32 ohm.)

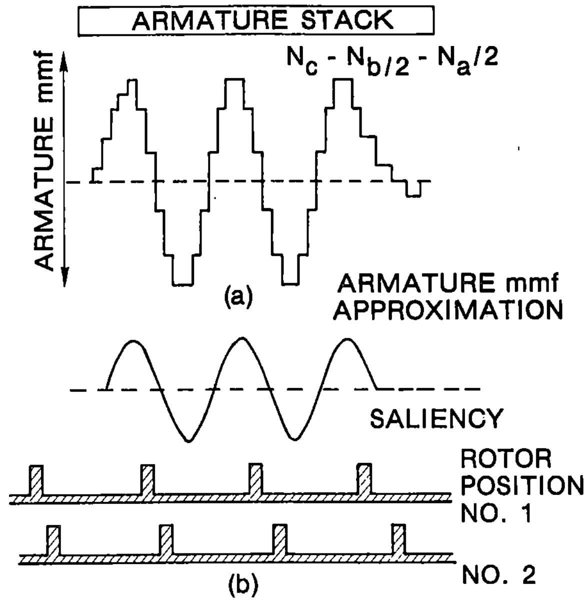

FIGURE 5-3. TWO POSITIONS OF SALIENCIES RELATIVE TO ARMATURE mmf DURING RELUCTANCE FORCE MEASUREMENTS. FORCE AT POSITION NUMBER 1 = 3/2 FORCE AT POSITION NUMBER 2.

The direct axis transient reactance was measured by recording the waveforms of one phase voltage and two phase currents during a step change from open circuit to short circuit on the stator with constant field current. One of the resulting waveforms is shown in Figure 5-5. The excitation frequency is 382 hertz. The envelopes of the waveforms have been traced to make them visible. The transient seen in the figure decays very quickly, in about 10 msec, in contrast to the behavior of small air gap machines where the decay may take several seconds. The time constant governing this decay is nearly equal to the ratio of field self-inductance to field resistance. Since the field flux crossing the air gap of a machine is inversely proportional to the length of the gap, the field inductance due to air gap flux in the LSM is several hundred times less than that of a round rotor synchronous machine. Because the field resistance is not a function of air gap, the subtransient time constant of the large air gap machine should be much smaller than that of the small air gap machine.

The value of the d-axis subtransient reactance is given by

$$x_d' = x_d \frac{I_{ss}}{I_{init}} \quad . \tag{5-1}$$

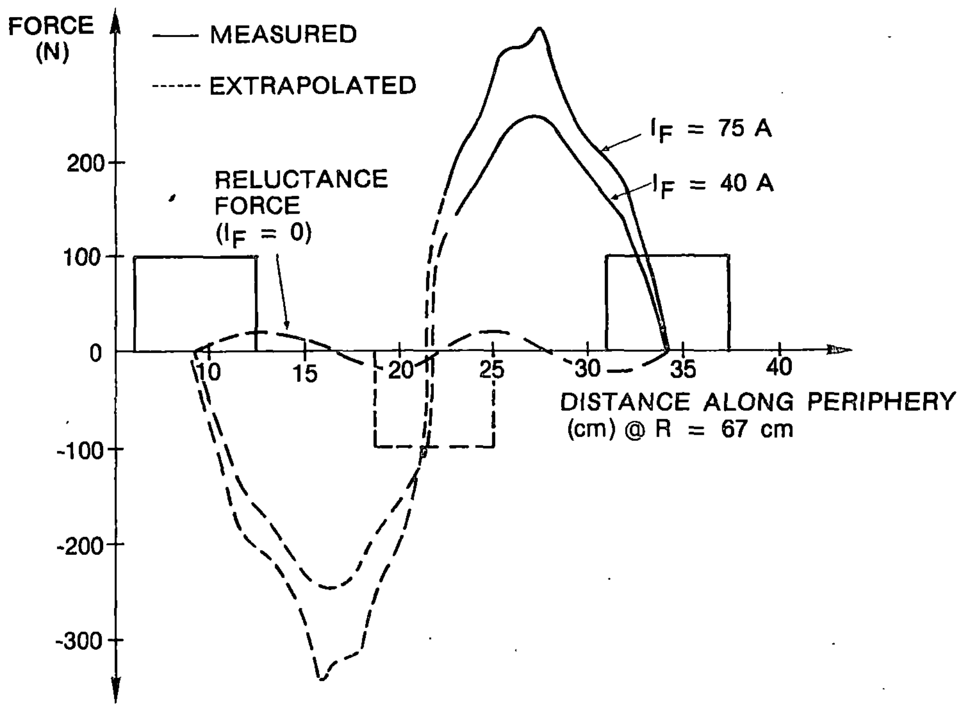

FIGURE 5-4a. FORCE VS. DISTANCE FOR HOMOPOLAR LSM; $2I_a = 2I_b = I_c = 200$ A dc.

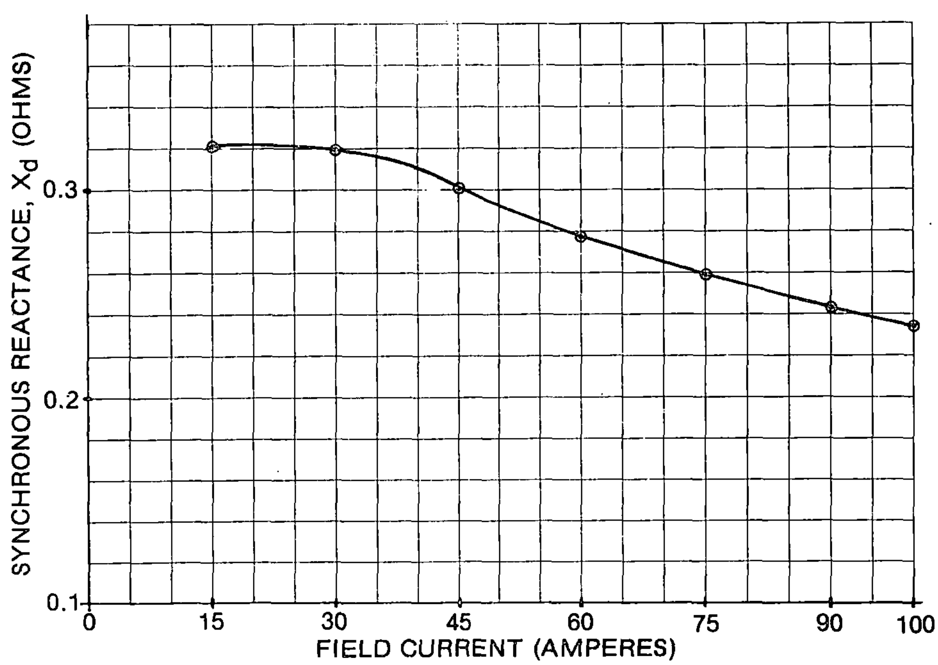

FIGURE 5-4b. LSM LAMINATED TRACK SYNCHRONOUS REACTANCE X_d VS. FIELD CURRENT - 382.5 Hertz, 1530 rpm.

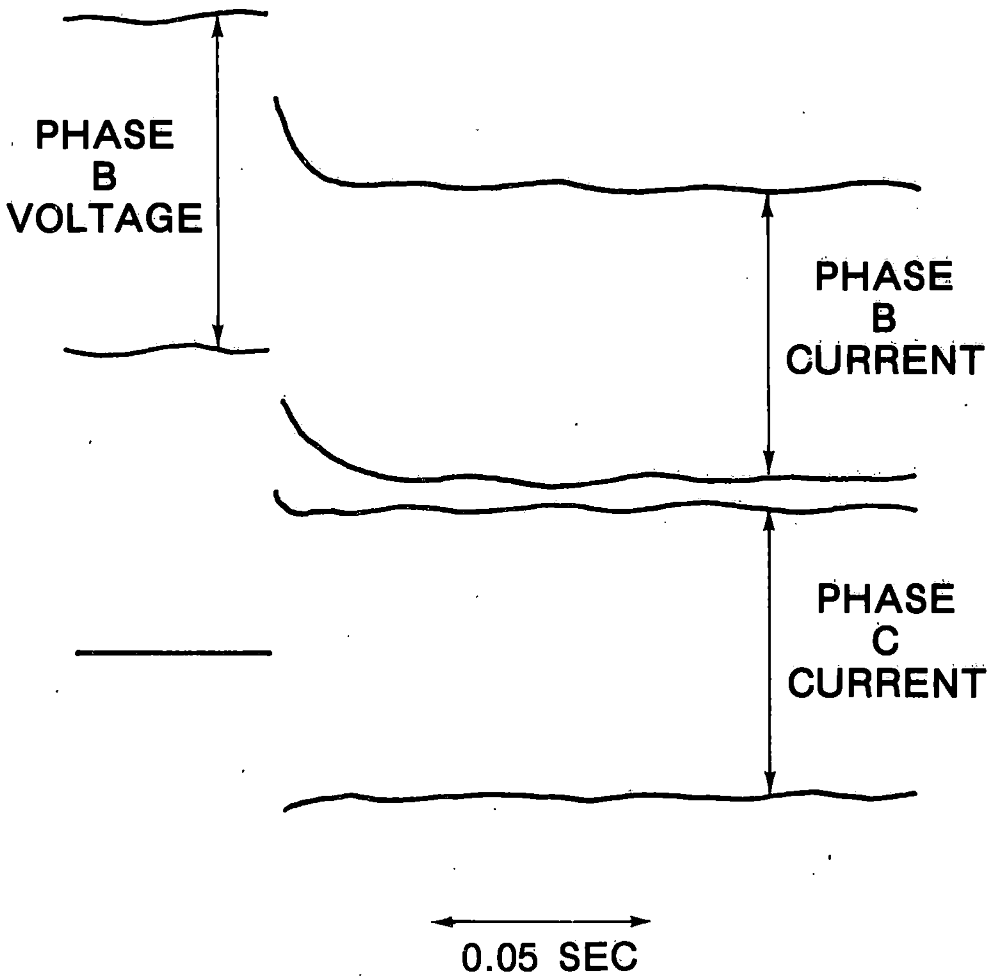

FIGURE 5-5. HOMOPOLAR LSM WAVEFORMS FOR AN OPEN CIRCUIT TO SHORT CIRCUIT STEP. FREQUENCY IS 382 HERTZ. FIELD CURRENT IS 75 AMPERES.

where X_d is the direct axis reactance, I_{ss} is the steady state phase current, and I_{init} is the initial value of the phase current. By this formula

$$X_d' = 0.90\ X_d \approx 0.27\ \Omega \quad 394 \text{ hertz} \tag{5-2}$$

where the saturated value of X_d has been used. This result is highly approximate due to the fast decay of the transient current.

Since the transient time constant was so short, no subtransient effects were visible. They should be slight since there are no amortisseur windings.

Two types of measurements were made to obtain a value of quadrature axis reactance. The first was a method based on reluctance torque given by Klingshirn[2] which says

[2] 1978 IEEE PES Winter Power Meeting.

$$L_d - L_q = \frac{8\ T_e}{3\ P\ I_m^2 \sin 2\ \delta} \tag{5-3}$$

where

L_d = d-axis inductance

L_q = q-axis inductance

T_e = developed torque in nt-m

P = number of poles (here saliencies)

I_m = dc current applied to armature

δ = torque angle in electrical degrees

The torque and current values of Figure 5-2 gives

$$L_d - L_q = \frac{8 \times 66 \times 0.67}{3 \times 3 \times 400^2 \times \sin(2 \times 45^\circ)} \tag{5-4}$$

The value of X_d-X_q is then 0.606 Ω @ 394 hertz. Since the unsaturated value of X_d is 0.45 Ω @ 394 hertz.

$$X_q \approx -\ 0.266\ \Omega\ @\ 394\ \text{hertz} \tag{5-5}$$

This negative value is clearly impossible. Further reflection has led to the conclusion that the difference in inductances measured by this method on an inductor machine is $L_{d(max)}-L_{d(min)}$ where $L_{d(max)}$ is the d-axis inductance in the center of the interpolar space and $L_{d(min)}$ is the d-axis inductance at the center of the pole piece. It appears that the q-axis reactance is not related to a static (dc excitation) force measurement in an inductor machine, a result caused by having saliencies only at every second direct-axis armature circuit.

The second method used to measure X_q was a slip test. For this measurement the machine was excited by a three-phase 60 hertz sinewave voltage source and driven at slightly less than synchronous speed. The field was open circuited. Figure 5-6 shows the waveforms of the b-phase voltage and current and the field voltage. The q-axis reactance is given by

$$X_q = X_d \frac{V_{b\ min}}{V_{b\ max}} \times \frac{I_{b\ min}}{I_{b\ max}} \tag{5-6}$$

$$= 0.34 \times 0.92 \times 0.91 = 0.284\ \Omega\ @\ 394\ \text{hertz}$$

The reactance X_d has the unsaturated value. This value of X_q is quite reasonable.

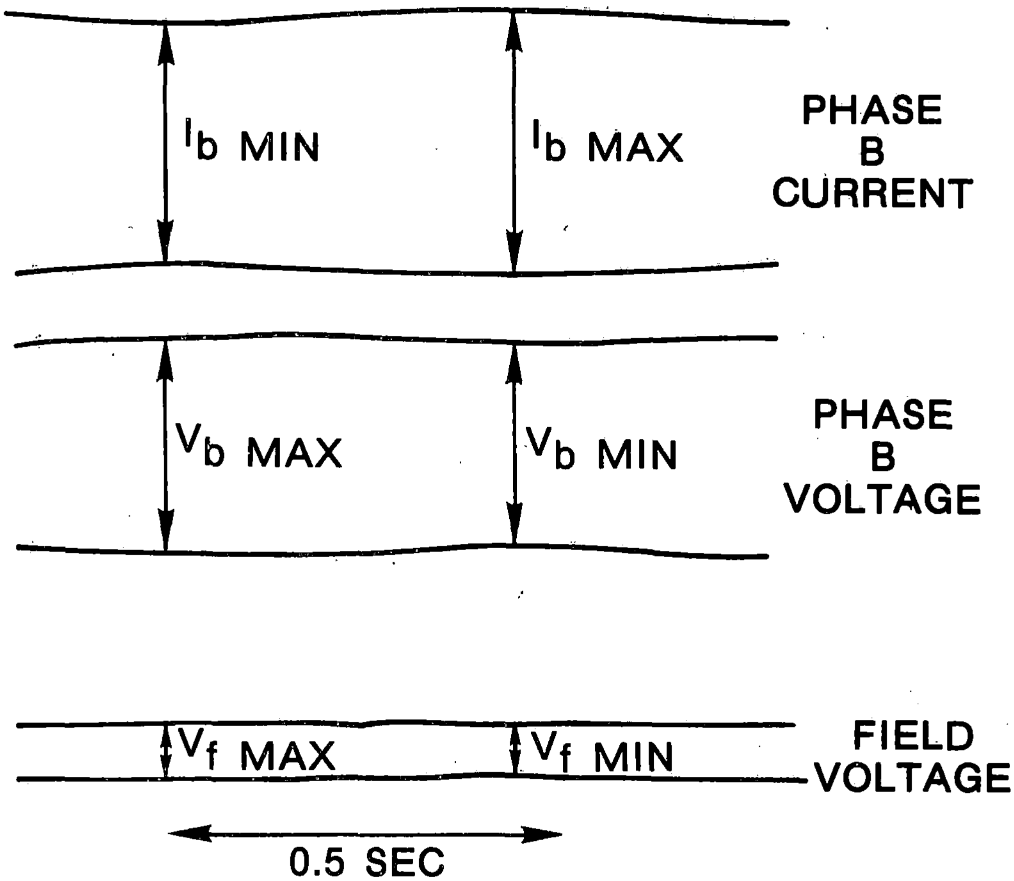

FIGURE 5-6. ENVELOPES OF PHASE VOLTAGE AND CURRENT WAVEFORMS DURING SLIP TEST:

$$X_q = X_d \frac{V_{b\ min}}{I_{b\ max}} \times \frac{I_{b\ min}}{V_{b\ max}}$$

The values of X_d and X_q are close to each other because leakage flux (~50% of X_d) is nearly equal for both reactances and because the ratio of d-axis to q-axis mutual flux is less than 2:1. (The ratio can even be less than 1:1 for large per unit pole arcs.) This relatively small ratio results because d-axis flux has to cross one large air gap in addition to one small air gap, while the q-axis flux crosses two large (interpolar) air gaps. (Recall that there are saliencies only at every other electrical pole.)

COMMUTATING REACTANCE MEASUREMENT

According to the Linear Synchronous Motor Test Plan (June 24, 1977), the commutating reactance of the LSM is given by

$$L_k = 2t_2^2/(\pi^2 c') \tag{5-7}$$

where t_2 is the zero to peak rise time of phase currents and c' is the equivalent capacitance of the inverter commutating capacitors. Using the rise time of Figure 5-7d (rated thrust) the commutating inductance is

$$L_k = \frac{2}{\pi^2} \frac{\times (220 \times 10^{-6})^2}{\times 90 \times 10^{-6}} = 109 \ \mu H \qquad (5\text{-}8)$$

($c' = 3/2\ c_c$, where c_c is the commutating capacitor), X_k is then

$$X_k = 0.27\ \Omega \ @ 394 \text{ hertz} \qquad (5\text{-}9)$$

this value corresponds well to the calculated value of

$$X_k = 0.5(X_d'' + X_q'') \qquad (5\text{-}10)$$

also given in the LSM Test Plan since

$$X_d'' \approx X_d' = 0.27\ \Omega \text{ and } X_q'' \approx X_q = 0.27\ \Omega \qquad (5\text{-}11)$$

for the 112 kW homopolar test machine.

FLUX MEASUREMENT

The modulated dc characteristic of the flux of this machine makes obtaining of flux data difficult, at least in comparison with a conventional ac flux machine. A combination of measurement techniques, including Hall-effect Gaussmeter and flux coil measurements, were used.

DC FLUX DISTRIBUTION

The machine was instrumented with coils wrapped around various parts and the coil terminals taken to a low-drift integrator calibrated in flux linkages or lines. The field coil was excited with dc ramped up from zero to 75 A in one or two seconds, and the linkages read from the integrator output. Figure 5-8 shows the coil locations and the values of flux associated with each in the test. It should be noted that a substantial amount of leakage is unaccounted for, as the yoke flux ϕ_y in the stator yoke structure exceeds the sum of the stator leakage ϕ_{yl}, the gap leakage ϕ_g and the rotor flux ϕ_{rt}. This amounts to

$$\phi_y - (\phi_{yl} + \phi_g + \phi_{rt}) = \left[6.06 - (1.65 + .37 + 2.34) \times 10^6\right] \qquad (5\text{-}12)$$

or 1.7×10^6 linkages that are not found by the test coils. The flux ϕ_{pl} is the leakage across the track between sides of the machine,

COMMUTATING REACTANCE - SLEM

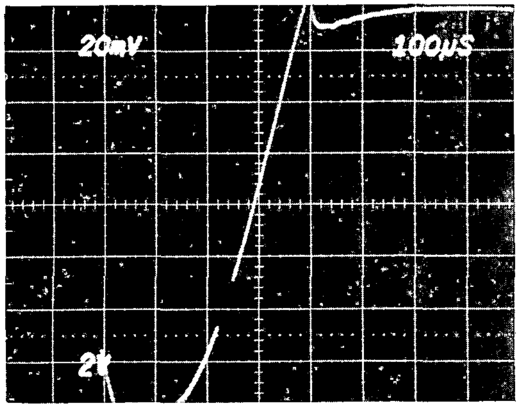

40 A FIELD
250 A ARMATURE
1530 RPM
382.5 Hz

(A)

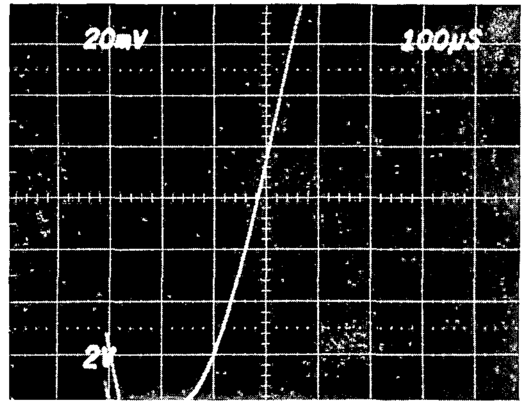

75 A FIELD
250 A ARMATURE
1530 RPM
382.5 Hz

(C)

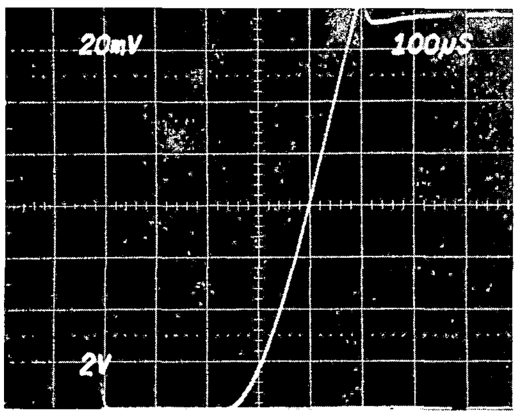

75 A FIELD
250 A ARMATURE
1530 RPM
382.5 Hz

(B)

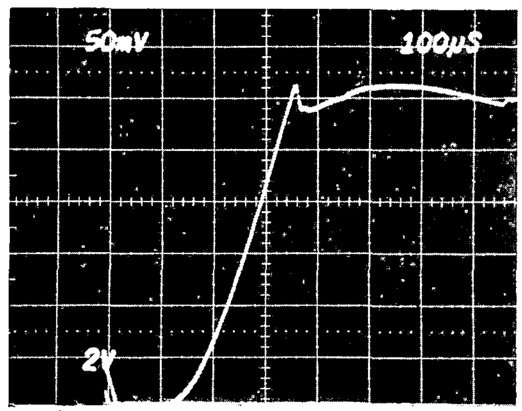

75 A FIELD
480 A ARMATURE
1530 RPM
382.5 Hz

(D)

FIGURE 5-7. PHASE CURRENT RISE TIMES.

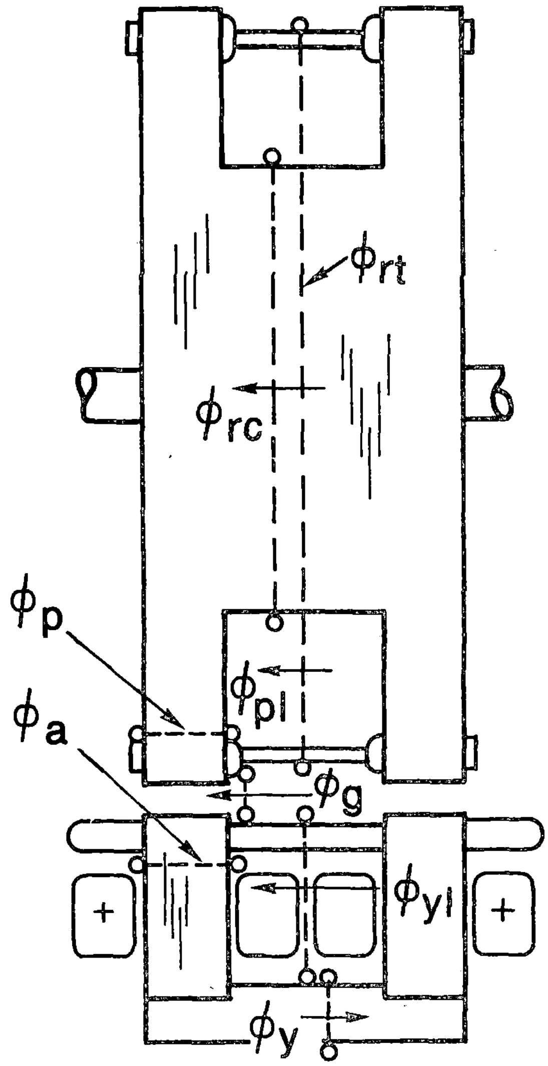

75 A FIELD

$\phi_y = 6.06 \times 10^6$ LINES
$\phi_a = 5.36 \times 10^6$
$\phi_{yl} = 1.65 \times 10^6$
$\phi_g = .374 \times 10^6$
$\phi_{rt} = 2.88 \times 10^6$
$\phi_{rc} = 2.34 \times 10^6$
$\phi_p = .427 \times 10^6$

(3 SALIENCIES OVER ARMATURE)

FIGURE 5-8. LSM LAMINATED TRACK SEARCH COIL LOCATIONS FOR FLUX MEASUREMENT, DEFINITION OF FLUX COMPONENTS.

$$\phi_{pl} = \phi_{rt} - \phi_{rc} = \left[2.88 - 2.34\right] \times 10^6 \qquad (5\text{-}13)$$

or $$\phi_{pl} = 0.54 \times 10^6 \text{ lines}$$

which amounts to $\frac{\phi pl}{15} = 0.036 \times 10^6$ lines per saliency.

These measurements also give an idea of the interpolar leakage flux. As with three saliencies over the stator, the flux in each saliency is

$$\phi_p = 0.427 \times 10^6 \text{ lines},$$

while the total rotor flux is

$$\phi_{rt} = 2.34 \times 10^6 \tag{5-14}$$

This leaves an interpolar leakage of

$$\frac{\phi_{rt}}{3} - \phi_p = \frac{2.34 \times 10^6}{3} - 0.427 \times 10^6 = \tag{5-15}$$

or 0.353×10^6 lines per pole pair

(45% of airgap flux) which is flux crossing the air gap between saliencies, making a negative contribution to the air gap flux variation.

These measurements also provide information on flux densities in the various parts of the machine. The density in the stator yoke is

$$B_y = \frac{6.06 \times 10^6 \text{ lines}}{1.59 \text{ in.} \times 32 \text{ in.}} = 119 \frac{\text{kl}}{\text{in.}^2} = 1.85 \text{ tesla.} \tag{5-16}$$

Pole waist flux density is

$$B_p = \frac{.427 \times 10^6 \text{ lines}}{1.71 \text{ in.} \times 2.125 \text{ in.}} = 118 \frac{\text{kl}}{\text{in.}^2} = 1.82 \text{ tesla} \tag{5-17}$$

while the pole surface is at

$$B_{ps} = \frac{.427 \times 10^6 \text{ lines}}{2.79 \text{ in.} \times 2.125 \text{ in.}} = 72.0 \frac{\text{kl}}{\text{in.}^2} = 1.12 \text{ tesla} \tag{5-18}$$

and the stator teeth are at

$$B_t = \frac{.520 \text{ in.} + .431 \text{ in.}}{.431 \text{ in.}} \times 1.12 \text{ tesla} = 2.46 \text{ tesla} \tag{5-19}$$

when under a saliency, assuming no fringing. From these values, it is clear that the stator yoke, stator teeth, and pole waists are all saturated at 75 A field current.

INITIAL AIR GAP FLUX TESTS

Initial flux density measurements were made with a Hall-effect Gaussmeter. A probe was secured in the air gap over a stator tooth, field was applied to the machine, and the wheel, or track, moved slowly by hand. The results of this test, for field currents of 30 and 75 A are shown in Figure 5-9. The peaks of flux correspond to the passage of track saliencies. For each of these cases a Fourier analysis was performed from the photos, and the dc average

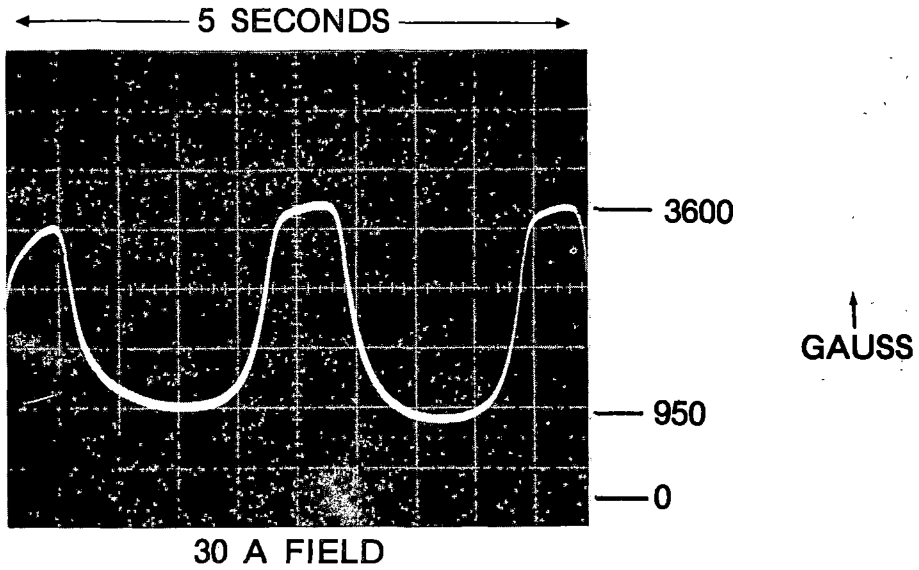

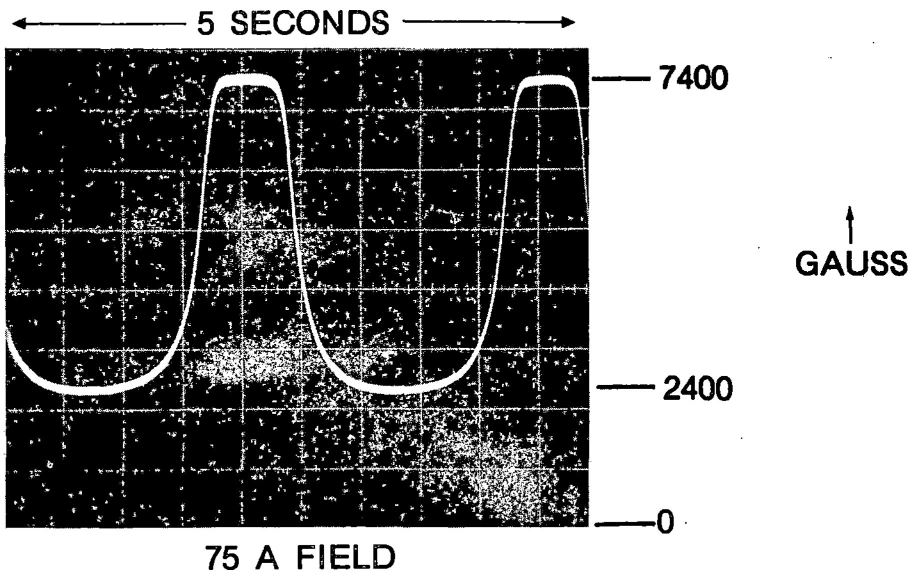

FIGURE 5-9. LSM LAMINATED TRACK QUASI-STATIC FLUX MEASUREMENTS (HALL GAUSSMETER).

and fundamental components were found. For the 30 A case, the dc average was 1.99 kG, and the fundamental was 1.38 kG. At 75 A field, the dc average was 4.04 kG, and the fundamental was 2.68 kG. These values of fundamental agree fairly closely with the densities required to produce the open circuit voltages observed in earlier tests. Attempts to measure flux densities with the Hall Gaussmeter at operating speeds were unsuccessful due to the poor frequency response of the instrument.

The circuitry attached to the flux coils in the air gap consists of an ac-coupled integrator and a true-rms converter. For preliminary tests, a coil near the longitudinal center of the stator

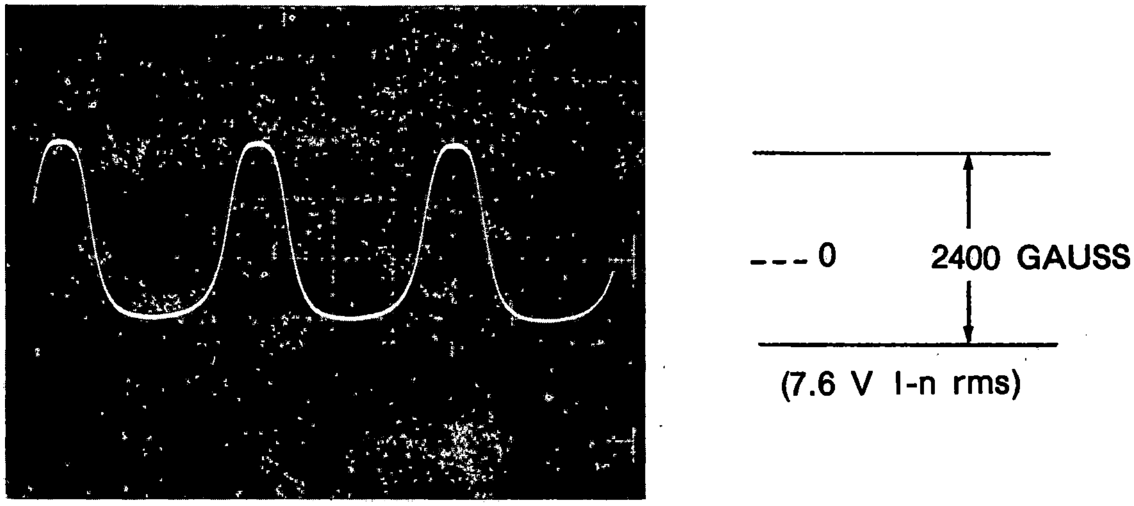

30 A FIELD

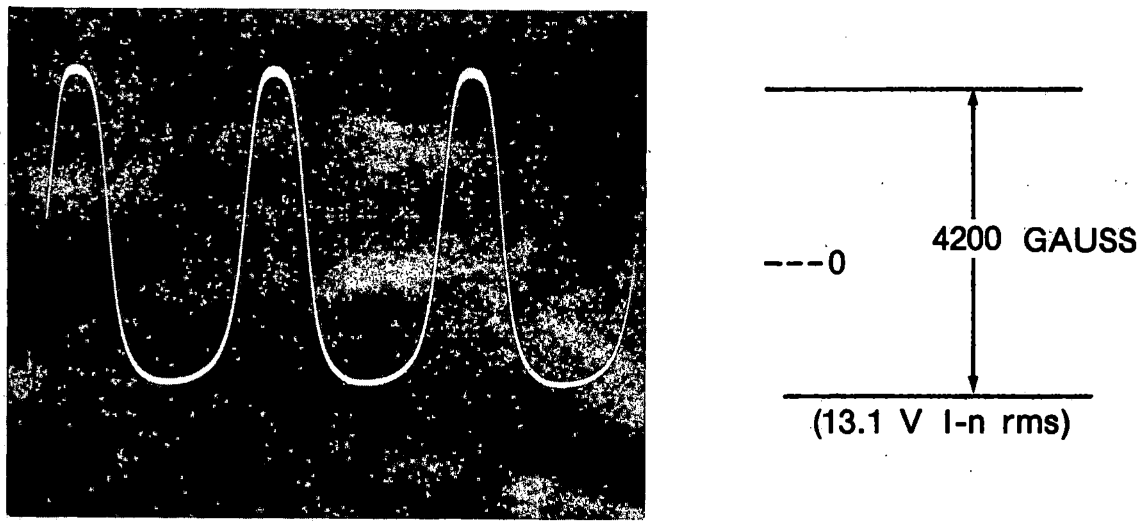

75 A FIELD

FIGURE 5-10. LSM LAMINATED TRACK FLUX MEASUREMENTS, FLUX COIL NEAR CENTER OF STATOR - 240 rpm (17.4 m/sec).

was selected, and its circuit tapped to the oscilloscope before the rms conversion. Figure 5-10 shows the flux waveforms obtained at field currents of 30 and 75 A. Scaling these output voltages with circuit parameters and coil dimensions results in a conversion factor of about 0.16 tesla per volt. The machine was operated at 240 rpm (17.4 meters per second) for this test, and the rms terminal voltages were recorded as shown in the figure. The results of this test, which indicate only the ac component of flux, are in agreement with the Hall Gaussmeter measurements within the limits of accuracy of the two measurement devices.

In Figure 5-11 the results of a static test of flux density over a stator tooth are presented. At various field currents from zero to 100 A the track was moved over the Hall probe on the stator to find maximum and minimum flux densities. These values, as well as the difference between maximum and minimum, are presented. The difference, labeled ΔB_{gap}, is closely related to the open circuit voltage generated by the machine, and a comparison with Figure 5-2, for example, will show this. The ΔB_{gap} actually decreases as the machine shows saturation in the vicinity of 100 A field current, just as the voltage decreases in this region.

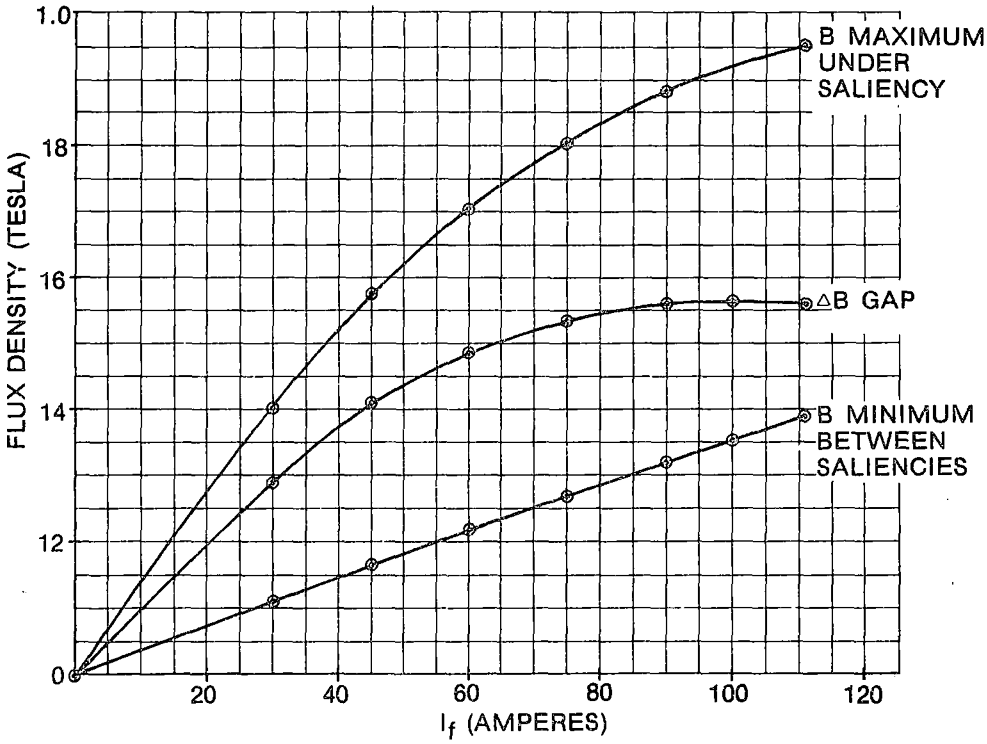

FIGURE 5-11. SLEM STATIC TEST OF AIR GAP FLUX - HALL PROBE CENTERED OVER STATOR TOOTH.

Air Gap Flux at Operating Speeds

Figure 5-12 shows the peak ac component of flux density as obtained from the stator flux coils through the data acquisition system. The three test frequencies were 60, 150 and 382.5 hertz, and there were no significant differences in the flux distribution with frequency. The shape of the distribution shows only a little variation of flux density from front to rear of the machine, and the magnitude is the same for all three cases. There is no end effect dependent on speed or frequency in the ac flux as seen from the stator side of the air gap.

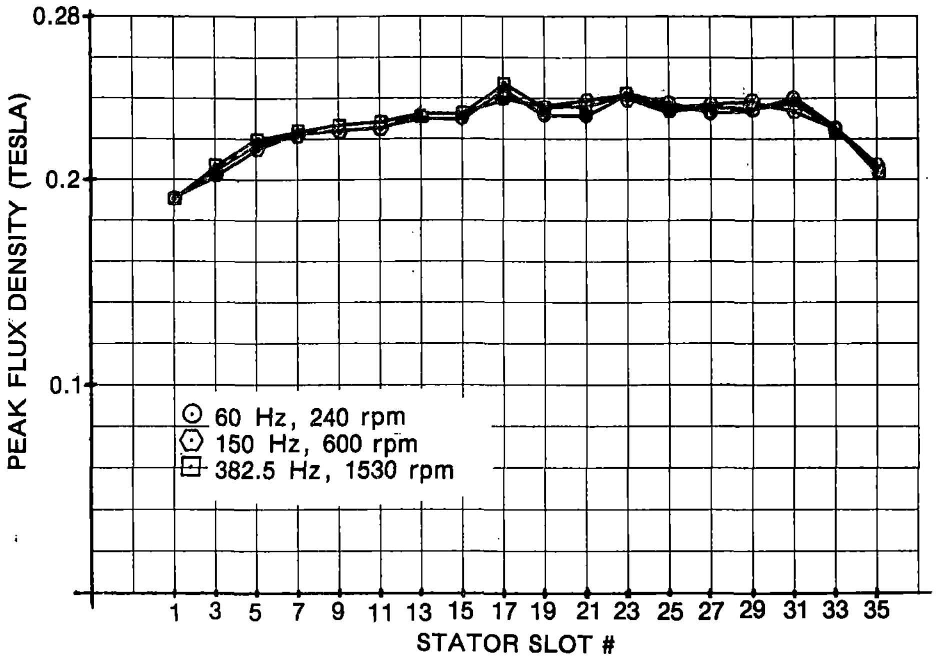

FIGURE 5-12. LSM LAMINATED TRACK PEAK AC FLUX DENSITY VS. SLOT POSITION - 60, 150, 382.5 Hertz.

Track Pole Flux

A coil of five turns was wrapped around the body of one track pole saliency and taken to slip rings, then to an oscilloscope or the DPO to be recorded. Figure 5-13 shows the voltage signals recorded for several conditions. The first run, at 60 hertz with 15 A field, shows a ripple due to the action of the field rectifier. The ripple frequency is 360 hertz, corresponding to the six-times ripple frequency in the rectifier output. As the field current is increased, this ripple disappears, as shown in the 60 hertz, 75 A case. The third case is one at rated speed and load and shows spikes due to current switching in the armature windings, these spikes appearing at six times the fundamental frequency, including both positive and negative going ones.

A second trace at the top of the third photo is the signal from the Number 2 Position sensor, which occurs when the track pole at the leading end of the machine is in the position indicated in Figure 5-14. This also corresponds to the greatest rate of change of flux (highest voltage) in the entrance period. The flux in the track pole begins to rise when the pole previous to it is entering over the stator, according to this test. The maximum decreasing flux occurs about 3.2 pole-pair pitches later, or approximately one inch after the theoretical end of the stator. Buildup and decay of flux appear to be symmetrical, and little or no end-to-end variation would be expected.

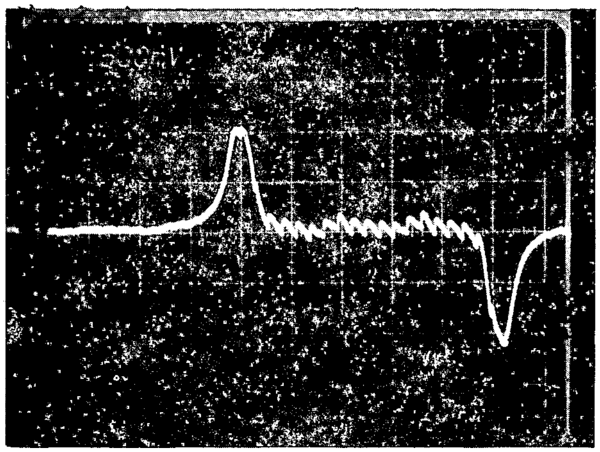

60 HERTZ

15 A FIELD

0.5 V/DIV.

10 MSEC/DIV.

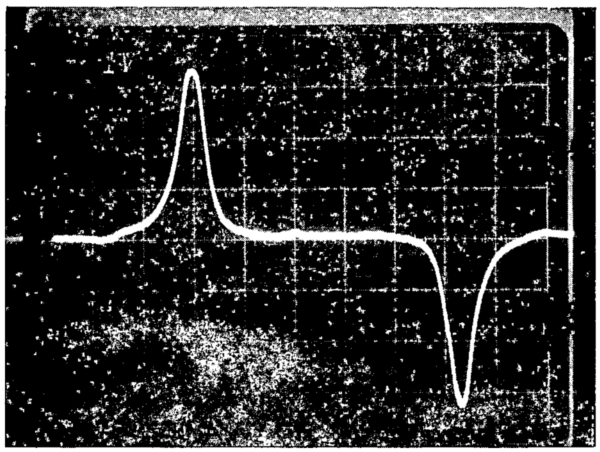

60 HERTZ

75 A FIELD

1.0 V/DIV.

10 MSEC/DIV.

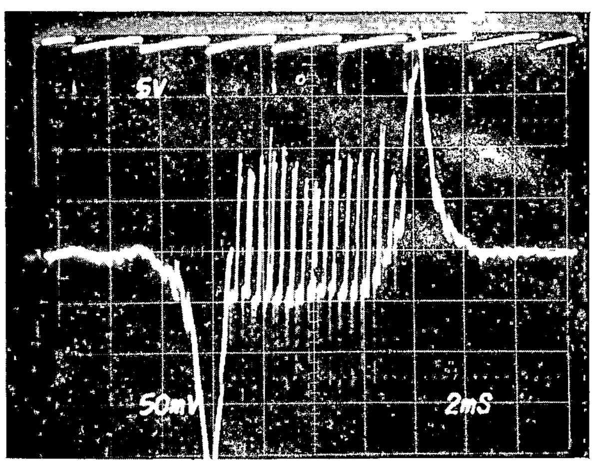

382.5 HERTZ

75 A FIELD

480 A ARMATURE

RATED LOAD

5V/DIV.

2 MSEC/DIV.

FIGURE 5-13. LSM LAMINATED TRACK POLE COIL VOLTAGE.

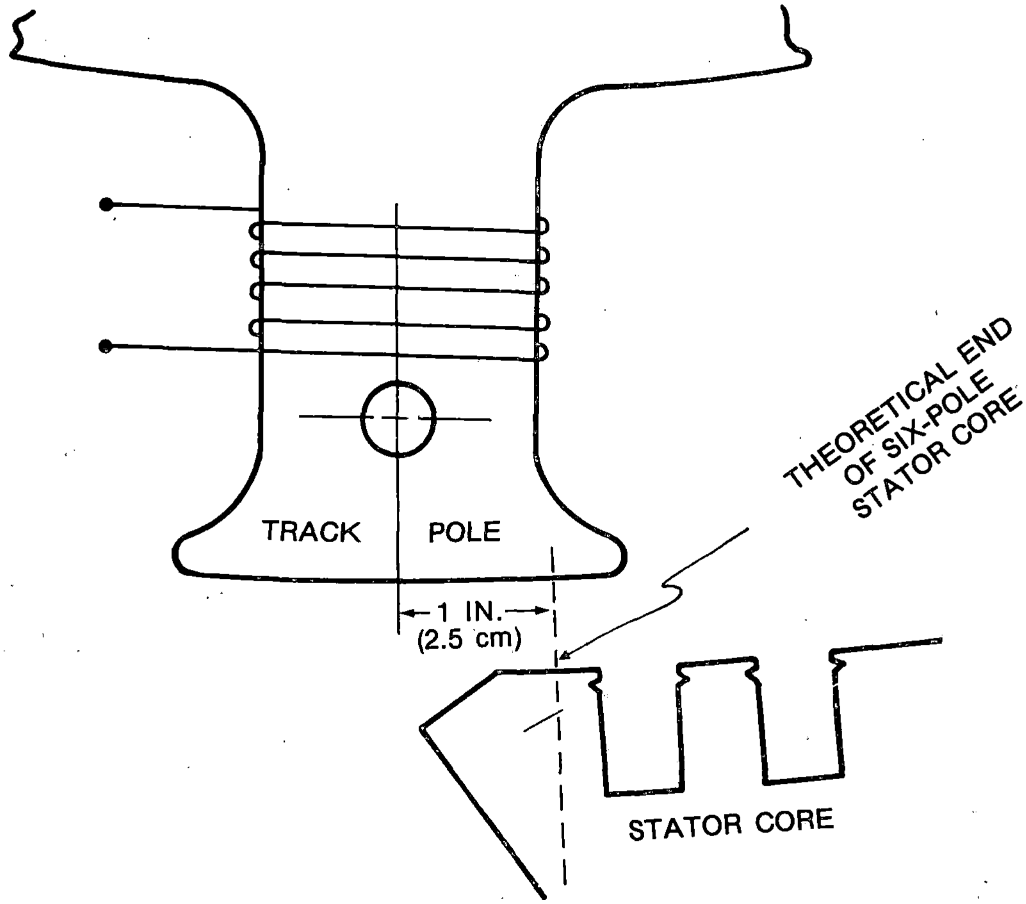

FIGURE 5-14. LSM LAMINATED TRACK - POSITION OF TRACK POLE OVER STATOR AT INTERRUPTION OF POSITION SENSOR NUMBER 2.

INTEGRATED TRACK COIL SIGNALS

The digital processing oscilloscope was used to record and process the voltage signal from the track pole coil under various operating conditions. Figure 5-15 shows the voltage obtained at 60 hertz speed with 40 A field applied. The DPO was used to divide this signal by the number of turns in the coil and integrate the result point-by-point with the result shown in Figure 5-16. The flux of 3.5×10^{-3} webers corresponds to a density of 1.49 tesla, and the pole waist is well below saturation.

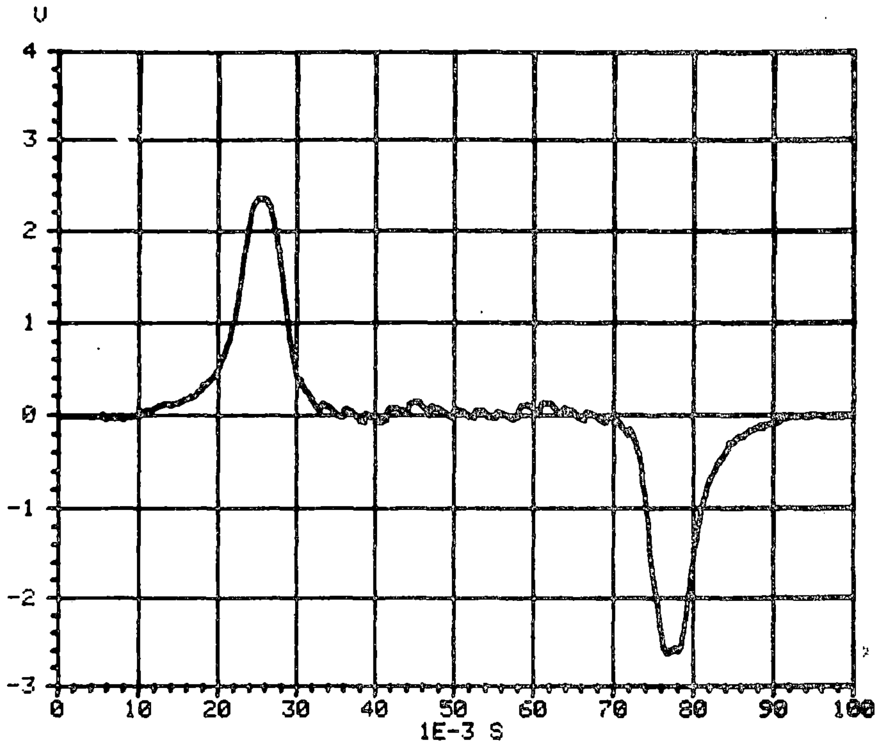

FIGURE 5-15. TRACK POLE COIL VOLTAGE VS. TIME - 60 Hertz, 240 rpm, 40 Ampere Field.

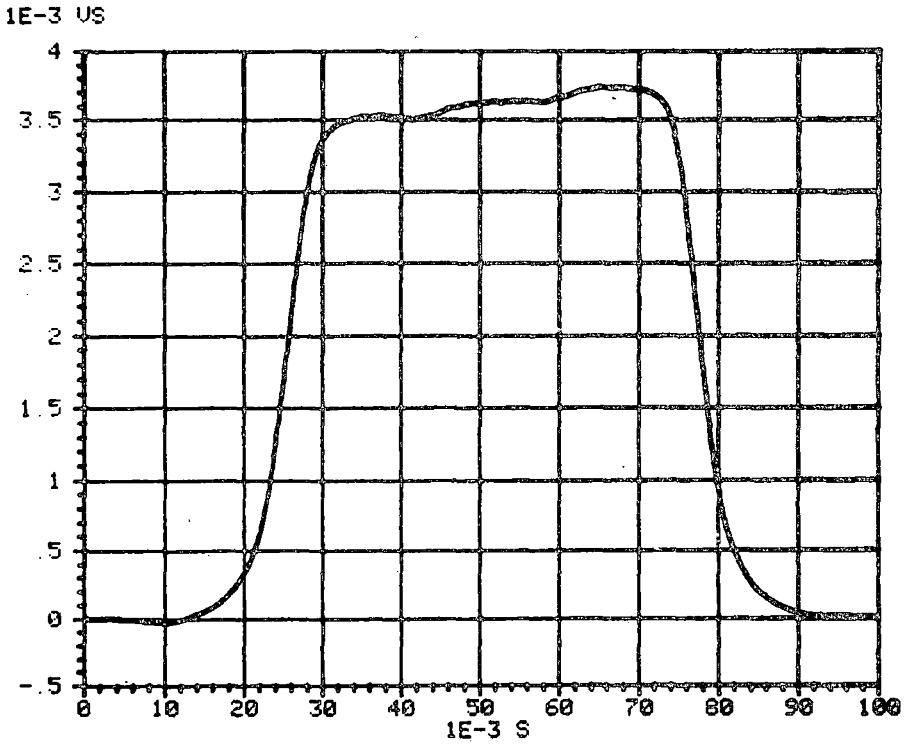

FIGURE 5-16. TRACK POLE FLUX VS. TIME - 60 Hertz, 240 rpm, 40 Ampere Field.

A rather interesting time and position variation of flux in the pole appears in this unsaturated case. There is a general slope upward from front to rear of the machine, amounting to about 0.2×10^{-3} webers, and there are two dips in this slope. The dips correspond to the entrance of the succeeding saliencies over the stator and the departure of the preceding ones. This slope and the dips indicate that the flux in the air gap and in the stator iron structure does not re-distribute instantaneously with the entrance and exit of saliencies, and that, in fact, the solid iron stator yoke influences the re-distribution of flux in a minor way. The solid iron structure delays the re-distribution of flux as a new saliency enters and causes a slight pileup of flux at the rear of the machine. The dips occur as the flux in each saliency is shared with the new entering one.

Figure 5-17 shows the flux in the track pole at 60 hertz speed with 75 A field applied. The effective length and approximate position of the stator core are also shown as they relate to the time scale. The peak flux of nearly 5×10^{-3} weber corresponds to a density of about 2.1 tesla. Figures 5-18 and 5-19 show the flux at 150 hertz speed and 382.5 hertz speed, respectively, and, except for time scale, these are identical to Figure 5-17. No effect of speed on flux buildup or maximum flux can be observed in these figures, and these results agree with those of Figure 5-12 in showing the absence of any appreciable end effect in the machine.

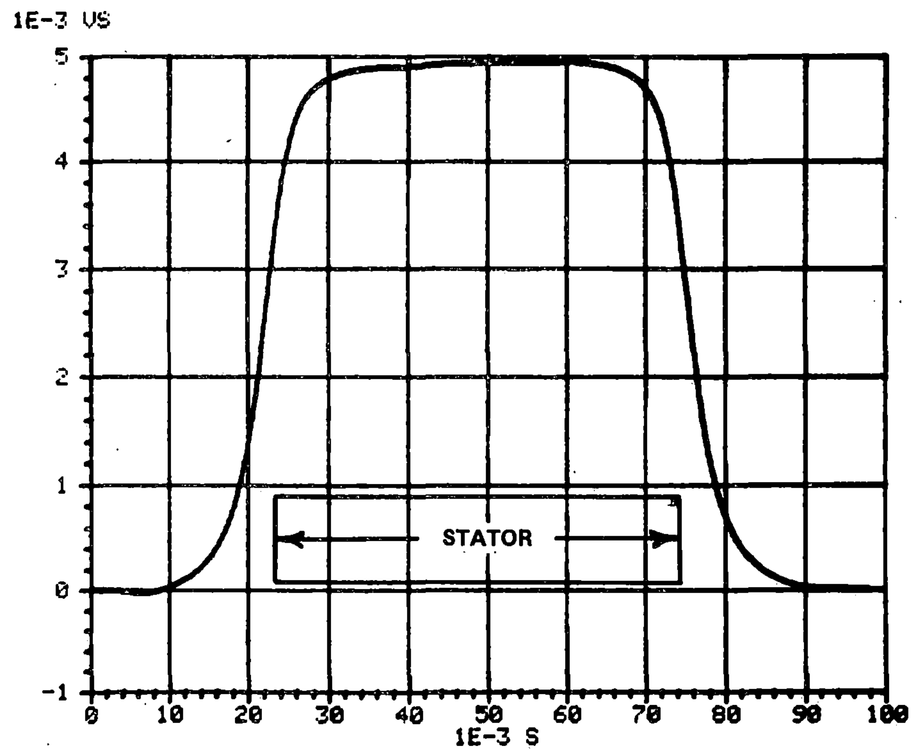

FIGURE 5-17. TRACK POLE FLUX VS. TIME (POSITION) - 60 Hertz, 240 rpm, 75 Ampere Field.

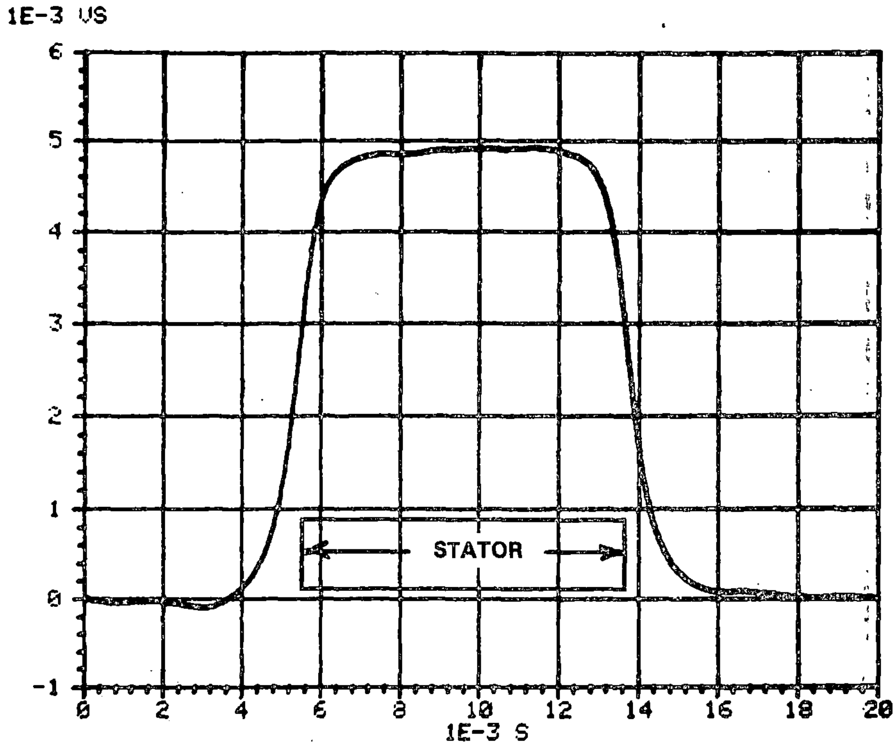

FIGURE 5-18. TRACK POLE FLUX VS. TIME (POSITION) - 150 Hertz, 600 rpm, 75 Ampere Field.

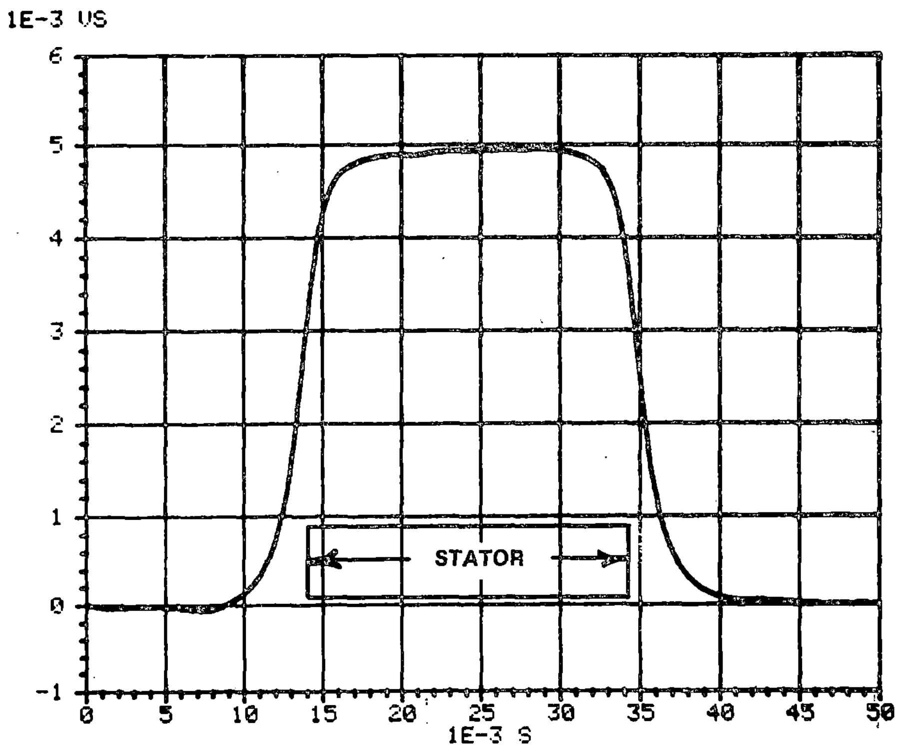

FIGURE 5-19. TRACK POLE FLUX VS. TIME (POSITION) - 382.5 Hertz, 1530 rpm, 75 Ampere Field.

Section 6

MODIFICATIONS AND CORRECTIONS TO THE HOMOPOLAR LSM DESIGN PROGRAM

The Homopolar Linear Synchronous Machine presently under test was designed with large margins of safety since the behavior of this type of machine was not well understood. First, a four-pole machine was designed which was to deliver rated thrust with 120 kW of input power. Then a fifth pole was added to the stator and taps installed so that, if necessary, the thrust could be increased by 25%. It resulted that the designer's prescience in over-designing the LSM in this way nearly compensated for the defects of the design program he was using. While the design program said the five-pole test machine should have an input power of 150 kW, the actual machine had only 95 kW of input power. (Input power is used as a performance measure since the program does not calculate losses.) By increasing the armature current above the design value, it was possible to achieve the 112 kW output power specified in the proposal.

It was thus clear that the design program had to be improved before it could be trusted to give the correct dimensions for a full-sized machine of a given rating. The program has now been modified, and agreement with the test machine data is much better. This section will describe the corrections made to the design program to achieve this improvement.

FORM FACTORS K_m AND K_u

The design program begins by reading the values of the form factors which establish the relationship between ac, dc, and peak flux density. Once these values are established, the program uses vector analysis and flux density calculations to determine the minimum required dimensions for the machine. These calculations are very similar to those performed in much more successful machine design programs. Therefore, unless this portion of the program contained a significant error, it was likely the greatest problem was with the form factor determination. When a careful study of the vector and flux density calculations revealed no major errors, a study of the form factors was begun.

The factors studied are designated K_m and K_u. The factor K_m is the ratio of peak air gap flux density to average air gap flux density. The factor K_u is equal to the total dc flux per pole divided by the ac fundamental flux per pole. Figure 6-1 shows the definition of K_m and K_u in terms of quantities measured from an air gap flux waveform. The values of K_m and K_u depend on the peak air gap flux density, the minimum air gap flux density, and fringing. The corrections made to the design program modify the value of the minimum air gap flux density to reflect the small (compared to conventional round machines) minimum-to-maximum air gap ratio and the effect of inter-armature leakage flux.

$$K_m = \frac{B_{max}}{B_{av}} \qquad K_u = \frac{\text{TOTAL DC FLUX}}{\text{FUND. AC FLUX}} = \frac{\pi B_{av}}{B_{al}}$$

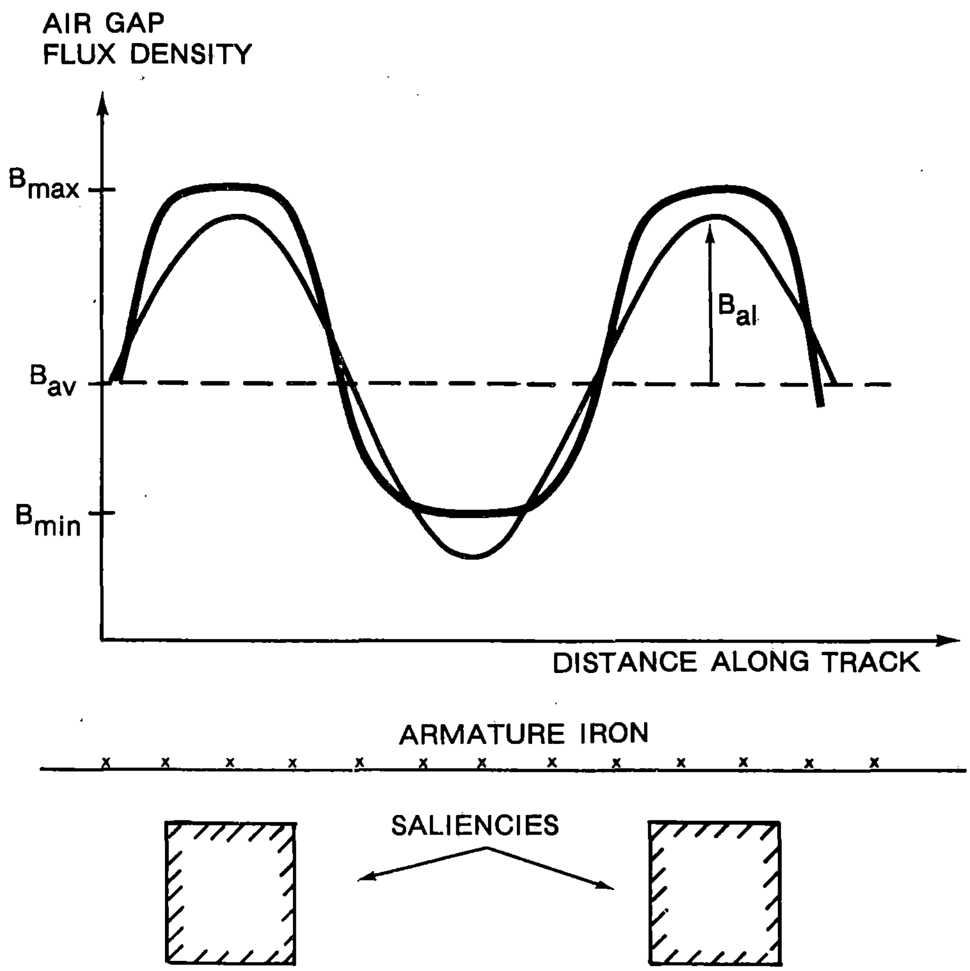

FIGURE 6-1. DESCRIPTION OF FORM FACTORS K_m AND K_u.

DEPENDENCE OF K_m AND K_u ON AIR GAP RATIO

The values of K_m and K_u are obtained from curves generated by flux plotting and assume a minimum-to-maximum gap ratio of 1/10. For small air gap machines these curves are quite satisfactory, but as the air gap ratio decreases, K_m and K_u begin to change rapidly. To find their dependence on air gap, the geometry of Figure 6-2 is used.

To simplify the calculations, the actual air gap flux distribution is replaced by a rectangular wave approximation. The average flux density is then

$$B_{aV} = B_{max}(\alpha'/2) + B_{min}(1-\alpha'/2) \tag{6-1}$$

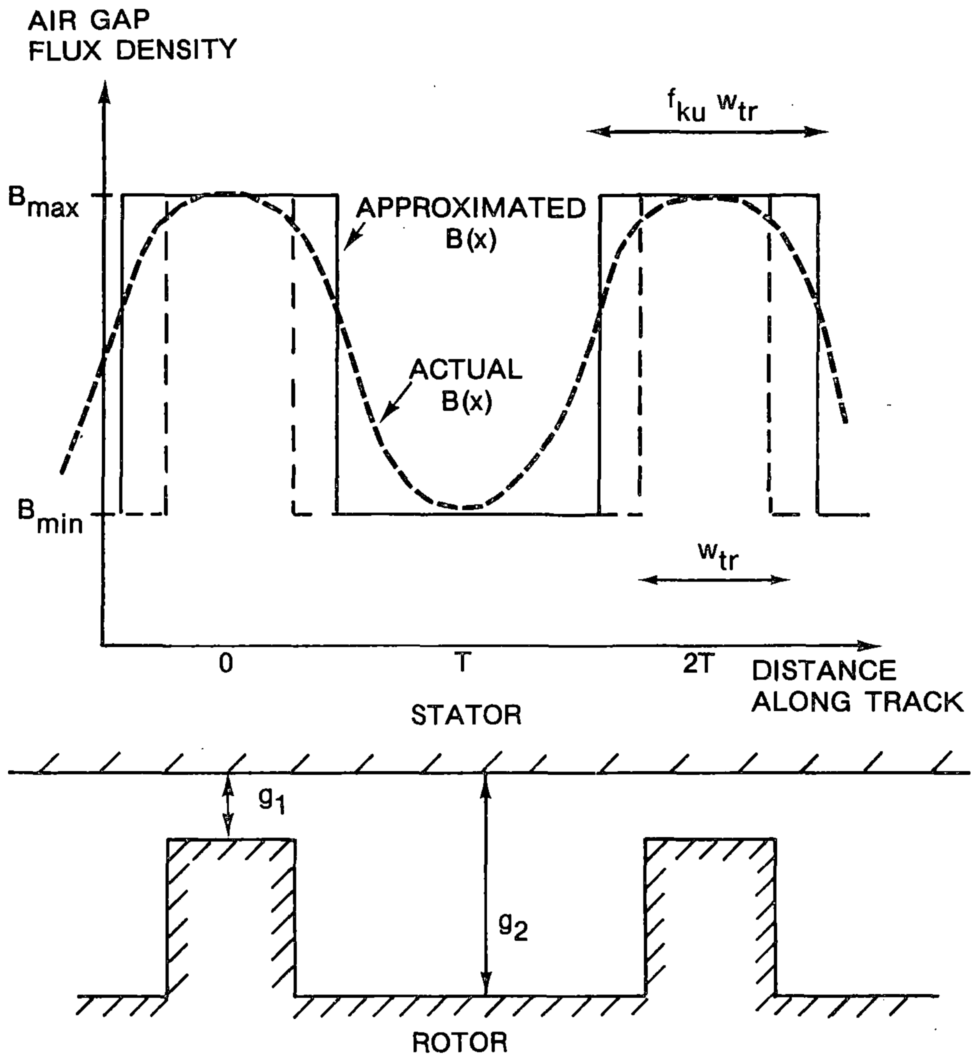

FIGURE 6-2. GEOMETRY FOR CALCULATION OF K_m AND K_u FOR VARYING GAP RATIO.

where

α' = αf_{ku}

α = per unit pole arc

f_{ku} = pole arc 'fringing' coefficient

B_{max} = maximum flux density

B_{min} = minimum flux density

The assumption that the flux density varies as the inverse of the air gap gives

$$B_{av} = B_{max}[(\alpha'/2) + (g_1/g_2)(1-\alpha'/2)] \quad (6\text{-}2)$$

where g_1 and g_2 are the minimum and maximum air gaps, respectively. The value of K_m is then

$$K_m = \frac{B_{max}}{B_{aV}} = \frac{2/\alpha'}{[1 + (g_1/g_2)(2-\alpha')/\alpha']} \tag{6-3}$$

Since the K_m curves assume $g_1/g_2 = 0.1$

$$\frac{K_m}{K_m^o} = c_{km} = \frac{1 + 0.1(2-\alpha')/\alpha'}{1 + (g_1/g_2)(2-\alpha')/\alpha'} \tag{6-4}$$

where K_m^o is the value of K_m from the flux plotting curves.

The fringing coefficient $f_{km} = \alpha'/\alpha$ is found by solving Eq. 6-3 for f_{km} yielding

$$f_{km} = \frac{2-2(g_1/g_2)K_m}{\alpha K_m - [1-(g_1/g_2)]} \tag{6-5}$$

and evaluating Eq. (4-5) at $(g_1/g_2) = 0.1$ to give

$$f_{km} = \frac{2 - 0.2\ K_m^o}{0.9\ \ \alpha\ K_m^o} \tag{6-6}$$

A corrected value of K_m is then calculated as $c_{km}\ K_m^o$. The process is iterative since the value of the interpolar gap, g_2, depends on K_m. A summary of the procedure will be given later in this report.

From Figure 6-1 the value of K_u is

$$K_u = \frac{\pi B_{aV}}{B_{a1}} = \frac{\pi B_{max}}{B_{a1}} \times \frac{B_{aV}}{B_{max}} = \frac{\pi B_{max}}{B_{a1}} \frac{1}{K_m} \tag{6-7}$$

Thus combining Eq. 6-4 with the effect of gap ratio on B_{max}/B_{a1} will be sufficient to derive the gap ratio correction factor for K_u.

Using the geometry of Figure 6-2, the fundamental fourier coefficient of the rectangular-wave flux density approximation is:

$$B_{a1} = \frac{2}{T} \int_{0}^{\alpha' T/2} B_{max} \cos \frac{\pi x}{T} dx + \frac{2}{T} \int_{\alpha' T/2}^{T} B_{min} \cos \frac{\pi x}{T} dx$$

$$= \frac{2}{\pi} B_{max} \sin \frac{\alpha' \pi}{2} - \frac{2}{\pi} B_{min} \sin \frac{\alpha' \pi}{2} \qquad (6\text{-}8)$$

$$= \frac{2 B_{max}}{\pi} (1 - g_1/g_2) \sin \frac{\alpha' \pi}{2}$$

where

T = electrical pole pitch

α' = $f_{ku} \alpha$

f_{ku} = K_u fringing coef.

α = per unit pole arc

The value of K_u is then

$$K_u = \frac{\pi}{K_m} \left(\frac{\pi}{2(1-g_1/g_2)\sin(\alpha' \pi/2)} \right) \qquad (6\text{-}9)$$

The ratio of K_u to K_u^o, the value given by the flux plotting curves, is

$$\frac{K_u}{K_u^o} = c_{ku} = \frac{K_m^o}{K_m} \left(\frac{1-0.1}{1-g_1/g_2} \right) = \frac{0.9}{c_{km}\left[1-g_1/g_2\right]} \qquad (6\text{-}10)$$

The procedure to calculate the correct value for K_u is again iterative since the interpolar gap is a function of K_u.

INTERARMATURE FLUX CORRECTION

The path for interarmature flux is shown in Figure 6-3a. This flux increases the flux density in the interpolar region and changes the values of K_m and K_u in much the same way as decreasing the interpolar gap does. Therefore, a relatively simple way to correct for the effect of interarmature flux is to decrease the effective interpolar gap.

The first step in determining this new gap is to calculate a permeance for the interpolar gap. The formula given by Professor Enrico Levi of Polytechnic Institute of New York

$$P_{IA} = (\mu_o/\pi) \ln (1 + w_a/w_f)$$

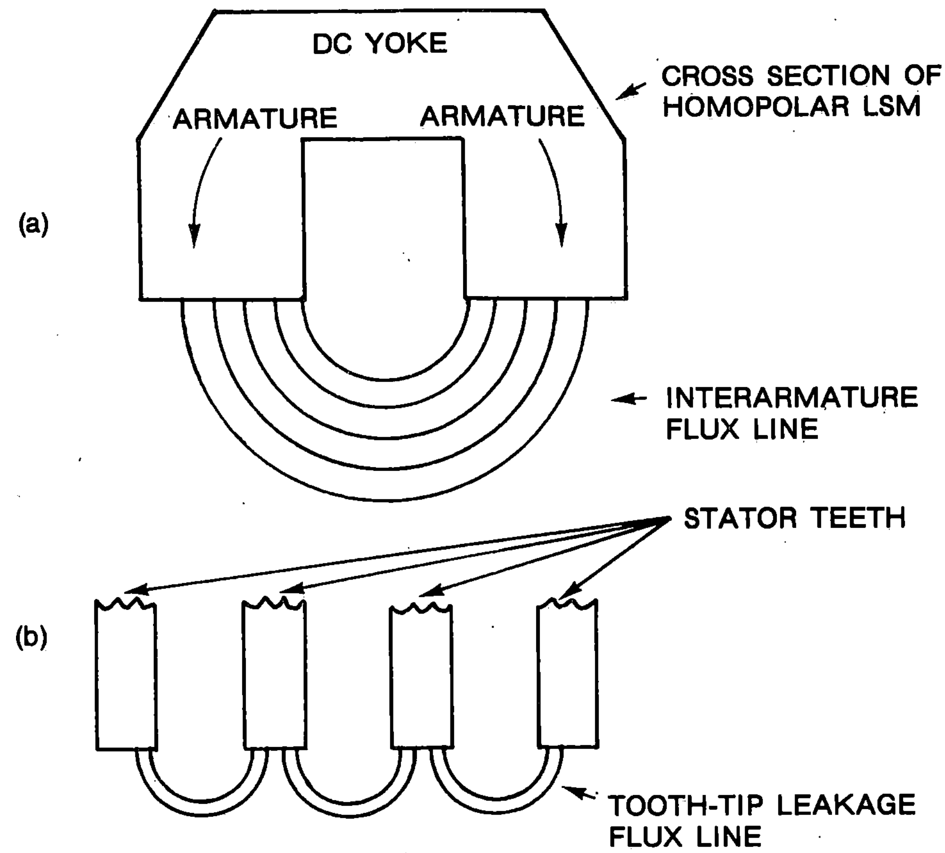

FIGURE 6-3. INTERARMATURE FLUX IN HOMOPOLAR LINEAR SYNCHRONOUS MOTOR AND ANALOGY TO TOOTH-TIP LEAKAGE FLUX.

where w_a and w_f are the widths of the armature (both sides), and field space, respectively, was not used since it is independent of the air gap. Such a formula cannot account for the fact that interarmature flux is much smaller for small air gap machines than for ones with large air gaps.

A more realistic expression was found by noting that flux paths very similar to those of the interarmature flux have long been identified between the stator teeth of conventional machines. Figure 6-3b shows this similarity by showing the flux lines of stator tooth-tip leakage flux. According to Liwschitz-Garik and Wipple[3] the permeance for tooth tip leakage is

$$P_{tt} = \frac{\mu_o g}{w_f + 0.8g}$$

[3] Electric Machinery, Vol. I.D. Van Nostrand, New York, 1946.

where g is the air gap. This formula is the result of a curve fit to data obtained by plotting the flux lines of a geometry like that of Figure 6-3a, further strengthening the argument that Eq. 6-11 is a good representation of interarmature flux permeance. Thus the permeance for interarmature flux will be taken as

$$P_{IA} = \frac{\mu_o \, g_2}{w_f + 0.8 \, g_2} \tag{6-11}$$

where g_2 is the interpolar gap. The flux density due to interarmature flux is then

$$B_{IA} = \frac{P_{IA} \times mmf_a}{w_a/2} \tag{6-12}$$

where mmf_a is the armature mmf. The interpolar flux density due to flux which enters the iron in the interpolar region is

$$B_{min} = \frac{\mu_o \, mmf_a}{g_2} \tag{6-13}$$

which gives a ratio of B_{IA} to B_{min} as

$$\frac{B_{IA}}{B_{min}} = \frac{2 \, g_2^2}{w_a (w_f + 0.8 \, g_2)} \tag{6-14}$$

The effect of interarmature flux can now be incorporated into B_{min} to form

$$B_{min} = B_{min} \left(1 + \frac{B_{IA}}{B_{min}} \right) = \frac{\mu_o \, mmf_a}{g_2} \tag{6-15}$$

where g_2 is a corrected interpolar air gap and is given by

$$g_2' = g_2 \left[1 + \frac{2 \, g_2^2}{w_a (w_f + 0.8 g_2)} \right]^{-1}$$

$$= \frac{g_2 \, w_a \, (w_f + 0.8 g_2)}{w_a (w_f + 0.8 g_2) + 2 \, g_2^2} \tag{6-16}$$

The revised design program replaces the calculated interpolar gap, g_2, by the value g_2 to account for the effect of interarmature flux.

PROGRAM SEQUENCE TO CORRECT K_m AND K_u

The corrections for variable interpolar gap and interarmature flux are incorporated into the design program by the following sequence:

1. Determine K_m^o and K_u^o from the flux plotting curves
2. Calculated f_{km} using Eq. 6-6.
3. Calculate the 'fringed' per unit pole arc $\alpha' = f_{km}\alpha$.
4. Calculate g_2' using Eq. 6-16 (the program supplies g_2).
5. Calculate c_{km} from Eq. 6-4 using g_2'.
6. Calculate c_{ku} from Eq. 6-10 using g_2'.
7. Calculate $K_m^1 = c_{km}\ K_m^o$ and $K_u^1 = c_{ku}\ K_u^o$.
8. Recalculate interpolar gap g_2 using K_m^1 and K_u^1.
9. Recalculate g_2' from new g_2.
10. Recalculate c_{km} and c_{ku} from new g_2'.
11. Calculate $K_m^2 = c_{km}\ K_m^o$ and $K_m^2 = c_{ku}\ K_u^o$.
12. Repeat sequence of steps 8 through 11 until $(K_m^n - K_m^{n-1})/K_m^n$ $<0.5\%$.

Usually two to four iterations are sufficient to meet the criterion of Step 12.

The original version of the design program is discussed in Section 6 of the Phase III Final Report. It has two main programs: one to calculate machine parameters and the second to calculate machine dimensions. The corrections discussed so far are incorporated into the second program, a list of which is given in the Phase III report.

Several other program modifications were also made to help design a more realistic machine or to correct errors. The more important of this category are:

1. Inclusion of a calculation of estimated temperature rise of armature and field windings.
2. Inclusion of a variable-sized space for cooling ducts in the field windings.
3. Modification of vector algebra to allow the design of a machine with a leading power factor.

4. Inclusion of field yoke ampere-turns into design procedure.

5. Modification of tooth-tip and end-turn armature leakage reactance calculations.

Modification Number 1 showed a serious heating problem in the field windings contained in the interpolar space.

VERIFICATION OF CORRECTIONS FOR 112 kW TEST LSM

As a verification of the modified design program a type of backward design was performed for the 112 kW homopolar linear synchronous machine presently being tested. Since the total length of the machine is fixed by the speed, frequency, and number of poles, armature width is the most important single dimension which specifies a machine's flux distribution and power. Accordingly, the rated voltage in the design program's input data was varied until the designed machine had the same armature width as the test LSM. Table 6-1 compares the main parameters and dimensions of the machine so designed to the test machine values. The first column of the table lists these values as given by the unmodified design program (in the run which finalized the test machine's dimensions).

The flux density levels needed to calculate the test values of K_m and K_u are taken from Section 5 of this report. These give the 75 A field current values of

$$K_m = \frac{7.40}{4.04} = 1.83 \tag{6-17}$$

and

$$K_u = \frac{\pi \times 4.04}{2.68} = 4.74 \tag{6-18}$$

The correlation to the modified design program values of $K_m = 1.75$ and $K_u = 4.83$ is very good. In addition the field current of the design program is 90 A while that of the test machine (for this data) is 75 A. A higher field current would lower K_m and raise K_u because of saturation effects, further improving the agreement.

The values taken from the original design program of $K_m = 2.03$ and $K_u = 2.82$ show K_m was reasonably close but the K_u was almost 60% too low. The effect of this error in K_u was to underestimate severely the total flux which had to cross the air gap to make a given rating. Thus when the originally calculated value of total air gap flux crosses the air gap of the test machine, the power delivered is only about 60% of the designed value.

This result is seen in the power calculations for the design programs and the test machine. While the December 1976 design said the machine would have an input power of 3 x 370 x 140 = 156 kW, the test machine had only 3 x 370 x 120 x 0.7 = 93 kW. The

TABLE 6-1. COMPARISON BETWEEN TEST DATA AND ORIGINAL AND REVISED VERSIONS OF DESIGN PROGRAM FOR 112 kW HOMOPOLAR LSM

	Dec. '76 Design Program (final design run	April '78 Design Program	Test Data
Speed (mph)	250.000	250.000	250.000
Frequency (Hz)	394.300	394.300	394.300
Poles	5.000	5.000	5.000
P.U. Pole Arc	0.500	0.500	0.500
Phase Current (A)	370.000	370.000	370.000
Voltage (L-N)	140.000	87.000	120.000
Power Factor	1.000	1.000	0.700
Phase Resistance (Ω@ 40^{o}C)	0.0134	0.0134	0.011
Arm. Leak. Reac. (Ω)	0.165	0.143	-
d-axis Reac. (Ω)	0.312	0.308	0.30$\pm$.01
d-axis Reac. (Ω)	0.284	0.279	0.27$\pm$.01
d-axis Trans. Reac. (Ω)	0.239	0.265	0.27$\pm$.02
Commutating Reac. (Ω)	0.261	0.272	0.27$\pm$.01
K_u (ratio dc to ac flux)	2.82	4.83	4.74
K_m (ratio peak to aug. flux density)	2.03	1.75	1.83
Field Current (A)	75.30	90.80	85.00
Field resistance (Ω@75^{o}C)	-	0.64	-
Stator width (cm)	25.00	25.00	25.00
Stator length (cm)	70.90	70.90	70.90
Stator height (cm)	9.08	12.47	-
Stator weight (kg)	170.00	212.00	-
Pole piece height (cm)	7.48	8.53	7.62
Pole piece weight (kg)	10.40	11.80	-

modified design program now says the test machine's input power would be 3 x 370 x 87 = 97 kW, a marked improvement.

Taken together, the results of this section indicate that the original design program did a poor job of determining the dimensions of the large air gap homopolar linear synchronous machines being studied; but also that the program as now modified should accurately determine the required size of the full-scale linear synchronous motors which appear in the Phase III SLEM final report.

Section 7

EXPERIMENTAL DATA

In this section, the method of data collection and reduction is explained, and the computer program(s) used for data reduction presented. A catalog of Appendix I is also included.

DATA ACQUISITION

The data presented here for the LSM was obtained using the data acquisition system described in Section 1 of the Phase II report, with appropriate changes of channel assignments to function with the synchronous machine. Table 7-1 contains a listing of the data channel assignments for this motor. Most of these are self-explanatory, but a few comments are in order. The force sensors A through J are ordered as shown in Figure 4-1 of Section 4. The airgap flux coils are centered over the odd-numbered stator slots, Numbers 1 - 35 (18 coils), while the yoke coils are wound around the laminated stack from the bottom of the associated slot to the bottom of the laminations. The butt coils cover the ends of the laminated stacks to measure axial flux out the ends.

Phase voltages and currents are measured as true rms values, while phase watts are averaged over time. The inverter firing angle signal is a dc voltage in the inverter control related to the angle-of-lead of firing pulses ahead of motor back emf. Speed and torque signals are averages coming from the shaft torque transducer, while dc link volts and amperes are averaged values from a scope probe and a current transducer attached to the link between rectifier and inverter.

The vertical force sensors can go both positive and negative in force, so their data channels have been given a 5.00 volt offset, upward force reducing the output voltage, downward increasing it. The lateral force sensors were preloaded against each other in pairs, as were the thrust or axial force sensors. This procedure increased the ability of the system to measure relatively small forces on the stator.

The airgap flux coils, all 18 of them, were 0.951 in. x 2.36 in. (2.42 x 5.99 cm) and were connected through RC integrators to produce a signal proportional to the ac flux cutting them. The yoke and butt coil outputs were treated similarly, but their areas differed. The yoke coils at Slots Numbers 6 and 30 were 4.938 x 2.313 in. (12.54 x 5.88 cm), at Slots Numbers 12 and 24 were 3.156 x 2.313 in. (8.02 x 5.88 cm), and the one at Slot Number 18 was 2.563 x 2.313 in. (6.51 x 5.88 cm). The butt coils were 1.813 x 7.063 in. (4.60 x 17.94 cm). All of these coils were treated to give flux densities as output in the data reduction program but can be used to give total flux, with the dimensions above.

TABLE 7-1. LSM DATA CHANNEL ASSIGNMENTS

1 - 3	Phase Volts A,B,C respectively
4 - 6	Phase A, A,B,C respectively
7 - 9	Phase Watts A,B,C respectively
10	Firing Angle of Inverter
11	Speed
12	Torque
13	dc Link Volts
14	dc Link A
15 - 18	Vertical Force Sensors A - D, respectively
19 - 22	Lateral Force Sensors E - H, respectively
23 - 24	Axial (Thrust) Force Sensors I, J respectively
25	Not Used
26 - 43	Airgap Flux Coils
44 - 48	Not Used
49	Yoke Flux Coil @ Slot #6
50	Yoke Flux Coil @ Slot #12
51	Yoke Flux Coil @ Slot #18
52	Yoke Flux Coil @ Slot #24
53	Yoke Flux Coil @ Slot #30
54	Butt Flux Coil - Lead - 752 Side
55	Butt Flux Coil - Lead LSM Side
56	Butt Flux Coil Trail - 752 Side
57	Butt Flux Coil Trail - LSM Side
58	Not Used
59	Temperature - Endturn Near Slot #8
60	Temperature - Endturn Near Slot #16
61	Temperature - Endturn Near Slot #23
62	Temperature - In Slot, #8
63	Temperature - In Slot, 752 Side, #16
64	Temperature - In Slot, 752 Side, #23
65	Temperature - In Slot, LSM Side, #16
66	Temperature - Care, LSM Side, Near Slot #8
67	Temperature - Dogbone
68	Temperature - Yoke
69	Temperature - Inboard Bearing
70	Temperature - Outboard Bearing
71	dc Motor Armature Volts
72	dc Motor Armature A
73	dc Motor Field A
74	Not Used
75	LSM Field Volts
76	LSM Field A
77	Not Used

Temperature channels were noisy in operation, but the average of three readings proved fairly accurate during testing. The dc motor armature current channel was never made meaningful, but voltage and field current were fairly accurate. LSM field voltage and current were obtained from the field rectifier output, averaged to get rid of rectifier ripple.

A sample data reduction program showing the conversion factors and logic used and a sample run from that program follow (Figure 7-1). These examples are from the analysis of the solid track machine, but differ only in minor detail from the laminated track ones. Variations on this program were made to suit different speeds and motoring and generating conditions as necessary. These variations included changes to voltage and watts channel calibrations, friction and windage calculations, and sign changes on torques and watts, and have not been included here due to their simple nature.

```
10*#RUN*:TSSLIB/RLINE,R=(NWARN)#DATA"10"
20 CHARACTER POS*1(10)/1HA,1HB,1HC,1HD,1HE,1HF,1HG,1HH,1HI,1HJ/
30 CHARACTER POBUTT*1(2)/1HI,1HO/
40 REAL NM1,NM2,NM3,MAX1,MAX2
50 REAL MAX3,MAX4,MAX5,MAX6,MAX7
60 CHARACTER STORE*18,STOR1*30
70 CHARACTER DATE*8,TIME*5
80 DIMENSION ISTART(5),C(400),F2(10)
90 DIMENSION V(3)
100 DIMENSION F(10)
110 CHARACTER IBUF*72
120 INTEGER RNO, DRPM, HZ, AMP
130C
140C IDENTIFICATION(DATE,TIME,RUN NUMBER,RPM, FREQUENCY,
150C AND AMPS) IS READ FROM THE FIRST
160C LINE OF FILE "DATA" AND PRINTED AT THE TOP OF THE REPORT.
170C THE FIRST 2 ITEMS ARE IN THE FORM XX/XX/XX AND XX:XX
180C AND THE REMAINING ARE INTEGERS. ALL ITEMS ARE SEPARATED
190C BY BLANKS.
200C
210C
220 READ (10,20) DATE,TIME,RNO,DRPM,HZ,AMP
230 PRINT 66
240 66 FORMAT(1X////////"DATE",T11,"TIME",T19,"RN#",T26,"RPM",
250 & T35,"HERTZ ",T45,"AMPS"//)
260 PRINT 67,DATE,TIME,RNO,DRPM,HZ,AMP
270 67 FORMAT(1X,A8,T12,A5,T19,I4,T27,I4,T35,I4,T45,I4,
280 & //////)
290 LSW=3
300 I=1
310C
320C THE REMAINING DATA ITEMS ARE READ AND PLACED IN THE ARRAY
330C (C). POINTERS ARE SET UP TO THE BEGINNING OF THE THREE SETS
340C OF DATA(-1 SIGNALS THE END OF A DATA SET: -2 SIGNALS THE
350C END OF DATA:THE FIRST ITEM IN EACH SET IS THE STARTING
360C CHANNEL NUMBER,WHICH IS IGNORED).
370C
380 10 CALL RLINE(10,IENT,LSW,IBUF,$30,$50,$50)
390 DECODE(IBUF,20)(C(I),I=I,I+(IENT-1))
400 I=I+1
410 20 FORMAT(V)
420 GO TO 10
430 30 N=1
440 ISTART(N)=2
450 DO 40 M=1,I
460 IF(C(M).NE.-1)GO TO 40
470 IF(C(M+1).EQ.-2)GO TO 60
480 N=N+1
490 ISTART(N)=M+2
500 40 CONTINUE
510 50 PRINT," ERROR RETURN"
520 GO TO 310
530 60 PRINT 65
540 65 FORMAT(1X,"SENSOR#",T15,"1ST READING",T30,"2ND READING",
```

FIGURE 7-1. SAMPLE RUN FROM A SAMPLE DATA REDUCTION PROGRAM.

```
550 & T45,"3RD READING",T60,"AVERAGE")
560C
570C THE THREE SETS OF DATA ARE AVERAGED AND THE VALUES STORED
580C AT THE END OF ARRAY (C). THESE VALUES ARE USED IN THE
590C CALCULATIONS. THE 3 VOLTAGE READINGS AND THE
600C AVERAGE ARE PRINTED OUT.
610C
620 I1=ISTART(1);I2=ISTART(2);I3=ISTART(3);I4=M+1
630 DO 62 I=1,ISTART(2)-4
640 C(I4)=(C(I1)+C(I2)+C(I3))/300.
650 PRINT 64,I,C(I1)/100.,C(I2)/100.,C(I3)/100.,C(I4)
660 64 FORMAT(1X,T3,I2,T14,F7.4,T29,F7.4,T44,F7.4,T59,F7.4)
670 I1=I1+1;I2=I2+1;I3=I3+1;I4=I4+1
680 62 CONTINUE
690C
700C THE REMAINDER OF THE PROGRAM DEALS WITH MAKING CALCULATIONS
710C (MULTIPLYING THE CONVERSION FACTOR BY THE VOLTAGE READING
720C FROM THE TAPE) AND PRINTING THEM FOR THE FIRST 79 SENSOR
730C READINGS.
740C
750 IB=M+1;IS=1
760 PRINT 23
770 STORE="VOLTS"
780 PRINT 11,STORE
790 11 FORMAT(" LINE",T20,"SENSOR#",T40,"CFACTOR",T60,A6)
800 DO 80 I=1,3
810 IF (I.EQ.1) V1=140.11
820 IF (I.EQ.2) V1=139.34
830 IF (I.EQ.3) V1=137.10
840 V2=V1*(C(IB))
850 V(I)=V2
860 PRINT 12,I,IS,V1,V2
870 12 FORMAT(I2,"-N",T22,I1,T39,F10.4,T58,F10.4)
880 IS=IS+1;IB=IB+1
890 80 CONTINUE
900 PRINT 24
910 STORE="AMPS"
920 PRINT 11,STORE
930 VOLAMP=0.
940 DO 90 I=1,3
950 IF (I.EQ.1) A1=94.97
960 IF (I.EQ.2) A1=96.71
970 IF (I.EQ.3) A1=94.44
980 A2=A1*(C(IB))
990 VOLAMP=A2*V(I)+VOLAMP
1000 PRINT 12,I,IS,A1,A2
1010 IS=IS+1;IB=IB+1
1020 90 CONTINUE
1030 PRINT 25
1040 STORE="KWATTS"
1050 PRINT 11,STORE
1060 RK3=0.
1070 DO 100 I=1,3
1080 IF (I.EQ.1) RK1=12.704
1090 IF (I.EQ.2) RK1=14.155
1100 IF (I.EQ.3) RK1=11.724
1110 RK2=RK1*(C(IB))
1120 PRINT 12,I,IS,RK1,RK2
```

FIGURE 7-1. SAMPLE RUN FROM A SAMPLE

```
RK3=RK2+RK3
IS=IS+1;IB=IB+1
100 CONTINUE
PRINT 122,RK3
122 FORMAT(1X/T39,"TOTAL KWATTS=",T58,F10.4/)
PRINT 44
44 FORMAT(1X,//T20,"SENSOR#",T40,"CFACTOR")
13 FORMAT(1X,A18,T22,I2,T39,F10.4,T58,F10.4)
DA1=30.93
DA2=DA1*(C(IB))-85.7
STORE="DELTA ANGLE"
PRINT 13,STORE,IS,DA1,DA2
IB=IB+1;IS=IS+1
RS1=200.
RS2=RS1*(C(IB))
STORE="ROTOR SPEED(RPM)"
PRINT 13,STORE,IS,RS1,RS2
IB=IB+1;IS=IS+1
NM1=300.
NM2=NM1*(C(IB))
STORE="SHAFT TORQUE(NM)"
PRINT 13,STORE,IS,NM1,NM2
FW=.00020633*(DRPM**2.0)
STORE="F&W TORQUE(NM)="; PRINT 13,STORE,IS,NM1,FW
NM3=FW+NM2
STORE="ELECTRO-MAG TORQUE(NM)=";PRINT 13,STORE,IS,NM1,NM3
IB=IB+1;IS=IS+1
DCV1=34.9
DCV2=DCV1*(C(IB))
STORE="DC LINK VOLTS"
PRINT 13,STORE,IS,DCV1,DCV2
IB=IB+1;IS=IS+1
DCA1=102.6
DCA2=DCA1*(C(IB))
STORE="DC LINK AMPS"
PRINT 13,STORE,IS,DCA1,DCA2
IB=IB+1;IS=IS+1
C
C CALCULATE AND PRINT POWER OUTPUT VALUES.
C
RKW=NM3*DRPM*.00010477
HP=RKW/.746
TR=NM3/.6929
EF=(RKW/RK3)*100.
PRINT 45
STOR1="KW=";PRINT 42,STOR1,RKW
STOR1="HP=";PRINT 42,STOR1,HP
STOR1="THRUST(NEWTONS)=";PRINT 42,STOR1,TR
STOR1="EFF(NOT INC FLD)=";PRINT 42,STOR1,EF
POFA=1000.0*RK3*100.0/VOLAMP
STOR1="POWER FACTOR(%)=";PRINT 42,STOR1,POFA
STOR1="KVA=";PRINT42,STOR1,(VOLAMP/1000.0)
STOR1="EFF X PF (PU)=";PRINT 42, STOR1,(EF*POFA/10000.0)
C FREQ IS CAL FROM HEADING RPM
STOR1="FREQUENCY(HZ)=";PRINT 42,STOR1,(.25*DRPM)
PRINT 26
PRINT 14
14 FORMAT(1X,"POSITION",T20,"SENSOR#",T40,"CFACTOR",T60,"NEWTONS")
```

DATA REDUCTION PROGRAM (CONTINUED).

```
1710C
1720C THE 10 FORCE CALCULATIONS ARE STORED IN ARRAY (F2) TO BE USED
1730C IN THE LATER CALCULATIONS ON THE FORCES.
1740C
1750 F(1)=890.; F(2)=F(1); F(3)=F(1); F(4)=F(1)
1760 F(5)=550.; F(6)=F(5)
1770 F(7)=558.; F(8)=F(7)
1780 F(9)=456.79; F(10)=F(9)
1790C
1800 DO 109 I=1,4
1810C ATTRACTION PRODUCES A POSITIVE F(2) FOR I=1,4
1820 F2(I)=F(I)*(5.00-C(IB))
1830 PRINT 15,POS(I),IS,F(I),F2(I)
1840 IB=IB+1; IS=IS+1
1850 109 CONTINUE
1860C
1870 DO 110 I=5,10
1880 F2(I)=F(I)*(C(IB))
1890 PRINT 15,POS(I),IS,F(I),F2(I)
1900 15 FORMAT(3X,A1,T22,I2,T38,F10.4,T58,F10.4)
1910 IB=IB+1; IS=IS+1
1920 110 CONTINUE
1930C
1940C A NUMBER OF CALCULATIONS ARE MADE USING THE FORCE VALUES
1950C IN THE ARRAY (F2) AND PRINTED OUT BY THE STATEMENTS FOLLOWING.
1960C
1970 RAD=.693; RL=.762; W=.1524; P=.203
1980 C1=(F2(10)-F2(9))/(F2(1)+F2(2)+F2(3)+F2(4))
1990 BETA=ATAN(C1)
2000 RES=(F2(10)-F2(9))/SIN(BETA)
2010 CC2=(((F2(4)+F2(3)-F2(2)-F2(1))*RL)/2.0)+(F2(9)-F2(10))*(RAD+P)
2020 ALPHA=ARSIN((SIN(BETA)*CC2)/(RAD*(F2(9)-F2(10))))
2030 THETA=BETA-ALPHA
2040 A=RES*COS(ALPHA)
2050 T=RES*SIN(ALPHA)
2060 FTAIL=F2(8)-F2(7)
2070 FLEAD=F2(6)-F2(5)
2080 PTQ=((F2(1)+F2(2))-(F2(3)+F2(4)))*(RL/2.0)
2085 PTQ=-PTQ
2090 YTQ = (FLEAD-FTAIL)*(RL/2.0)
2100 RTQ=((F2(2)+F2(4))-(F2(1)+F2(3)))*(W/2.0)
2105 RTQ=-RTQ
2110 FLAT = FLEAD+FTAIL
2120 PRINT 41
2122 SVS=F2(1)+F2(2)+F2(3)+F2(4)
2123 STOR1="SUM OF VERTICAL FORCES="; PRINT 42, STOR1, SVS
2127 STOR1="DIFFERENCE OF THRUSTS="; PRINT 42, STOR1, (F2(10)-F2(9)
2130 STOR1="RESULTANT OF TZA=";PRINT 42,STOR1,RES
2140 STOR1="FORCE ANGLE OF RESULTANT=";PRINT 42,STOR1,ALPHA
2150 STOR1="LOCATION OF RESULTANT=";PRINT 42,STOR1,THETA
2160 STOR1="RADIAL FORCE=";PRINT 42,STOR1,A
2170 STOR1="TANGENTIAL THRUST=";PRINT 42,STOR1,T
2180 STOR1="PITCH TQ=";PRINT 42,STOR1,PTQ
2190 STOR1="ROLL TQ=";PRINT 42,STOR1,RTQ
2200 STOR1="YAW TQ=";PRINT 42,STOR1,YTQ
2210 STOR1="LATERAL FORCE=";PRINT 42,STOR1,FLAT
2220 STORE="POSITION"
2230 PRINT 27
2240 PRINT 16,STORE
2250 16 FORMAT(1X,A11,T14,"SENSOR#",T24,"CFACTOR",T36,
```

FIGURE 7-1. SAMPLE RUN FROM A SAMPLE

```
2260 & "PEAK",T48,"CFACTOR",T60,"RMS")
2270C
2280C
2290 MAX1=.228; RMS1=MAX1/1.414
2300 IB=IB+1; IS=IS+1
2310 DO 120 I=1,35,2
2320 RMS2=RMS1*(C(IB))
2330 MAX2=MAX1*(C(IB))
2340 PRINT 17,I,IS,MAX1,MAX2,RMS1,RMS2
2350 17 FORMAT(1X,"SLOT ",I2,T16,I2,T22,F10.4,T34,F10.4,T46,
2360 & F10.4,T59,F10.4)
2370 IB=IB+1;IS=IS+1
2380 120 CONTINUE
2390 IB=IB+5; IS=IS+5
2400 STORE="YOKE BELOW:"
2410 PRINT 16,STORE
2420 DO 130 I=6,30,6
2430 IF(I.EQ.6) MAX1=.0863
2440 IF(I.EQ.12) MAX1=.1351
2450 IF(I.EQ.18) MAX1=.1664
2460 IF(I.EQ.24) MAX1=.1351
2470 IF(I.EQ.30) MAX1=.0863
2480 RMS1=MAX1/1.414
2490 RMS4=RMS1*(C(IB))
2500 MAX4=MAX1*(C(IB))
2510 PRINT 17,I,IS,MAX1,MAX4,RMS1,RMS4
2520 IB=IB+1;IS=IS+1
2530 130 CONTINUE
2540 DO 131 I=1,2,1
2550 MAX1=.077; RMS1=MAX1/1.414
2560 RMS6=RMS1*(C(IB))
2570 MAX6=MAX1*(C(IB))
2580 PRINT 18,"BUTT-LEAD ",POBUTT(I),IS,MAX1,MAX6,RMS1,RMS6
2590 18 FORMAT(1X,A10,T13,A1,T16,I2,T22,F10.4,T34,F10.4,T46,
2600 & F10.4,T59,F10.4)
2610 IB=IB+1;IS=IS+1
2620 131 CONTINUE
2630 DO 132 I=1,2,1
2640 RMS7=RMS1*(C(IB))
2650 MAX7=MAX1*(C(IB))
2660 PRINT 18,"BUTT-TRAIL",POBUTT(I),IS,MAX1,MAX7,RMS1,RMS7
2670 IB=IB+1;IS=IS+1
2680 132 CONTINUE
2690 PRINT 28
2700 PRINT 19,"CELSIUS  "
2710 19 FORMAT(1X,"  POSITION",T20,"SENSOR#",T40,"CFACTOR",T60,A9)
2720 IB=IB+1;IS=IS+1
2730 T1=21.33
2740 DO 140 I=1,12
2750 T2=T1*(C(IB))
2760 PRINT 21,I,IS,T1,T2
2770 21 FORMAT(1X,T6,I2,T22,I2,T39,F10.4,T58,F10.4)
2780 IB=IB+1;IS=IS+1
2790 140 CONTINUE
2800 PRINT 29
2810 V1=54.7
2820 V2=V1*(C(IB))
2830 STORE="VOLTS"
2840 PRINT 13,STORE,IS,V1,V2
2850 IB=IB+1;IS=IS+1
```

DATA REDUCTION PROGRAM (CONTINUED).

```
AM1=50.
AM2=AM1*(C(IB)-5.00)
STORE="AMPS"
PRINT 13,STORE,IS,AM1,AM2
IB=IB+1;IS=IS+1
FAM1=20.04
FAM2=FAM1*(C(IB))

STORE="FLD AMPS"
PRINT 13,STORE,IS,FAM1,FAM2
IB=IB+1; IS=IS+1
IB=IB+1; IS=IS+1
PRINT 47
47 FORMAT(1X//T25,"SLEW FIELD"//T20,"SENSOR#",T40,"CFACTOR")
S1=11.19
S2=S1*(C(IB))
STORE="VOLTS"
PRINT 13,STORE,IS,S1,S2
IB=IB+1; IS=IS+1
S3=12.66
S4=S3*(C(IB))-4.2
STORE="AMPS"
PRINT 13,STORE,IS,S3,S4
S24=S2*S4/1000.
PRINT 48,S24
48 FORMAT(1X,"KILOWATTS=",T15,F10.4)
EF2=(RKW/(RK3+S24))*100.
PRINT 49,EF2
49 FORMAT(1X,"EFF(INC FLD)=",T15,F10.4)
IB=IB+1; IC=IC+1
23 FORMAT(1X//T20,"VOLTS - LINE TO NEUTRAL"//)
24 FORMAT(1X//T25,"AMPS - LINE"//)
25 FORMAT(1X//T20,"KWATTS - LINE TO NEUTRAL"//)
26 FORMAT(1X//T25,"FORCE"//)
27 FORMAT(1X//T20,"FLUX DENSITY IN TESLA"//)
28 FORMAT(1X//T25,"MOTOR TEMP"//)
29 FORMAT(1X//T25,"DC MOTOR"//T20,"SENSOR#",T40,"CFACTOR")
41 FORMAT(1X,///T18,"REDUCTION OF SENSOR FORCES TO
& RESULTANT FORCES"//)
42 FORMAT(1X,A30,F10.4)
45 FORMAT(1X//T25,"POWER OUTPUT"//)
310 STOP;END
   SUBROUTINE TEST
   CHARACTER PAUSE*4
   PRINT, "   WHAT NEXT?"
   READ, PAUSE
   IF(PAUSE .EQ. "RUN") RETURN
   STOP
   END
```

DATE

6/21/78

SENSOR#
1
2
3
4
5
6
7
8
9
10
11
12
13
14
15
16
17
18
19
20
21
22
23
24
25
26
27
28
29
30
31
32
33
34
35
36
37
38
39
40

FIGURE 7-1. SAMPLE RUN FROM A SAMPLE DATA

TIME	RN#	RPM	HERTZ	AMPS
18:14	212	1530	383	575

1ST READING	2ND READING	3RD READING	AVERAGE
1.5600	1.6200	1.6200	1.6000
1.6700	1.6800	1.6600	1.6700
1.5900	1.5900	1.5800	1.5867
5.9000	5.8700	5.8900	5.8867
5.8100	5.8000	5.8100	5.8067
5.9500	5.9900	5.9800	5.9733
3.6400	3.5000	3.6200	3.5867
3.6500	3.6700	3.6500	3.6567
3.6900	3.6300	3.6800	3.6667
1.8300	1.8300	1.8400	1.8333
7.8600	7.8600	7.8500	7.8567
0.6700	0.6800	0.7100	0.6867
7.9400	7.8800	7.8300	7.8833
7.3500	7.3600	7.3400	7.3500
3.5300	3.5700	3.4900	3.5300
4.0500	4.0400	4.0100	4.0333
2.8200	3.0200	2.9500	2.9300
2.9200	2.6800	2.6600	2.7533
0.2600	0.3900	0.4200	0.3567
0.7200	0.6700	0.6200	0.6700
0.7800	0.8300	0.9300	0.8467
0.8800	0.9100	0.8400	0.8767
0.0100	0.	0.	0.0033
4.0500	4.0700	2.0800	3.4000
0.1900	0.1900	0.1900	0.1900
0.4100	0.3800	0.4000	0.3967
0.7300	0.7400	0.7400	0.7367
0.9200	0.9100	0.9500	0.9267
1.0200	1.0500	1.0300	1.0333
1.1200	1.1400	1.1800	1.1467
1.2100	1.2200	1.2200	1.2167
1.2300	1.2400	1.2100	1.2267
1.2100	1.2200	1.2000	1.2100
1.2800	1.2700	1.2600	1.2700
1.2600	1.2400	1.2700	1.2567
1.2900	1.3100	1.2900	1.2967
1.3400	1.3200	1.3000	1.3200
1.2900	1.3000	1.3000	1.2967
1.2600	1.2700	1.2700	1.2667
1.2000	1.1800	1.2000	1.1933

REDUCTION PROGRAM (CONTINUED).

41	1.2900	1.2800	1.2900	1.2867
42	0.9100	0.9200	0.9200	0.9167
43	0.9100	0.9100	0.9200	0.9133
44	0.5900	0.6100	0.6100	0.6033
45	0.1600	0.1400	0.1400	0.1467
46	0.1300	0.1200	0.1200	0.1233
47	0.	0.0200	0.	0.0067
48	0.0700	0.0800	0.1000	0.0833
49	1.6500	1.6500	1.6400	1.6467
50	2.1100	2.1300	2.1100	2.1167
51	2.0600	2.0400	2.0800	2.0600
52	1.9500	1.9500	1.9600	1.9533
53	2.1000	2.1200	2.1200	2.1133
54	0.1700	0.1800	0.1700	0.1733
55	0.1800	0.1700	0.1500	0.1667
56	0.0800	0.0700	0.0800	0.0767
57	0.0700	0.0900	0.0700	0.0767
58	0.	0.	0.	0.
59	4.9900	4.0600	2.0100	3.6867
60	4.8200	3.2200	3.6500	3.8967
61	4.9000	4.2200	3.5900	4.2367
62	9.9900	7.2400	8.7000	8.6433
63	9.9900	9.9900	4.9200	8.3000
64	8.3200	9.0500	9.9900	9.1200
65	9.9900	9.9900	8.1300	9.3700
66	3.4700	2.3200	2.7300	2.8400
67	2.4300	2.5000	2.4800	2.4700
68	2.4000	2.4200	2.4600	2.4267
69	2.2900	1.7300	2.8200	2.2800
70	2.3900	2.3900	2.3900	2.3900
71	9.9900	9.9900	9.9900	9.9900
72	2.5100	2.5500	2.5800	2.5467
73	0.5900	0.5900	0.5900	0.5900
74	0.0600	0.0100	0.	0.0233
75	9.9900	9.9900	9.9900	9.9900
76	6.1000	6.1000	6.1000	6.1000
77	0.0200	0.0300	0.0300	0.0267

VOLTS - LINE TO NEUTRAL

LINE	SENSOR#	CFACTOR	VOLTS
1-N	1	140.1100	224.1760
2-N	2	139.3400	232.6978
3-N	3	137.1000	217.5320

AMPS - LINE

LINE	SENSOR#	CFACTOR	AMPS
1-N	4	94.9700	559.0567
2-N	5	96.7100	561.5627
3-N	6	94.4400	564.1216

KWATTS - LINE TO NEUTRAL

LINE	SENSOR#	CFACTOR	KWATTS
1-N	7	12.7040	45.5650
2-N	8	14.1550	51.7601
3-N	9	11.7240	42.9880
		TOTAL KWATTS=	140.3131

	SENSOR#	CFACTOR	
DELTA ANGLE	10	30.9300	-28.9950
ROTOR SPEED(RPM)	11	200.0000	1571.3333
SHAFT TORQUE(NM)	12	300.0000	206.0000
F&W TORQUE(NM)=	12	300.0000	482.9979
ELECTRO-MAG TORQUE	12	300.0000	688.9979
DC LINK VOLTS	13	34.9000	275.1283
DC LINK AMPS	14	102.6000	754.1100

POWER OUTPUT

KW=	110.4451
HP=	148.0497
THRUST(NEWTONS)=	994.3685
EFF(NOT INC FLD)=	78.7133
POWER FACTOR(%)=	37.0497
KVA=	378.7160
EFF X PF (PU)=	0.2916
FREQUENCY(HZ)=	382.5000

FORCE

POSITION	SENSOR#	CFACTOR	NEWTONS
A	15	890.0000	1308.3000
B	16	890.0000	860.3333
C	17	890.0000	1842.3000
D	18	890.0000	1999.5333
E	19	550.0000	196.1667
F	20	550.0000	368.5000
G	21	558.0000	472.4400
H	22	558.0000	489.1800
I	23	456.7900	1.5226
J	24	456.7900	1553.0860

REDUCTION OF SENSOR FORCES TO RESULTANT FORCES

SUM OF VERTICAL FORCES=	6010.4666
DIFFERENCE OF THRUSTS=	1551.5634
RESULTANT OF TZA=	6207.5001

FIGURE 7-1. SAMPLE RUN FROM A SAMPLE DATA REDUCTION PROGRAM (CONTINUED).

FORCE ANGLE OF RESULTANT=	0.1759
LOCATION OF RESULTANT=	0.0767
RADIAL FORCE=	6111.7351
TANGENTIAL THRUST=	1086.1639
PITCH TQ=	637.4892
ROLL TQ=	22.1539
YAW TQ=	59.2811
LATERAL FORCE=	189.0733

FLUX DENSITY IN TESLA

POSITION	SENSOR#	CFACTOR	PEAK	CFACTOR	RMS
SLOT 1	26	0.2280	0.0904	0.1612	0.0640
SLOT 3	27	0.2280	0.1680	0.1612	0.1188
SLOT 5	28	0.2280	0.2113	0.1612	0.1494
SLOT 7	29	0.2280	0.2356	0.1612	0.1666
SLOT 9	30	0.2280	0.2614	0.1612	0.1849
SLOT 11	31	0.2280	0.2774	0.1612	0.1962
SLOT 13	32	0.2280	0.2797	0.1612	0.1978
SLOT 15	33	0.2280	0.2759	0.1612	0.1951
SLOT 17	34	0.2280	0.2896	0.1612	0.2048
SLOT 19	35	0.2280	0.2865	0.1612	0.2026
SLOT 21	36	0.2280	0.2956	0.1612	0.2091
SLOT 23	37	0.2280	0.3010	0.1612	0.2128
SLOT 25	38	0.2280	0.2956	0.1612	0.2091
SLOT 27	39	0.2280	0.2888	0.1612	0.2042
SLOT 29	40	0.2280	0.2721	0.1612	0.1924
SLOT 31	41	0.2280	0.2934	0.1612	0.2075
SLOT 33	42	0.2280	0.2090	0.1612	0.1478
SLOT 35	43	0.2280	0.2082	0.1612	0.1473
YOKE BELOW:	SENSOR#	CFACTOR	PEAK	CFACTOR	RMS
SLOT 6	49	0.0863	0.1421	0.0610	0.1005
SLOT 12	50	0.1351	0.2860	0.0955	0.2022
SLOT 18	51	0.1664	0.3428	0.1177	0.2424
SLOT 24	52	0.1351	0.2639	0.0955	0.1866
SLOT 30	53	0.0863	0.1824	0.0610	0.1290
BUTT-LEAD I	54	0.0770	0.0133	0.0545	0.0094
BUTT-LEAD O	55	0.0770	0.0128	0.0545	0.0091
BUTT-TRAIL I	56	0.0770	0.0059	0.0545	0.0042
BUTT-TRAIL O	57	0.0770	0.0059	0.0545	0.0042

MOTOR TEMP

POSITION	SENSOR#	CFACTOR	CELSIUS
1	59	21.3300	78.6366
2	60	21.3300	83.1159
3	61	21.3300	90.3681
4	62	21.3300	184.3623
5	63	21.3300	177.0390
6	64	21.3300	194.5296
7	65	21.3300	199.8621
8	66	21.3300	60.5772
9	67	21.3300	52.6851
10	68	21.3300	51.7608

FIGURE 7-1. SAMPLE RUN FROM A SAMPLE

11	69	21.3300	48.6324
12	70	21.3300	50.9787

DC MOTOR

	SENSOR#	CFACTOR	
VOLTS	71	54.7000	546.4530
AMPS	72	50.0000	-122.6667
FLD AMPS	73	20.0400	11.8236

SLEM FIELD

	SENSOR#	CFACTOR	
VOLTS	75	11.1900	111.7881
AMPS	76	12.6600	73.0260
KILOWATTS=	8.1634		
EFF(INC FLD)=	74.3855		

GENERAL ELECTRIC

DATA REDUCTION PROGRAM (CONTINUED).

CATALOG OF TEST DATA

The following is a catalog of all runs used in the analysis presented in this report. It is to be used in referring to the actual copies of the runs contained in Appendix I. Some runs are not included, either because their results were unsatisfactory, or because the numbers were not, in fact, used. In most cases, these conditions are noted.

CATALOG

60 & 150 Hertz Performance Tests

100 - 108	Preliminary 60 Hz Motoring
109 - 116	60 Hz, 75 A Field, Motoring - Preliminary
117 - 124	60 Hz, 40 A Field, Motoring - Preliminary
125 - 133	60 Hz Angle Tests - 400 A
134 - 140	60 Hz Angle Tests - 500 A
141 - 146	60 Hz Motoring, 75 A Field
147 - 152	60 Hz Motoring, 40 A Field
153 - 160	60 Hz Open Ckt. Saturation
161 - 167	150 Hz Open Ckt. Saturation
168	Not Used
169 - 176	60 Hz Short Ckt. Saturation
177 - 184	150 Hz Short Ckt. Saturation
185 - 190	60 Hz Motoring, 75 A Field
191 - 197	60 Hz Generating, 75 A Field
198 - 203	60 Hz Generating, 40 A Field
204 - 211	60 Hz Angle Tests - 100 A
212 - 219	60 Hz Angle Tests - 200 A
220 - 227	60 Hz Angle Tests - 300 A
228 - 235	60 Hz Angle Tests - 470 A
236 - 240	60 Hz Motoring - 16.3 mm gap
241 - 248	60 Hz Motoring - 11.2 mm gap
249 - 256	60 Hz Open Ckt. Saturation - 11.2 mm
257 - 264	150 Hz Open Ckt. Saturation - 11.2 mm
265 - 272	60 Hz Short Ckt. Saturation - 11.2 mm
273 - 280	150 Hz Short Ckt. Saturation - 11.2 mm
281 - 288	60 Hz Motoring - 21.3 mm gap
289 - 296	60 Hz Open Ckt. Saturation - 21.3 mm
297 - 304	150 Hz Open Ckt. Saturation - 21.3 mm
305 - 312	60 Hz Short Ckt. Saturation - 21.3 mm
313 - 320	150 Hz Short Ckt. Saturation - 21.3 mm
321 - 327	150 Hz Motoring - Preliminary
328 - 337	150 Hz Angle Tests - 500 A
338 - 344	150 Hz Motoring - 75 A Field
345 - 350	150 Hz Motoring - 40 A Field

351 - 352	Runs for DPO Data
353 - 359	150 Hz Generating - 40 A Field
360 - 365	150 Hz Generating - 75 A Field
366 - 370	150 Hz Motoring - 16.3 mm gap
371 - 378	150 Hz Motoring - 11.2 mm gap
379 - 384	150 Hz Motoring - 21.3 mm gap
385 - 398	150 Hz Generating - 75 A Field
399 - 403	150 Hz e = o
	150 Hz G - Table Tests
404 - 408	150 Hz e = o
409 - 413	150 Hz e = +12.5 mm
414 - 419	150 Hz e = +25 mm
420 - 424	150 Hz e = 12.5 mm
425 - 430	150 Hz e = 25 mm
431 - 435	150 Hz e = o, f = o
436 - 440	150 Hz b = +.0224 rad
441 - 445	150 Hz b = +.0448 rad
446 - 450	150 Hz b = -.0224 rad
451 - 455	150 Hz b = -.0448 rad
456 - 460	150 Hz b = o, a = o
461 - 465	150 Hz a = +.00148 rad
466 - 470	150 Hz a = -.00148 rad
471 - 475	150 Hz a = +.00296 rad
476 - 480	150 Hz a = +.00296 rad
481 - 485	150 Hz a = o, c = o
486 - 490	150 Hz c = +.00456 rad
491 - 495	150 Hz c = -.00456 rad
496 - 500	150 Hz c = o
501 - 505	60 Hz e = o
	60 Hz 6 - Table Tests
506 - 510	60 Hz e = +12.55 mm
511 - 516	60 Hz e = +25 mm
517 - 521	60 Hz e = -12.5 mm
522 - 527	60 Hz e = -25 mm
528 - 532	60 Hz e = o, b = o
533 - 537	60 Hz b = +.0224
538 - 542	60 Hz b = +.0448
543 - 547	60 Hz b = -.0224
548 - 532	60 Hz b = -.0448
533 - 557	60 Hz b = o, a = o
558 - 562	60 Hz z = +.00296 rad
563 - 567	60 Hz a = -.00296 rad
568 - 572	60 Hz a = o, c = o
573 - 577	60 Hz c = +.00456 rad
578 - 582	60 Hz c = -.00456 rad
583 - 587	60 Hz c = o

	382.5 Hz Performance Tests
588 - 590	1500 rpm Friction Windage
591 - 598	382.5 Hz Open Circuit Saturation
599 - 606	382.5 Hz Short Circuit Saturation
607 - 609	382.5 Hz Preliminary Motoring Test
610 - 616	382.5 Hz Angle Tests - 550 A
617 - 622	382.5 Hz Angle Tests - 550 A
623 - 631	382.5 Hz Motoring, 75 A Field
632 - 639	382.5 Motoring, 40 A Field
640 - 644	382.5 Hz Motoring, d = 16.3 mm
645 - 652	382.5 Hz Motoring, d = 21.3 mm
653 - 660	382.5 Hz Open Ckt. Saturation, d = 21.3 mm
661 - 668	382.5 Hz Short Ckt. Saturation, d = 21.3 mm
669 - 676	382.5 Hz Short Ckt. Saturation, d = 11.2 mm
677 - 684	382.5 Hz Open Ckt. Saturation d = 11.2 mm
685 - 692	382.5 Hz Motoring, d = 11.2 mm
	382.5 Hz G - Table Tests
693 - 697	382.5 Hz Runs for DPO, e = o
698 - 702	382.5 Hz e = +12.5 mm
703 - 708	382.5 Hz e = +25 mm
709 - 713	382.5 Hz e = -12.5 mm
714 - 719	382.5 Hz e = -25 mm
720 - 724	382.5 Hz e = o, b = o
725 - 729	382.5 Hz b = -.0224 rad
730 - 734	382.5 Hz b = -.0448 rad
735 - 739	382.5 Hz b = +.0224 rad
740 - 744	382.5 Hz b = -.0448 rad
745 - 749	382.5 Hz b = o, a = o
750 - 754	382.5 Hz a = +.00296 rad
755 - 759	382.5 Hz a = -.00296
760 - 764	382.5 Hz a = o, c = o
765	1530 rpm - Friction & Windage
766 - 770	382.5 Hz c = +.00456 rad
771 - 775	382.5 Hz c = -.00456 rad
776 - 780	382.5 Hz c = o
781 - 783	382.5 Hz Motoring, Photos
784, 785	382.5 Hz DPO Runs
786 - 790	382.5 Hz Motoring, 85 A Field
791 - 794	382.5 Hz Rotor Flux Plots
795 - 804	150 Hz Unity Displacement Factor
805	60 Hz Motoring - Photos

Section 8

CONCLUSION

The tested performance of the single-sided high-speed homopolar Linear Synchronous Motor differed significantly from the initial design predictions. Revision of the design program to model the interpolar gap and interpolar leakage flux resulted in good agreement between design prediction and performance. The machine, tested with a laminated track structure, showed a high power factor and an absence of end effects.

Misalignments of the stator relative to the rotor showed a strong tendency for the machine to hold itself in proper alignment laterally. A strong force of attraction, increasing with any reduction of air gap, made the machine unstable in the pitch mode or in any other variation of air gap dimension.

The weakest portion of the data obtained for the machine was measurement of input power from the controlled current inverter. The waveforms produced by the inverter provided a challenge to both analog and digital methods of power measurement. Use of several alternative methods of power measurement and assignment of losses gave reasonable measures of input power, efficiency, and power factor.

Revision of the Linear Synchronous Motor design program showed the output power of the test machine could be increased nearly 35% by doubling the height of the pole pieces. Initial calculations had shown that a small to large gap ratio of one to six was sufficient to approximate an infinite interpolar gap, but test results and later calculations showed a ratio of nearly one to twelve was needed. A larger interpolar gap improves motor performance by increasing the fundamental ac component of the field flux. This problem does not appear when the pole pieces are mounted on a nonmagnetic material instead of the large iron wheel used by the test motor.

Track weight could be decreased by decreasing the field space width. However, since the width of this space is determined by the space needed for the crossover of the figure eight windings, it would be very difficult to make it significantly narrower.

Optimal performance of the test machine was obtained by using a leading power factor of about 60°. Drawing a vector diagram for this mode of operation shows that the air gap voltage and armature current vectors are aligned which, for fixed vector lengths, gives the maximum energy conversion. Thus, to achieve a given output power, operation at unity power factor requires a heavier machine and track than does operation at a leading power factor.

Performance of a Linear Synchronous Motor with Laminated Track Poles and with Various Misalignments, 1980
US DOT, FRA, William R Mischler, Thomas A Nondahl